IDENTIFYING AND CHARACTERIZING THE ROLES OF TRANSMEMBRANE PROTEINS IN DIRECTING ASYMMETRIC Q NEUROBLAST MIGRATIONS

By

Lakshmi Sundararajan

Submitted to the graduate degree program in Molecular Biosciences and the Graduate Faculty of the University of Kansas in partial fulfillment of the requirements for the degree of Doctor of Philosophy.

_____
Chairperson – Dr. Erik Lundquist

_____
Dr. Brian Ackley

_____
Dr. Robert Ward

_____
Dr. Yoshiaki Azuma

_____
Dr. Eli Michaelis

Date Defended: July 3, 2014

The Dissertation Committee for Lakshmi Sundararajan
certifies that this is the approved version of the following dissertation:

IDENTIFYING AND CHARACTERIZING THE ROLES OF TRANSMEMBRANE PROTEIN IN DIRECTING ASYMMETRIC Q NEUROBLAST MIGRATIONS

_____
Chairperson – Dr. Erik Lundquist

Date approved: July 3, 2014

Abstract

Migration of neurons is essential for proper nervous system development. Defects in neural development can lead to several neurological disorders. Hence it is important to understand the mechanism of neuronal migration along with the signaling pathways required. *Caenorhabditis elegans* is a useful system to study neuronal migration due to its well-characterized nervous system and fully sequenced genome. We use Q neuroblasts to study neuronal cell migration. The QR and QL neuroblasts, born in the posterior lateral region of the worm, undergo initial polarizations in the anterior and posterior directions respectively. They then migrate in the direction of protrusion and divide to produce three neurons of which AQR (from QR) migrates anteriorly to near the anterior deirid, and PQR (from QL) posteriorly to near the phasmid ganglia.

Secreted Wnt ligands control the direction of Q descendent migrations, but the initial protrusions and migrations are independent of the EGL-20/Wnt signal. Previous studies have shown that the transmembrane proteins UNC-40/DCC, PTP-3/LAR and MIG-21 are required to direct the early Q cell migrations (Honigberg and Kenyon, 2000) (Middelkoop et al., 2012). To elucidate the genetic interaction between *unc-40*, *ptp-3* and *mig-21*, we built double mutants and used statistics to compare the defects observed to the single mutants. Our mutant analyses showed that MIG-21 and PTP-3 function in the same genetic pathway in both QR and QL. In QL, UNC-40 acts redundant to MIG-21/PTP-3 in directing posterior migration. In QR, UNC-40 and MIG-21/PTP-3 inhibit each other's role in posterior migration to direct anterior migration. Cell specific rescue experiments showed that *unc-40*, *ptp-3* and *mig-21* act cell autonomously in directing Q neuroblast migration.

We wanted to identify other genes that function with *unc-40, ptp-3* and *mig-21* in QR and QL. We isolated *cdh-4*, a fat like cadherin from a forward genetic screen. Previous work (Schmitz et al., 2008) has shown that CDH-4 is required for Q descendent migration. *cdh-4* mutants show defects in early QL and QR(~75% migrate posterior) migrations. To understand how *cdh-4* interacts

with *unc-40, ptp-3* and *mig-21*, we built double mutants of *cdh-4* with the above genes. In QR, both *unc-40RNAi* and *ptp-3RNAi* significantly suppressed the posterior migration seen in *cdh-4* mutants suggesting that, the posterior migration seen in *cdh-4* mutants required functional UNC-40 and PTP-3. The above result shows that CDH-4 has a role in both UNC-40 and PTP-3 pathways, which might explain why *cdh-4* mutants show a high percentage of QR migrating posterior. In QL however, *unc-40RNAi; cdh-4* mutants show an increase in percentage of QL migrating anterior, suggesting that UNC-40 and CDH-4 are required in redundant pathways for posterior QL migration. In contrast, *ptp-3RNAi; cdh-4 mutants* resembled *cdh-4* mutants alone, suggesting that PTP-3 and CDH-4 might function in the same genetic pathway.

CDH-4 driven by its endogenous promoter is expressed in Q cells during its migrations. We wanted to check further if *cdh-4* functions in the Q cell to direct its migration. Mosaic analysis experiments showed that *cdh-4* functions non-cell autonomously to regulate Q cell migrations despite being expressed in the Q cell during its migration.

Together, we have identified the roles of transmembrane proteins UNC-40, PTP-3, MIG-21 and CDH-4 in directing Q cell migrations. We have also characterized a signaling network through which these proteins function and thereby provide some insight into mechanism of neuronal cell migration.

As mentioned earlier, we have identified and characterized the role of genes that are required to direct both early and subsequent descendant Q neuroblast migration. However, genes like *egl-20/Wnt* and *mab-5/Hox* are exclusively required to direct Q descendant migration. We wanted to identify other genes that function to direct QR and QL descendant migrations. We identified *sdn-1/Syndecan*, a heparan sulfate proteoglycan, and characterized its role in directing anterior QR descendant migration. To understand how *sdn-1* interacts with *mig-13*, a previously characterized gene in anterior QR guidance, we built *sdn-1; mig-13* double mutants. In AQR, *sdn-1; mig-13* double mutants significantly enhanced the defects observed in the single mutant backgrounds suggesting that they function in parallel pathways to direct AQR migrations. Also,

sdn-1 mutants suppressed the anterior migration of PQR seen in a *mab-5* loss of function background, suggesting that SDN-1 functioned genetically downstream of MAB-5 and was possibly regulated by MAB-5.

In sum, we are starting to classify the genetic pathways required to direct both early QR and QL and their descendant neuron migration. These signaling pathways characterize the inherent asymmetry between these left-right cells. Understanding these interactions will help us uncover the more complex signaling systems in mammalian nervous system development.

Acknowledgments

The entire period of my graduate career has been one of the most gratifying yet challenging experiences that I have ever encountered. I left my family, country and friends behind at the age of 21 to come to a place where no one I knew even spoke the same mother tongue as mine. The reward for pushing myself to take that leap came in the form of some great friends and a wonderful Ph.D. experience in the University of Kansas. But I could not have come so far without the unconditional support of my family members. I'd really like to thank my mother, Bhooma for never questioning my desire to leave home for a career in research despite the anguish she experienced at me leaving indefinitely, and my father, Sundararajan for being a constant source of strength and support. My brother Niranjan has been my best friend and has always encouraged me to stand by my dreams. He has also shown me that it's a good thing to take a break and have some fun despite having a busy schedule. I would also like to acknowledge my grandparents Kousalya and Ramanujam for letting me know every single day how proud they are of my accomplishments. I also have to acknowledge my aunts Sudha and Geetha for always providing me with a home away from home and for being the coolest aunts ever.

I would like to earnestly thank my mentor, Dr. Erik Lundquist for teaching me how to be an independent researcher. He has not only provided me with the knowledge but has constantly encouraged and pushed me to do the best that I am capable of. Erik's enthusiasm for science has always helped me feel motivated to keep at my projects even through failed experiments and his personal work ethics on the bench has been a visual tool for me to learn. For all that and more I am extremely thankful.

My graduate experience would not have been as much fun without my exceptional colleagues in the Lundquist Lab. They have not only provided me with extraordinary scientific conversation and suggestions but they have also been wonderful friends and I do treasure the time I've spent with each one of them. I have to specifically mention Jamie Dyer, for making the first year in the

lab so comfortable and Jamie Alan, for being the best big sister ever. I also want to extend my gratitude to Vinidhra Sridharan, a fellow graduate student and the best friend anyone could have. I cannot imagine have gone through grad school without her by my side. I'd also like to thanks Samantha Hartin for introducing me to her delightful family who have never let me feel left out during any holiday celebration like Thanksgiving or Christmas. It made me miss my family a little less.

I'd also like to acknowledge Dr. Brian Ackley for his helpful suggestions during lab meetings and his generosity with his reagents and the time taken to teach me microscope techniques. I'd also like to thank the members of his lab. Finally, I'd like to thank my committee members for their insightful suggestions, encouragement and guidance.

Table of contents

List of figures

List of Tables

Chapter I

Introduction

1.2 Introduction:

Neuronal cell migration constitutes an essential part of nervous system development. During the development of the cerebral cortex, cells migrate in a defined direction to populate different layers of the cortex (Solecki et al., 2006). This defined directional migration required a few steps. First, the cell in response to a signaling cue will send out protrusions in direction of migration. Then, the protrusions condense to a single protrusion after which the cell will adhere to the migrating surface. Then the cell retracts to push itself to a newer destination along the surface of migration.

An essential part of cell migration involves the specific interaction between transmembrane molecules on the surface of the cell and an external signaling cue. This interaction triggers a specific downstream signaling pathway that culminates in the modulation of the actin cytoskeleton. The actin cytoskeleton aids in formation of lamellopodial and filopodial structures that aid the cell to migrate. However, the specificity of the direction of migration is conferred by the interaction between the transmembrane proteins and a signaling cue and the downstream signaling pathway generated by the specific interaction.

Caenorhabditis elegans is an ideal model system to identify and study the role of signaling pathways involved in neuronal cell migration. *C. elegans* has a simple nervous system with 302 neurons that are well characterized (White et al., 1986) . Also, the transparent nature of the nematodes makes it easier to observe and characterize cell migration *in vivo* making the system ideal to study the mechanisms of migration.

We use the Q neuroblasts in *C. elegans* as a system to study neuronal cell migration. The Q neuroblasts in *Caenorhabditis elegans* are born in the posterior lateral region of the worm on the right (QR) and left side (QL) (Sulston and Horvitz, 1977). QR subsequently migrates anterior and QL migrates posterior. The Q neuroblasts constitute a good model system to study signaling pathways involved in asymmetrical cell migrations. QR and QL are daughters of

V5 hypodermal seam cells and are born about half an hour after hatching (Chapman et al., 2008; Dyer et al., 2010; Honigberg and Kenyon, 2000). By about five hours post hatching, the Q cells migrate and then undergo their first division. QR migrates and divides anterior on the seam cell V4 while QL migrates and divides posterior on the seam cell V5. The Q descendants after the first Q cell division further undergo a series of programmed cell death, migrations, and cell divisions to from three neurons each. AQR from QR migrates the farthest anteriorly to near the anterior deirid. Similarly, PQR from QL migrates farthest in the posterior direction, to near the phasmid ganglia (Chalfie and Sulston, 1981; Chapman et al., 2008; Sulston and Horvitz, 1977; White et al., 1986). After QL undergoes it's first cell division, it requires an EGL-20/Wnt directed MAB-5/Hox expression for further posterior migration. MAB-5/Hox is a transcription factor and is required cell autonomously in Q descendants to direct posterior migration. QR descendants migrate away from the EGL-20/Wnt induced MAB-5/Hox signal and thus migrate anterior (Chalfie et al., 1983; Eisenmann, 2005; Harris et al., 1996; Kenyon, 1986; Korswagen et al., 2000; Salser and Kenyon, 1992, 1996; Whangbo and Kenyon, 1999; Zhao et al., 2003). MAB-5 is necessary and sufficient to cause posterior migration (Figure 1.1). In *mab-5* loss-of-function mutants, both QR and QL descendants migrate anterior. Furthermore, in a *mab-5* gain of function mutant, both QR and QL descendants migrate posterior. However, the intial Q neuroblast migration and division occurs independent of a MAB-5 signal (Chapman et al., 2008). Recent work has shown that the initial migration can influence the expression of MAB-5 in the Q descendants. MIG-21 mediates a differential sensitivity to MAB-5 between QR and QL resulting in QL being more sensitive to MAB-5 when compared to QR (Middelkoop et al., 2012).

Previous studies identified the roles of transmembrane proteins UNC-40/DCC, PTP-3/LAR and MIG-21 in directing anterior-posterior QR and QL migrations (Sundararajan and Lundquist, 2012). UNC-40/DCC and PTP-3/LAR have been extensively studied with respect to their roles in the nervous system development (Ackley et al., 2005; Aicher et al., 1997; Alexander et al., 2009; Chan et al., 1996; Harrington et al., 2002; Honigberg and Kenyon, 2000; Keino-

Masu et al., 1996). UNC-40/DCC is an UNC-6/Netrin receptor that functions as an attractive signal for axons that migrate along the dorsal-ventral axis (Keino-Masu et al., 1996). However, previous studies have shown that UNC-6/Netrin does not play a role in directing anterior-posterior Q neuroblast migrations (Honigberg and Kenyon, 2000). This suggests that UNC-40/DCC might function in an UNC-6 independent manner possibly with a different ligand to direct anterior-posterior Q neuroblast migrations. Also, previous studies with PTP-3/LAR have shown that it can function as a receptor often with SDN-1 acting as a ligand in the nervous system (Hudson et al., 2006; Johnson et al., 2006; Wang et al., 2012).

In an effort to identify potential ligands that could function with UNC-40 and PTP-3, we performed an EMS screen to isolate mutants with defects in direction of AQR and PQR migrations. Through the screen we identified three new mutations in *mig-21* gene. MIG-21 is a small thrombospondin domain containing transmembrane protein that has been implicated in directing early Q neuroblast migrations and Q descendent migrations (Middelkoop et al., 2012).

To identify the nature of genetic interaction between *unc-40*, *ptp-3* and *mig-21*, we constructed combination of double and triple mutants between the genes. Our genetic analyses revealed distinct interactions between *unc-40*, *ptp-3* and *mig-21* in QR Vs. QL. In QR and QL, we found that UNC-40/DCC, PTP-3/LAR and MIG-21 direct posterior migration. In QL, PTP-3/LAR and MIG-21 function in the same pathway redundant to UNC-40/DCC to direct posterior QL migration. However in QR, UNC-40/DCC and PTP-3/MIG-21 mutually inhibit each other's role in posterior migration to direct anterior QR migration (Sundararajan and Lundquist, 2012). Next, we wanted to see whether *unc-40*, *ptp-3* and *mig-21* is required cell autonomously in the Q cells to direct their migrations. Our cell specific rescue and RNAi experiments showed that *unc-40*, *ptp-3* and *mig-21* act cell autonomously in both QR and QL (Sundararajan and Lundquist, 2012).

Our work has established a signaling system required for early Q neuroblast migration independent of the EGL-20/MAB-5 signaling. The

transmembrane proteins UNC-40/DCC (Deleted in Colorectal Cancer), PTP-3/LAR (Leukocyte common Antigen Receptor Tyrosine Phosphatase) and MIG-21 (a thrombospondin repeat containing protein) are required for directing posterior QR and QL migrations. Despite the role of UNC-40, PTP-3 and MIG-21 in directing posterior Q migrations, we hypothesized an asymmetrical interaction between these proteins in QR and QL that contribute to an inherent left-right asymmetry in the Q cells. Our genetic analysis showed that PTP-3 and MIG-21 worked in the same pathway in parallel to UNC-40 in both QR and QL. In QR, these pathways mutually inhibited each other's role in posterior migration to direct the cell anterior. In QL, these pathways acted redundantly to direct posterior cell migration (Sundararajan and Lundquist, 2012).

To identify other genes that interact with *unc-40*, *ptp-3* and *mig-21* in contributing to the left-right asymmetry in QR and QL, we performed a forward genetic screen using Ethyl Methyl Sulfonate and isolated mutations in genes that caused defects in AQR/PQR migrations. Through the screen we isolated two novel mutations in *cdh-4* gene that coded for early stop codons in the coding region. CDH-4 is a cadherin repeat containing transmembrane protein that has been implicated in axon fasciculation and cell migration (Najarro et al., 2012; Schmitz et al., 2008). Schmitz *et al* showed that *cdh-4* plays a role in directing AQR and PQR migration.

CDH-4 is homologous to mammalian Fat (Abou Jamra et al., 2008; Loveless and Hardin, 2012; Najarro et al., 2012; Schmitz et al., 2008). Fat has been implicated in bipolar disorder development and schizophrenia (Abou Jamra et al., 2008; Jung and Jun, 2013; Light et al., 2007; Redies et al., 2012). Fat like cadherins have been studied extensively in Drosophila and mammalian systems. In Drosophila, Fat along with Dachsous plays an important role in establishing planar cell polarity. Earlier studies have shown that Fat along with the other PCP components interacts with the Wnt signaling pathway to generate planar cell polarity (Ishiuchi et al., 2009; Rawls et al., 2002; Saburi et al., 2008; Strutt and Strutt, 2002, 2005; Wodarz, 2005; Yang et al., 2002). In *C. elegans,* a similar interaction is seen between the PCP components and Wnt signaling in patterning

the nervous system, regulating axon guidance, and synaptogenesis (Ackley, 2013; Najarro et al., 2012; Schmitz et al., 2008). Much of the PCP-Wnt interaction remains conserved in vertebrate systems (Goodrich and Strutt, 2011; Ishiuchi et al., 2009; Saburi et al., 2008). Thus, Fat has been implicated strongly as a part of the PCP pathway in multiple systems.

As mentioned earlier, Q cells undergo a Wnt signal independent initial migration and division (Chapman et al., 2008). Mutations in *cdh-4* cause directional defects in early Q neuroblast migrations indicating that CDH-4 might play Wnt independent roles in cell migration. Schmitz *el al.,* also showed that *cdh-4* acts independent of *mab-5*, a Wnt target through quantifying AQR and PQR migration defects in *cdh-4* loss of function alleles built with *mab-5* loss of function and gain of function alleles. To identify if *cdh-4* interacts with the Wnt independent signaling system of *unc-40*, *ptp-3* and *mig-21* in directing early Q neuroblast migration, we analyzed double and triple mutants of *cdh-4* with *unc-40*, *ptp-3* and *mig-21*. We found that *cdh-4* contributed to the differential interactions between *unc-40*, *ptp-3* and *mig-21* in QR *vs.* QL. In QR, our analysis showed that mutations in *unc-40*, *ptp-3* and *mig-21* significantly suppressed the posterior migration observed in a *cdh-4* mutant background. Hence, CDH-4 is possibly acting in both UNC-40 and PTP-3/MIG-21 pathways to facilitate a mutual inhibition of their directed posterior migration and cause anterior QR migration. In QL, our quantification of *cdh-4; unc-40*, *cdh-4; ptp-3* and *cdh-4; mig-21* double mutants showed that CDH-4 functioned with PTP-3 and MIG-21 redundantly with UNC-40 directing posterior migration. Mosaic analysis experiments showed that CDH-4 functioned non-cell autonomously regulated Q cell migrations despite being expressed in the Q cell during its migration.

Together, we have identified a novel Wnt independent role of CDH-4 in regulating early Q neuroblast migrations. CDH-4 interacts with both UNC-40 and PTP-3/MIG-21 in QR by facilitating a mutual inhibition of each other's role in posterior migration and cause anterior migration. In QL, CDH-4 acts with PTP-3 and MIG-21 in parallel to UNC-40 in directing posterior migration. These distinct interactions between QR and QL contribute to the inherent left-right asymmetry

that causes bilaterally symmetrical cells to migrate in an anterior-posterior direction.

Our results so far have characterized the role of genes required for the directional migration of early Q neuroblast and Q descendant migrations. However previous work has shown that there are genes that control the migrations of Q descendants but do not affect early Q neuroblast migrations (Chapman et al., 2008; Sym et al., 1999). A well characterized example of this is the EGL-20/Wnt directed MAB-5/Hox expression that is required for posterior QL descendant migrations but is not required for early QR or QL migrations (Chapman et al., 2008). Another example is MIG-13, a single pass transmembrane protein that is required to direct anterior QR descendant migration but not the early anterior QR migration (Sym et al., 1999). Previous work has shown that MAB-5/Hox inhibits the posterior expression of MIG-13 and keeps MIG-13 expression restricted to the anterior and central regions of the worm (Sym et al., 1999). These intersecting anterior versus posterior directing signaling pathways contribute to the inherent left-right asymmetry between these neurons (AQR and PQR). We identified the role of SDN-1/Syndecan, a Heparan Sulfate Proteoglycan in directing both the extent and direction of QR descendant migration. Our results showed that SDN-1 and MIG-13 function in redundant pathways to direct anterior QR descendant migrations and that SDN-1 was required cell autonomously in QR to direct their migrations. Also, our genetic analyses put SDN-1 downstream of MAB-5, with MAB-5 possibly regulating the posterior function of SDN-1.

In sum, we are starting to identify signaling pathways that are required to direct both early and subsequent descendant migrations of the Q neuroblasts. We have characterized the roles of genes that contribute to the inherent left-right asymmetry between these cells, and we are beginning to identify the complex genetic interactions between these genes. Uncovering these complex genetic pathways is a step toward understanding the more multifaceted intricate signaling pathways that are required to regulate vertebrate neuronal development.

Figure 1.1.

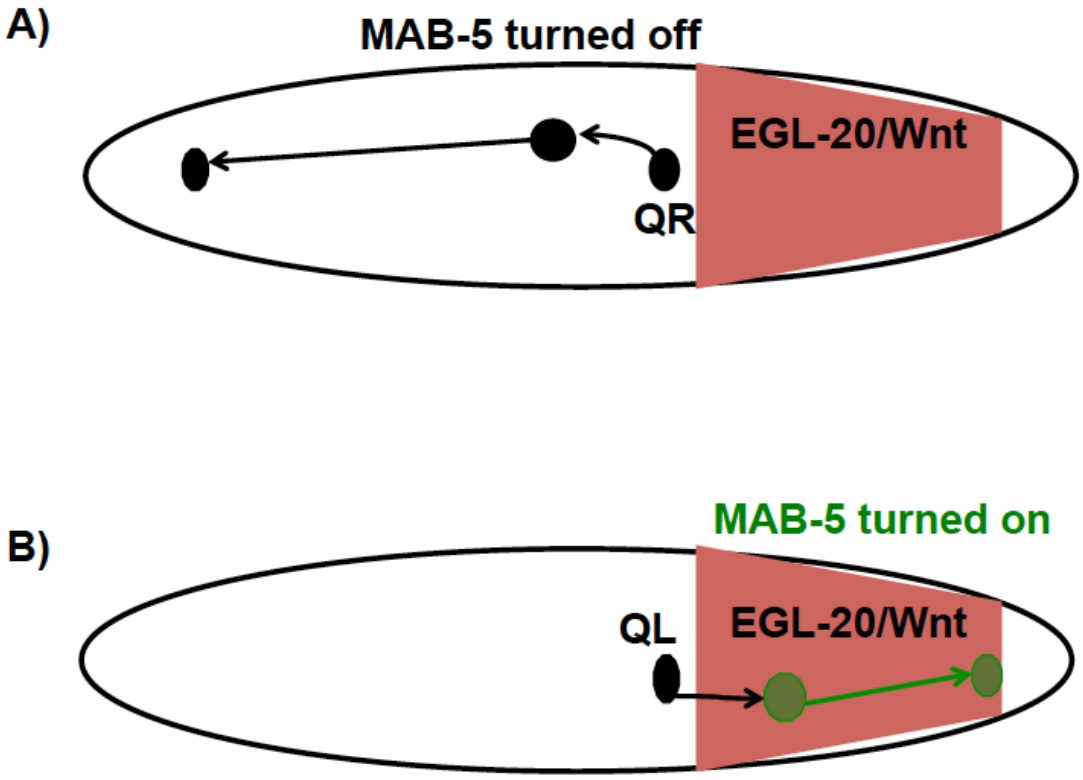

Figure 1.1. A model for early and subsequent descendant migration in presence of EGL-20 directed MAB-5 signal: A) QR undergoes an initial anterior migration away from the EGL-20/Wnt signal and its descendants migrate anterior since MAB-5 does not turn on. B) QL migrates posterior into the EGL-20/Wnt signal, which turns on MAB-5 in its descendants that direct them posterior.

Chapter II

Transmembrane proteins UNC-40/DCC, PTP-3/LAR and MIG-21 Control Anterior-Posterior Neuroblast Migration with Left-Right Functional Asymmetry

2.1 Abstract

Migration of neurons and neural crest cells is of central importance to the development of nervous systems. In *C. elegans*, the QL neuroblast on the left migrates posteriorly, and QR on the right migrates anteriorly, despite similar lineages and birth positions with regard to the left-right axis. Initial migration is independent of a Wnt signal that controls later anterior-posterior Q descendant migration. Previous studies showed that the transmembrane proteins UNC-40/DCC and MIG-21, a novel thrombospondin type-I repeat containing protein, act redundantly in left-side QL posterior migration. Here we show that the LAR receptor protein tyrosine phosphatase PTP-3 acts with MIG-21 in parallel to UNC-40 in QL posterior migration. We also show that in right-side QR, the UNC-40 and PTP-3/MIG-21 pathways mutually inhibit each other's role in posterior migration, allowing anterior QR migration. Finally, we present evidence that these proteins act autonomously in the Q neuroblasts. These studies indicate an inherent left-right asymmetry in the Q neuroblasts with regard to UNC-40, PTP-3, and MIG-21 function that results in posterior versus anterior migration.

2.2 Introduction

Cell migration is a fundamental event in the development of nervous systems. In the vertebrate central nervous system, neurons and neuroblasts migrate radially to populate distinct layers in the cerebellar and cerebral cortices, and neural crest cells migrate along distinct paths in the vertebrate embryo to give rise to the peripheral nervous system. The Q neuroblasts in *C. elegans* are a useful model to study the migration of neuroblasts and neurons in the anterior-posterior axis. The Q neuroblasts are a bilaterally symmetric pair of cells in the posterior-lateral region of the animal, with QR on the right side and QL on the left side (Sulston and Horvitz, 1977). The Q neuroblasts are born in embryogenesis and are the sisters of the V5 hypodermal seam cells. By 5 hours after hatching, QR has migrated anteriorly and divided over the V4 seam cell, and QL has migrated posteriorly and divided over the V5 seam cell (Chapman et al., 2008; Dyer et al., 2010; Honigberg and Kenyon, 2000). The resulting Q cell descendants then undergo a pattern of migration, division, and programmed cell death resulting in three neurons each (AQR, SDQR, and AVM on the right from QR; and PQR, SDQL, and PVM on the left from QL) (Chalfie and Sulston, 1981; Sulston and Horvitz, 1977). The QR descendant AQR migrates the longest distance to a region near the anterior deirid ganglion in the head, and the QL descendant PQR migrates the longest distance posteriorly to the phasmid ganglion in the tail (Chapman et al., 2008; Sulston and Horvitz, 1977; White et al., 1986). The posterior migration of QL descendants requires the activity of the MAB-5/Hox transcription factor, expression of which is induced in QL descendants by an EGL-20/Wnt signal emanating from the posterior (Chalfie et al., 1983; Eisenmann, 2005; Harris et al., 1996; Herman, 2001; Kenyon, 1986; Korswagen et al., 2000; Salser and Kenyon, 1992; Whangbo and Kenyon, 1999). QR migrates anteriorly and does not normally receive this EGL-20/Wnt signal, and thus does not express MAB-5/Hox.

The initial anterior and posterior migrations of the QR and QL neuroblasts do not depend on MAB-5 or EGL-20/Wnt, as QL and QR protrude and polarize normally in *mab-5* and *egl-20* mutants (Chapman et al., 2008). While initial Q

migration is independent of EGL-20/Wnt, the five *Wnt* genes are involved in subsequent Q descendant guidance along the anterior-posterior axis (Harterink et al., 2011; Pan et al., 2006; Zinovyeva et al., 2008).

The initial Q migrations can affect subsequent MAB-5 expression in the Q descendants (Chapman et al., 2008; Middelkoop et al., 2012). The extent of posterior protrusion correlates with *mab-5* expression, with more *mab-5* expression in cells that protrude posteriorly (Middelkoop et al., 2012), consistent with exposure to the posterior EGL-20/Wnt signal. QR is inherently less sensitive to the EGL-20/Wnt signal than QL (Middelkoop et al., 2012; Whangbo and Kenyon, 1999), a difference that seems to be mediated by the MIG-21 molecule (i.e. in *mig-21* mutants the differential sensitivity is abolished) (Middelkoop et al., 2012).

Previous studies have revealed mechanisms of initial Q neuroblast migration that is independent of EGL-20/Wnt and MAB-5/Hox. The transmembrane immunoglobulin superfamily receptor UNC-40/Deleted in Colorectal Cancer (DCC) controls the anterior-posterior protrusion and migration of both QR and QL (Honigberg and Kenyon, 2000; Middelkoop et al., 2012). UNC-40/DCC is an UNC-6/Netrin receptor that regulates cell and growth cone migrations in the dorsal ventral axis (Hedgecock et al., 1990; Keino-Masu et al., 1996). UNC-6/Netrin is not involved with UNC-40/DCC in anterior-posterior Q migration (Honigberg and Kenyon, 2000), nor does it act with UNC-40 in muscle arm extension (Alexander et al., 2009), suggesting that UNC-40/DCC might utilize other ligands in these processes.

To identify additional genes that might act with UNC-40 in initial Q protrusion and migration, we conducted a forward genetic screen for mutants with altered migrations of the QL and QR descendant neurons AQR and PQR, with the idea that they might also affect Q protrusion and migration. This screen identified three new mutations in the *mig-21* gene (Du and Chalfie, 2001), which encodes a small transmembrane molecule with two extracellular thrombospondin type I domains. MIG-21 was shown previously to affect Q protrusion and migration and Q descendant migration, and to control differential sensitivity of QL

and QR to the EGL-20/Wnt signal (Du and Chalfie, 2001; Middelkoop et al., 2012).

A previous screen for Q descendant migration mutants identified *qid-5(mu245)* (Ch'ng et al., 2003), which we found caused misdirected AQR and PQR similar to *unc-40* and *mig-21*. We sequenced the genome of a *qid-5(mu245)* strain and discovered that *qid-5(mu245)* is a new and potential null allele of the *ptp-3* gene, which was previously implicated in Q protrusion and migration (Williams, 2003) and which encodes a LAR-type receptor protein tyrosine phosphatase (Ackley et al., 2005; Harrington et al., 2002). The *ptp-3* locus encodes a family of transmembrane molecules characterized by extracellular immunoglobulin and fibronectin type III repeats and two intracellular phosphatase domains. PTP-3/LAR related molecules are involved in multiple aspects of nervous system development, including axon guidance, neurite development and synaptic organization (Ackley et al., 2005; Hofmeyer and Treisman, 2009; Johnson et al., 2006; Pawson et al., 2008; Wang et al., 2012), cell movements in gastrulation (Harrington et al., 2002), and germline stem cell maintenance (Srinivasan et al., 2012).

Analysis of double and triple mutants involving *unc-40, ptp-3, and mig-21* revealed distinct interactions in QL versus QR. In QL we found that UNC-40 and MIG-21 act redundantly in posterior migration, similar to a recently published study (Middelkoop et al., 2012). We also found that PTP-3 acts in parallel to UNC-40 in QL posterior migration, and might act in the same pathway as MIG-21. Surprisingly, we found that the abnormal posterior migration of QR in *ptp-3* and *mig-21* mutants was suppressed by *unc-40*, and *vice versa,* leading us to speculate that in QR, UNC-40 and a PTP-3/MIG-21 pathway might mutually inhibit each other's role in posterior migration, allowing for anterior migration of QR. Cell-specific rescue and RNAi experiments indicate that MIG-21, UNC-40, and PTP-3 can act cell-autonomously in the Q cells to guide Q migrations.

In sum, we have identified three transmembrane molecules, UNC-40, MIG-21, and PTP-3 that control posterior Q cell migration. UNC-40 and MIG-21/PTP-3 act in parallel in QL, and act as mutual inhibitors of one another in QR.

These novel interactions between UNC-40, PTP-3, and MIG-21, indicate that complex transmembrane receptor interactions guide initial Q cell protrusion and migration, and that, despite apparent bilateral symmetry, QL and QR use inherently distinct mechanisms to guide initial anterior-posterior migration.

2.3 Materials and Methods

***C. elegans* genetics.** All experiments were conducted at 20^{o} C using standard culture techniques (Sulston and Hodgkin, 1988). The following mutations were used: LGI *unc-40(e1430), unc-40(e271), unc-40(n324)*; LGII *ptp-3(mu256), ptp-3(mu245), ptp-3(ok244), muIs32[mec-4::gfp]*; LGIII *mig-21(u787), mig-21(lq37), mig-21(lq78), mig-21(lq84)*; LGIV *lqIs80[Pscm promoter::gfp::caax]*; LGV *sid-1(pk3321), lqIs58[Pgcy-32 promoter::cfp] ayIs9[Pegl-17::gfp] (Branda and Stern, 2000)*; LG unassigned *lqIs146[Pscm promoter::unc-40(RNAi)], lqEx661[Pscm promoter::mig-21(RNAi)], lqIs166[Pscm promoter::ptp-3(RNAi)]*; *lqIs151[Pscm promoter::unc-40(+)::gfp], lqEx637[Pscm promoter::ptp-3B(+)::gfp)], juIs197[ptp-3B(+)::gfp], lqEx593[mig-21(+)], lqEx712 [Pdpy-7::ptp-3B(+)], lqEx714 [Pegl-17::unc-40(+)], lqEx716 [Pegl-17::ptp3B(+)].* Trangenes were constructed by standard gonadal microinjection to produce extrachromosomal arrays and were stably integrated into the genome using standard UV-TMP techniques (Mello and Fire, 1995).

Isolation of *mig-21* alleles and characterization of the *mig-21* locus. The *mig-21* alleles *lq37, lq78*, and *lq84* were isolated in an EMS screen for new mutations that affect the positions of the Q cell descendants AQR and PQR (E.A.L., unpublished). Single nucleotide polymorphism (snp) mapping was used to assign these mutations to linkage groups as described in (Davis et al., 2005). Briefly, males from the polymorphic Hawaiian strain CB4856 were mated to hermaphrodites harboring the new mutation in the N2 background, which also contained the *lqIs58 V* and *lqIs80 IV* marker transgenes. Single F1 heterozygous hermaphrodites were plated singly, and 10-20 F2 animals with AQR and PQR migration defects (mutant segregants) were subjected to PCR using the snp primers described in (Davis et al., 2005). The PCR products were digested with *DraI* restriction enzyme to detect the snp. Relative agarose gel electrophoresis band intensities were used to determine which CB4856-associated snps were underrepresented in the mutant segregants. *lq37, lq78*, and *lq84* all showed

linkage to snps on LGIII, and each failed to complement each other and *mig-21(u787)* for AQR and PQR defects (data not shown). The *mig-21* locus from each strain was amplified by polymerase chain reaction (PCR), and the PCR products were sequenced to identify the lesions associated with each allele (primer sequences available upon request). *lq37* was a G to A transition (position LGIII 5877678 WS228) resulting in a C to Y missense change; *lq78* was a G to A transition (position LGIII 5877466 WS228) resulting in a G to E missense; and *lq84* was a G to A missense (position LGIII 5877289 WS228) resulting in an altered 3' splice site.

A transgene containing the wild-type *mig-21(+)* locus was generated by amplifying and cloning the *mig-21* gene from N2 genomic DNA. This fragment consisted of the entire region from the predicted upstream and downstream genes relative to *F01F1.13* (LGIII 5878514 to 5876277, Wormbase WS229). The region was sequenced to ensure that no mutations had been introduced by PCR. This construct (*lqEx593*) rescued the AQR and PQR migration defects of *mig-21(u787)*.

In an unrelated experiment, the transcriptomes of L1 larvae approximately 5 hours after hatching were sequenced using next-generation RNA seq on the Illumina Genome Analyzer IIx (GAIIx) platform (Cofactor Genomics, St. Louis, MO USA). Sequencing reads were mapped to the *C. elegans* reference genome using TopHat (Langmead et al., 2009)and visualized using the Integrated Genomics Viewer 2.0.15 (Robinson et al., 2011; Thorvaldsdottir et al., 2013). The reads that mapped to the *mig-21* locus are shown in Figure 2.S1, and confirmed the gene structure diagrammed in Figure 2.S2. The 3' end of the gene structure is identical to that described in (Middelkoop et al., 2012). The 5' end differed from the Middelkoop et al., 2012 prediction, and was confirmed by a transcript sequencing read as shown on Wormbase. The prediction described here contains a predicted N-terminal signal sequence not found in the Middelkoop et al., 2012 prediction.

***ptp-3(mu245)* identification.** The previously-identified *qid-5(mu245)* mutant affected AQR and PQR migration in a manner similar to *mig-21*. To identify the gene affected by *qid-5(mu245)*, we subjected a strain harboring the mutation (LE2577; *qid-5(mu245) muIs32 II; lqIs80 Iv; lqIs58 V*) to genome resequencing using the Illumina GAIIx platform (special thanks to O. Hobert and A. Boyanov, Columbia University). LE2577 reads were compared to the *C. elegans* reference genome using MAQgene (Bigelow et al., 2009), which also categorized the predicted effects the polymorphisms on gene structure and function. LE2577 harbored a predicted C to A mutation (position LGII 10995118 in WS229) that resulted in a premature stop codon in the *ptp-3* gene. *qid-5(mu245)* had been previously mapped to a region of LGII that contains *ptp-3*. *qid-5(mu245)* failed to complement *ptp-3* for AQR and PQR migration defects (data not shown), indicating that *mu245* is an allele of *ptp-3*.

Scoring AQR and PQR migration defects. Defects in AQR and PQR migration were quantified as described previously (Chapman et al., 2008). AQR and PQR were assayed using the *gcy-32::cfp* transgene *lqIs58* in L4 or young adult animals. Five regions along the anterior-posterior axis of the animal were considered. Position 1 represents the wild-type position of AQR in the anterior deirid ganglion just posterior to the pharynx; position 2 represents a region anterior to the vulva but posterior to the anterior deirid; position 3 represents a region proximal to the vulva (~10 AQR or PQR cell body widths to the anterior and posterior of the vulva); position 4 represents the birthplace of the Q neuroblasts near the posterior deirid ganglion; and position 5 represents the wild-type position of PQR posterior to the anus in the phasmid ganglion. At least 100 animals of each genotype were scored for AQR and PQR position relative to this scale. Only positions 1 and 5, the unambiguous positions of wild-type AQR and PQR, were used in statistical analysis. Significance was determined using Fisher's Exact test.

Scoring Q neuroblast migration defects. The protrusion and migration of the Q neuroblasts was quantified as described previously (Chapman et al., 2008).

To synchronize animals, adults and larvae were washed from plates, leaving behind eggs. At one-half-hour time points, newly hatched larvae were washed from these plates and allowed to develop on freshly-seeded NGM plates. Q cells were analyzed at 2, 3, and 4 hours after synchronization. At 2-2.5 h post hatch, the Q neuroblasts extend anterior (QR) and posterior (QL) protrusions. By 3-3.5h, the Q neuroblasts have migrated above their respective seam cells (V4 for QR; V5 for QL). At 4-4.5h, the Q neuroblasts undergo their first division above the seam cells. Protrusion at 2-2.5 h was scored as anterior if the cell protruded over the V4 seam; as no protrusion if it failed to protrude, and posterior if it protruded over the V5 seam cell. Migration at the 3-3.5 h stage was scored as anterior if the Q cells migrated over the V4 seam cell; as migration failure if the Q cells failed to migrate; and as posterior if the Q cells migrated over the V5 seam cell. Position of division at 4-4.5 h was scored as anterior if the Q cells divided over the V4 seam cell; as between if the Q cells divided between the V4 and V5 seam cells; and posterior if the Q cells divided over the V5 seam cell. At least 25 cells were scored for each genotype, and significance of difference in migration between genotypes was determined by Fisher's Exact analysis. Only position of division at 4-4.5h was included in Figure 2.6, but the data at the other time points is not significantly different from 4-4.5h alone.

***ptp-3* and *unc-40* transgenes** A transgene consisting of the wild-type *ptp-3B* gene and upstream region fused in frame to *gfp* (*juIs197[ptp-3B::gfp]*) (Ackley et al., 2005)rescued AQR and PQR defects of *ptp-3(mu256)*. We amplified the coding region from this construct, and placed it behind the *scm* promoter to drive *ptp-3B::gfp* expression specifically in the seam cells and early Q cells (*lqEx637[scm promoter::ptp-3B::gfp]*) (Chapman et al., 2008). Primer and plasmid sequences are available upon request. We created an *scm promoter::unc-40::gfp* transgene (*lqIs151[scm promoter::unc-40(+)::gfp]*) by amplifying the *unc-40::gfp* coding region from the previously described *mec-4 promoter::unc-40::gfp* plasmid (Levy-Strumpf and Culotti, 2007), and placing it behind the *scm* promoter. The *dpy-7* promoter (Gilleard et al., 1997) (LGX:

7537743-7538087; WS232) was amplified by PCR and placed upstream of *ptp-3B(+),* and the *egl-17* promoter (Branda and Stern, 2000; Cordes et al., 2006) (LGX: 485131-489794; WS232) was amplified by PCR and placed upstream of *unc-40(+)* and *ptp-3B(+)*. The coding regions of these transgenes were sequenced to ensure that no errors had been introduced by PCR.

Transgenic RNA mediated gene interference (RNAi). We used a cell-specific transgenic RNAi approach as described previously (Esposito et al., 2007). Fragments of the *mig-21, unc-40,* and *ptp-3* coding regions were amplified by PCR and inserted behind the *scm* promoter in a plasmid (primer and plasmid sequences available upon request). For each gene, a "sense" and "antisense" orientation relative to the *scm* promoter was isolated. An equimolar mixture of the sense and antisense plasmids was used to construct transgenic animals. These transgenic animals were predicted to express both sense and antisense RNAs driven by the *scm* promoter in the seam cells and Q cells, which was expected to trigger a double-stranded RNA response in these cells (RNAi). Using this approach, *mig-21(RNAi)* phenocopied *mig-21* mutations in AQR and PQR migration. While *ptp-3(RNAi)* and *unc-40(RNAi)* had no effect on their own, they both enhanced the effects of mutations in the other. Transgenes were crossed into the *sid-1(pk3321)* background to test potential dsRNA spreading and systemic effects of the transgenes

2.4 Results

***mig-21* allele isolation and the *mig-21* locus.** In a screen for new mutations with AQR and PQR migration defects, we identified three new mutations, *lq37, lq78,* and *lq84*, that caused directional migration defects of both AQR and PQR. These three alleles mapped to linkage group III (see Materials and Methods) and failed to complement one another for AQR and PQR migration (data not shown), suggesting they affected the same gene. The *mig-21* gene, which was previously shown to affect Q descendant migrations (Du and Chalfie, 2001; Middelkoop et al., 2012), resides on linkage group III. *mig-21(u787)* failed to complement *lq37, lq78*, and *lq84* for AQR and PQR migration defects (data not shown), indicating that these mutations were new alleles of *mig-21*.

mig-21 corresponds to the F01F1.13 gene in Wormbase (Middelkoop et al., 2012). To confirm the *mig-21* locus structure, we sequenced transcripts from early L1 animals using next generation sequencing (RNA seq) (see Materials and Methods). From these reads (Figure 2.S1) and from cDNAs reported on Wormbase, a *mig-21* gene structure was determined as depicted in Figures 2.S1 and 2.S2. The 3' end (exons 2-5) was identical to that reported by (Middelkoop et al., 2012). The first exon defined by RNA seq in our prediction differed from the first exon of the model (Figure 2.S1), which is upstream and non-overlapping with our first exon. The initiator ATG in the (Middelkoop et al., 2012) model is 167 bp upstream of our predicted ATG. No RNA seq reads aligned to this 167 bp upstream exon region (Figure 2.S1), indicating that it is not actively transcribed and is not an exon of *mig-21*. A transcript with our predicted structure could be produced by transgenes described in (Middelkoop et al., 2012), as these included our entire predicted region as well as the 167 bp upstream sequence.

The *mig-21* locus described here can encode a 313-residue type I transmembrane molecule with an N-terminal signal sequence, two predicted extracellular thrombospondin type I domains, a transmembrane domain, and a short cytoplasmic tail with no obvious similarity to other molecules (Figure 2.1 and Figure 2.S2). This MIG-21 molecule contained a predicted N-terminal signal

sequence not found in the (Middelkoop et al., 2012) prediction, supporting the accuracy of exon 1 in our gene model.

Sequencing of the *mig-21* gene from *lq37, lq78*, and *lq84* revealed nucleotide lesions associated with each allele (Figure 2.S1 and Figure 2.1). *lq37* contained a G to A transition resulting in a missense cysteine to phenylalanine change in the first thrombospondin type I domain. *lq78* showed a G to A transition resulting in a glycine to glutamic acid missense change in an unconserved region of the predicted extracellular domain, and *lq84* harbored a G to A transition in the 3' splice site of the fourth intron. The previously characterized *mig-21(u787)* mutation is G to A transition resulting in a premature stop codon (tryptophan 65).

MIG-21 controls AQR and PQR migration. Our *mig-21* results reported here with the Q cell descendants AQR and PQR migration are similar to those reported in (Middelkoop et al., 2012), who used the position of the QL.pax and QR.pax neurons (SDQL/R, AVM, and PVM) also derived from QL and QR. AQR and PQR were visualized with a *gcy-32::cfp* transgene described previously (Chapman et al., 2008). In wild-type, the QR descendant AQR on the right migrates anteriorly to the anterior deirid ganglion, and the QL descendant PQR on the left migrates posteriorly to the phasmid ganglion in the tail (Figure 2.2A, B and C). We found that mutations in *mig-21* caused directional defects in both AQR and PQR migration, with PQR affected more strongly (Figures 2.2 and 2.3). PQR sometimes migrated anteriorly, and AQR sometimes migrated posteriorly. *mig-21(u787)*, a predicted premature stop codon, was consistently the strongest allele, especially in AQR migration, and is likely a null (Figure 2.3). The other alleles *lq37*, *lq78*, and *lq84* might be hypomorphic alleles. A transgene harboring a wild-type copy of the *mig-21* locus (see Materials and Methods) rescued the AQR and PQR migration defects of *mig-21(u787)* (Figure 2.3). These results indicate that MIG-21 is involved in determining the direction of AQR and PQR migration.

MIG-21 controls early Q neuroblast migration. Previous results suggested that defects in AQR and PQR migration could be due to earlier defects in the protrusion and migration of the Q neuroblasts from which AQR and PQR are derived (Chapman et al., 2008; Dyer et al., 2010). We analyzed early Q cell protrusion and migration using the *scm::GFP::CAAX* reporter gene described previously (Chapman et al., 2008; Dyer et al., 2010). At 1-1.5 h post hatching, protrusions starts as small filopodial structures that later become large protrusions at 2-2.5h after hatching (Figure 2.4A, B, and C). QR protrudes anteriorly over the V4 seam cell and QL protrudes posteriorly over V5. At 3-3.5h hours after hatching, the Q cell bodies migrate to reside atop V4 (for QR) and V5 (for QL) (Figure 2.4A, D and E). At 4-4.5h hours after hatching, the Q cells undergo their first division atop the respective seam cells (Figure 2.4A, F and G).

mig-21(u787) and *mig-21(lq37)* mutants displayed defects in the direction of Q neuroblast protrusion (Figure 2.5A and B), similar to results observed previously (Middelkoop et al., 2012). QR sometimes protruded and migrated posteriorly, and QL sometimes protruded and migrated anteriorly. Directional protrusion defects were noted at the first sign of protrusion, suggesting that MIG-21 affects the initial decision about direction of protrusion. We also noted that some protrusions were shorter compared with wild-type. *mig-21* Q cell bodies also migrated in the wrong direction and divided atop the incorrect seam cell; QR sometimes migrated posteriorly and divided over V5, and QL sometimes migrated posteriorly and divided over V4. In some cases MIG-21 Q cells failed to migrate (Figure 2.5F) and divided between the V4 and V5 cells or on their posterior or anterior edges, respectively.

Defects in *mig-21* at the stage of division (4-4.5h after hatching) are quantified in Figure 2.6. QL migration was essentially randomized in both *mig-21(u787)* and *mig-21(lq37)*, and QR was less severely affected. These data are consistent with (Middelkoop et al., 2012). We also quantified initial protrusion at 2-2.5 h and migration at 3-3.5 h, and similar trends were observed (data not shown).

UNC-40/DCC controls early Q neuroblast migration. Previous studies have shown that the immunoglobulin superfamily receptor molecule UNC-40/Deleted in Colorectal Cancer controls early Q neuroblast protrusion (Honigberg and Kenyon, 2000; Middelkoop et al., 2012). We found similar results using the *scm::GFP::CAAX* reporter to visualize the Q cells (Chapman et al., 2008). In *unc-40* mutants, Q cells often initially protruded and migrated in the wrong direction and failed to migrate fully atop the seam cells before dividing (Figures 2.5E and Figure 2.6). While similar to *mig-21,* the penetrance of the *unc-40(n324)* and *unc-40(e1430)* phenotypes were consistently lower than those of *mig-21(u787)* and *mig-21(lq37)*.

unc-40 also displayed defects in AQR and PQR direction and extent of migration (Figure 2.3). PQR was more strongly affected than AQR, and the defects were less penetrant than those in *mig-21*. PQR migration defects were significantly less severe in *unc-40(e1430)* compared to *unc-40(n324)*, suggesting that *unc-40(e1430)* might retain some function, although AQR migration and QL/QR migration were not significantly different between *unc-40(e1430)* and *unc-40(n324)*. A third *unc-40* allele, *e271*, caused defects similar to *unc-40(n324)* that were significantly more severe than *unc-40(e1430)* (Figure 2.3). Furthermore, the *n324/e1430 trans*-heterozygote resembled *n324* alone (Figure 2.3). Together, these data suggest that *unc-40(e1430)* is a hypomorph, although it is also possible that *unc-40(e1430)* carries a linked recessive suppressor mutation not found in the other strains.

PTP-3/LAR controls early Q neuroblast migration. To identify other molecules with roles in Q migration similar to MIG-21 and UNC-40, we assayed mutants that had been shown previously to affect Q descendant migrations. *qid-5(mu245)* (Ch'ng et al., 2003) was shown to affect the placement of the AVM and PVM Q descendants. We found that *qid-5(mu245)* also affected AQR and PQR direction and extent of migration similar to *unc-40* and *mig-21*. We used next generation sequencing to determine the genome sequence of a *qid-5(mu245)* strain (see

Materials and Methods). *qid-5(mu245)* had been previously mapped to region of linkage group II (Ch'ng et al., 2003), and in this region of the genome we discovered a premature stop codon in the *ptp-3* gene. *ptp-3* had been shown previously to affect Q and descendant migrations (Williams 2003), and we found that *qid-5(mu245)* failed to complement *ptp-3(mu256)* for AQR and PQR migration (data not shown).

The previously-described *ptp-3(mu256)* allele is a single nucleotide insertion in the coding region for the first phosphatase domain (Figure 2.1 and Figure 2.S3) (Ackley et al., 2005). *ptp-3(mu245)* introduces a TCA/serine to TAA premature stop at codon 905 in the *ptp-3A* open reading frame and is predicted to affect all known *ptp-3* transcripts except the shortest, *ptp-3C* (Figure 2.1 and Figure 2.S3). As described below, the *ptp-3B* transcript is the relevant transcript for Q cell migration. *ptp-3B* encodes an isoform of a LAR receptor tyrosine phosphatase-like molecule, and consists of an extracellular domain with two fibronectin III repeats, a transmembrane domain, and an intracellular domain with two tyrosine phosphatase domains (Figure 2.1) (Harrington et al., 2002).

Both *ptp-3(mu245)* and *ptp-3(mu256)* caused defects in AQR and PQR migration that resembled *mig-21* and *unc-40* (Figure 2.3). *ptp-3(mu256)* was shown previously to affect early Q direction and extent of protrusion (Williams 2003), and we found that *ptp-3(mu245)* also affected initial Q direction of protrusion and migration similar to *unc-40* and *mig-21* (Figure 2.6). The *ptp-3(ok244)* deletion allele affects only a subset of *ptp-3* predicted transcripts with extended 5' exons (*ptp-3A, D,* and *E*; Wormbase). *ptp-3(ok244)* caused no defects in AQR or PQR migration (Figure 2.3) or in early Q neuroblast protrusion and migration (data not shown), suggesting that the *ptp-3A,D,E* products are not involved in Q migrations. The *ptp-3B* transcript is the only known transcript affected by *mu245* and not affected by *ok244* (Figure 2.S3), suggesting that *ptp-3B* is the relevant isoform in Q and descendant migrations. As shown below, a *ptp-3B* transgene rescued *ptp-3(mu256)*, consistent with this notion.

ptp-3(mu245) displayed significantly more posteriorly directed QR cells and AQR neurons and anterior QL migration than *ptp-3(mu256)* (Figures 2.3 and

2.6), suggesting that *ptp-3(mu245)* might be a stronger loss of function allele than *ptp-3(mu256)* and might be a null for the affected isoforms, including *ptp-3B*. While *unc-40, ptp-3,* and *mig-21* mutations all affected Q and descendant migrations in a similar manner, *mig-21* and *ptp-3* mutants generally had stronger effects than *unc-40* mutants.

MIG-21 and UNC-40 act redundantly in posterior QL migration. *mig-21* and *unc-40* mutations both displayed defects in QL posterior protrusion and migration, with some QL cells protruding and migrating to the anterior. *mig-21(u787); unc-40(n324)* double mutants had QL migration defects that were significantly and synergistically more severe than either mutant alone (Figure 2.6). This phenotypic synergy suggests that UNC-40 and MIG-21 normally act redundantly to control QL posterior migration. These results are consistent with (Middelkoop et al., 2012), who also found that MIG-21 and UNC-40 redundantly control posterior QL protrusion. The *unc-40(e1430); mig-21(u787)* defects were not significantly different from *mig-21(u787)* alone (Figure 2.6), supporting the idea that *unc-40(e1430)* is a hypomorph.

PQR migration was also significantly more severely affected in double mutants of two distinct *unc-40 and mig-21* alleles than the single mutants alone (Figure 2.7). In *unc-40(n324); mig-21(u787)* doubles, the putative double null, only 2% of PQR neurons migrated posteriorly. These results indicate that UNC-40 and MIG-21 redundantly control posterior protrusion and migration of QL and posterior migration of PQR.

Anterior QR migration is regulated through mutual antagonism of MIG-21 and UNC-40. *mig-21* and *unc-40* mutants both displayed abnormal posterior protrusion and migration of QR, which normally migrates anteriorly (Figure 2.6). Surprisingly, *unc-40; mig-21* double mutants displayed significantly reduced posterior QR protrusion and migration compared to either single mutant alone (Figure 2.6). In fact, in no *unc-40; mig-21* double mutant scored did we observe a QR that had migrated posteriorly. These data suggest that wild-type UNC-40

activity was required for posterior QR migration in *mig-21* mutants, and that wild-type MIG-21 activity was required for posterior QR migration in *unc-40* mutants. These results imply that in QR, MIG-21 and UNC-40 might normally inhibit the other's role in posterior migration, resulting in the normal anterior migration of QR. When either MIG-21 or UNC-40 are missing, the other is free to drive posterior protrusion and migration.

A similar trend was observed in AQR migration, as significantly fewer AQRs migrated posteriorly in the *unc-40; mig-21* double mutants compared to *mig-21* alone (Figure 2.7). The exception was the *unc-40(e1430); mig-21(lq37)* combination, which was not significantly different from *mig-21(lq37)* alone, again suggesting that *unc-40(e1430)* is a hypomorph.

In sum, these experiments indicate that MIG-21 and UNC-40 are required for posterior Q cell and descendant migration. In QL, MIG-21 and UNC-40 act redundantly to drive posterior protrusion and migration. In QR, MIG-21 and UNC-40 might reciprocally inhibit each other, allowing anterior protrusion and migration. In other words, mutation of one revealed a latent ability of QR to protrude and migrate posteriorly that was dependent on the other.

PTP-3 acts redundantly with UNC-40 in QL, similar to MIG-21. We found that the *unc-40(n324); ptp-3(mu256)* double mutant resulted in embryonic lethality (data not shown), and we were unable to score Q cells and descendants in these mutants. To circumvent this lethality, we used a transgenic RNAi approach to knock down *unc-40* and *ptp-3* in the seam cells and Q cells based on the approach described in (Esposito et al., 2007) (see Materials and Methods). Plasmids were generated to drive expression of sense and antisense RNA complementary to the *unc-40* and *ptp-3* genes under the control of the seam cell promoter (*scm* promoter), which is active in the seam cells and early Q cells (Chapman et al., 2008; Terns et al., 1997). Animals were made transgenic with a mix of the sense and antisense plasmids, and the resulting transgenes were used in analysis. On their own, *scm::ptp-3(RNAi)* and *scm::unc-40(RNAi)* lines, from hereon called *ptp-3(RNAi)* and *unc-40(RNAi)*, showed no defects in QR or

QL migration (data not shown). However, *unc-40(RNAi); ptp-3(mu256)* and *unc-40(RNAi); ptp-3(mu245)* showed significantly more anterior QL migration compared to *ptp-3(mu256)* and *ptp-3(mu245)* alone (Figure 2.6). PQR migration was similarly affected (Figure 2.7). These results indicate that UNC-40 and PTP-3 act redundantly in QL protrusion and migration. *unc-40(RNAi)* had no effect on its own, indicating that *unc-40(RNAi)* eliminated some, but not all, *unc-40* activity. *ptp-3(RNAi)* also had no effect alone but enhanced the PQR migration defects of *unc-40(n324)* (Figure 2.7). These results indicate that PTP-3 and UNC-40 redundantly control the posterior protrusion and migration of QL and the posterior migration of PQR, similar to MIG-21 and UNC-40.

PTP-3 and UNC-40 display mutual antagonism in QR, similar to MIG-21 and UNC-40. The *unc-40(RNAi); ptp-3(mu245)* double mutant displayed significantly fewer posterior QR and AQR migrations compared to *ptp-3(mu245)* alone (Figure 2.6 and 2.7), suggesting mutual antagonism in posterior QR migration as described for UNC-40 and MIG-21. *unc-40(RNAi)* in the *ptp-3(mu256)* hypomorphic background resulted in fewer posterior QR, but this was not statistically significant. This could be due to the fact that neither *unc-40(RNAi)* nor *ptp-3(mu256)* completely eliminates function of either gene, and the hypomorphic *ptp-3(mu256)* had fewer posterior QR/AQR than the null *ptp-3(mu245)*.

In reciprocal experiments targeting *ptp-3* with RNAi, we found that *ptp-3(RNAi); unc-40(n324)* animals showed no posterior AQR migration compared to 3% for *unc-40(n324)* alone (Figure 2.7). While not statistically significant, this result is consistent with PTP-3 function being required for posterior AQR migration in *unc-40* mutants.

In sum, interactions between *ptp-3* and *unc-40* were similar to those observed between *mig-21* and *unc-40*: redundancy in QL/PQR posterior migration, and mutual suppression of posterior QR/AQR migration.

PTP-3 and MIG-21 act in the same genetic pathway. *ptp-3; mig-21* double mutants showed no significant change in percentages of QL and QR that migrated to the posterior compared to single *mig-21(u787)* mutants, suggesting that they act in the same pathway (Figure 2.6). This is in contrast to *unc-40(n324); mig-21(u787)* double mutants, which strongly synergized in QL, suggesting action in parallel pathways (Figure 2.6). AQR and PQR defects in *mig-21; ptp-3* doubles were also not different from *mig-21* alone (Figure 2.7). The lack of strong genetic enhancement in *mig-21; ptp-3* double mutants indicates that PTP-3 and MIG-21 act in the same pathway in Q migrations.

The triple *unc-40(RNAi); ptp-3(mu245); mig-21(u787);* displayed significantly more QL and PQR defects than *ptp-3(mu245); mig-21(u787)*, indicating redundancy between *unc-40* and *ptp-3/mig-21* (Figure 2.6 and 2.7). Triple mutant *ptp-3(mu245); mig-21(u787); unc-40(RNAi)* QL and PQR defects were not significantly more severe than *unc-40(n324); mig-21(u787)* or *unc-40(RNAi); ptp-3* doubles (Figure 2.6 and 2.7), consistent with MIG-21 and PTP-3 acting in the same pathway in parallel to UNC-40. The *unc-40(RNAi)*; *ptp-3(mu245); mig-21(u787)* triple also displayed significantly fewer posterior QR and AQR migrations than *ptp-3(mu245); mig-21(u787)* (Figure 2.6 and 2.7), indicating mutual antagonism of UNC-40 and PTP-3/MIG-21 in QR and AQR posterior migration.

This genetic analysis indicates UNC-40, MIG-21, and PTP-3 all function to promote posterior Q cell and Q descendant migration. In QL, MIG-21 and PTP-3 act in the same pathway in parallel to UNC-40. In QR, UNC-40 and MIG-21/PTP-3 might define two pathways that mutually antagonize the other's activity in posterior migration, such that anterior migration of these cells can result.

UNC-40, MIG-21, and PTP-3 can act autonomously in the Q cells. We drove the expression of the *unc-40* coding region fused to *green fluorescent protein (gfp)* in the seam cells and Q cells using the *scm* promoter (see Materials and Methods). This construct was expressed in these cells, and UNC-40::GFP accumulated at the cell margins of the seam cells and Q cells (Figure 2.8A).

Furthermore, *Pscm::unc-40::gfp* rescued the AQR and PQR migration defects of *unc-40(n324)* (Figure 2.8D), suggesting that UNC-40 activity in the seam cells and/or Q cells is sufficient for AQR and PQR migration.

We also generated a transgene driving *unc-40* expression in the Q cells and not the seam cells using the *egl-17* promoter (Branda and Stern, 2000; Cordes et al., 2006). At the time of Q cell migration and division in early L1 (0-6 hours post-hatching), the *egl-17* promoter drove *gfp* expression in the Q cells in the posterior, with no detectable expression in other posterior cells (Figure 2.8C and (Middelkoop et al., 2012)). In the anterior, some pharyngeal cells, the M4 pharyngeal neuron, and a cell that might be the head mesodermal cell expressed *egl-17::gfp* (Figure 2.8C). After Q migration and division (6-10 hours post hatching), *egl-17::gfp* expression was detected in the P cells (the vulval precursor cells) in the posterior (data not shown). However, at the time of Q migration, *egl-17::gfp* expression was limited to the Q cells in the posterior.

The *Pegl-17::unc-40* transgene rescued AQR and PQR migration defects of *unc-40(n324)* (Figure 2.8D). As the *egl-17* promoter was active only in Q cells in the posterior at the time of Q migration and division, Q cell expression is the most likely source for *unc-40* rescue. Although non-Q sources cannot be definitively excluded, this result suggests that UNC-40 acts autonomously in the Q cells.

unc-40 RNAi driven by the *scm* promoter enhanced QL/QR and AQR/PQR migration defects of *ptp-3* and *mig-21* (Figure 2.7), suggesting that UNC-40 acts in the seam cells and/or Q cells. However, RNAi can spread from one tissue to another (systemic RNAi) (Tabara et al., 1998), so it is possible that RNAi expressed from the *scm* promoter might spread to other tissues, and that knockdown in other tissues is responsible for AQR and PQR migration defects. The SID-1 protein is required for spreading of RNAi, as SID-1 affects the ability of cells to accumulate extracellular dsRNA molecules (Winston et al., 2002). Previous studies have used transgenic expression of *sid-1* to sensitize neurons to systemic RNAi (Calixto et al., 2010). Here, we test if SID-1 function is required for the effects of cell-specific RNAi expressed by the *scm* promoter. We tested

the efficacy of *unc-40(RNAi)* enhancement of *ptp-3(mu256)* in a *sid-1(pk3321)* background and found that AQR and PQR defects were slightly but not significantly reduced compared to the *sid-1(+)* background (Figure 2.9). Together with rescue of *unc-40* mutants by the *Pscm::unc-40* and *Pegl-17::unc-40* construct, these data indicate that UNC-40 acts in the Q cells in AQR and PQR migration.

MIG-21 expression in the Q cells using the *egl-17* promoter rescued defects, indicating that MIG-21 acts autonomously in the Q cells (Middelkoop et al., 2012). We were unable to obtain cell-specific rescue of *mig-21* with a transgene containing the *scm* promoter driving the *mig-21(+)* coding region fused to *gfp,* nor could we detect GFP expression. The endogenous expression of *mig-21* is transient in the Q neuroblasts at the time that they are extending protrusions (1-2 h after hatching), and diminishes rapidly as the cell bodies migrate (Middelkoop et al., 2012). Possibly, the *Pscm::mig-21::gfp* construct is not expressed at the correct time or level to rescue *mig-21* mutants.

We found that *mig-21* RNAi expressed from the *scm* promoter caused AQR and PQR migration defects (Figure 2.9). Furthermore, *mig-21(RNAi)* significantly enhanced PQR migration defects of *unc-40(n324)*, and *unc-40(n324)* significantly suppressed AQR posterior migration of *mig-21(RNAi)*, similar to *mig-21(u787)* (Figure 2.9). *unc-40(n324); mig-21(RNAi); sid-1(pk3321)* mutant AQR and PQR defects were not significantly different from the *sid-1(+)* background (Figure 2.9), suggesting that *mig-21* knockdown in the seam cells and/or Q cells was causing the defects. This is consistent with previous studies showing cell autonomy of *mig-21* function in the Q cells (Middelkoop et al., 2012).

Similar studies were conducted on *ptp-3*. A transgene containing the endogenous *ptp-3B* gene under its own promoter fused to *gfp* (see Materials and Methods) rescued AQR and PQR migration defects of *ptp-3(mu256)*, as did expression from the *dpy-7* promoter active in all hypodermis including the seam cells and the early Q cells (Gilleard et al., 1997)(Figure 2.8C). Q-cell specific *Pegl-17::ptp-3B* expression also rescued *ptp-3(mu256)* and *ptp-3(mu245)* AQR and PQR migration defects, suggesting autonomy of *ptp-3* function in the Q cells.

However, expression of *ptp-3B::gfp* from the *scm* seam cell promoter did not significantly rescue *ptp-3(mu256)* (Figure 2.8C), despite robust expression of PTP-3B::GFP in the seam and Q cells and cell margin accumulation (Figure 2.8B). Furthermore, *ptp-3* RNAi driven by the *scm* promoter enhanced PQR migration defects of *unc-40(n324)* but the enhancement was abolished in a *sid-1(pk3321)* mutant background (Figure 2.9). That *Pegl-17::ptp-3B* rescued *ptp-3* mutants argues that *ptp-3* can act cell-autonomously, as the *egl-17* promoter was active only in the Q cells in the posterior at the time of initial Q migration (Figure 2.8C). However, expression in other cells driven by the *egl-17* promoter (pharyngeal cells, the M4 neuron, and later P cell expression) cannot be excluded. Lack of rescue by *Pscm::ptp-3B* and *sid-1* sensitivity of *scm* promoter-driven RNAi suggest that *ptp-3* might also have a non-autonomous role in Q cell migration.

2.5 Discussion

Previous results showed that MIG-21 and UNC-40 act redundantly in posterior QL migration (Middelkoop et al., 2012). Our results presented here confirm this finding in QL, and suggest that MIG-21 and UNC-40 might repress each other in posterior QR migration, allowing QR to migrate anteriorly (Figure 2.9). In the *mig-21; unc-40* double null mutant, there was no posterior migration of either QL or QR, consistent with a central role of UNC-40 and MIG-21 in promoting posterior migration. The LAR receptor tyrosine phosphatase PTP-3 has been implicated in Q cell and descendant migration (Williams 2003). We present evidence here that UNC-40 and PTP-3 act redundantly in posterior QL migration, and that MIG-21 and PTP-3 might act in the same pathway in parallel to UNC-40. *unc-40* RNAi knockdown consistently reduced posterior QR migration in *ptp-3*, similar to *unc-40* suppression of this defect in *mig-21*, and *mig-21; ptp-3* double mutants showed posterior QR migration similar to either single alone. Thus, MIG-21 and PTP-3 might act in the same pathway in parallel to UNC-40 in Q migration (Figure 2.10).

The initial protrusion and migration of QL and QR affect the subsequent expression of MAB-5 in the Q descendants and thus their anterior posterior migration (Chapman et al., 2008; Middelkoop et al., 2012). QR is inherently less sensitive than QL to the EGL-20/Wnt signal that activates MAB-5 expression (Whangbo and Kenyon, 1999), and MIG-21 appears to mediate this differential sensitivity (Middelkoop et al., 2012). That AQR and PQR defects generally follow the trend of QL and QR migration defects in these mutants is consistent with this idea that initial Q protrusion and migration affects *mab-5* expression and subsequent Q descendant migration.

MIG-21 and UNC-40 mutual inhibition in QR. We found that *unc-40; mig-21* double mutants displayed no posterior QR migration, in contrast to each single mutant alone, which showed significant QR posterior migration. This result suggests that UNC-40 and MIG-21 can promote posterior migration in QR as in QL, but in QR they mutually repress each other's activity, allowing anterior

migration (Figure 2.10). In a *mig-21* mutant, UNC-40 was free to promote posterior QR migration; and in an *unc-40* mutant, MIG-21 was free to promote posterior QR migration. Thus, QL and QR have an inherently distinct mechanism involving UNC-40, PTP-3, and MIG-21 to control posterior versus anterior migration. In both QL and QR, these three molecules promote posterior migrations. However, in QR, UNC-40 and MIG-21 repress each other's activity, allowing QR to migrate anteriorly. The nature of this inherent difference in UNC-40 and MIG-21 function in QL versus QR is not understood, but it might be that QL and QR express distinct cytoplasmic molecules that govern this differential action, or that there are differences in the extracellular environments on the left versus the right side leading to this effect. There is precedence for differences in QL versus QR, as QR is inherently less sensitive than QL to the EGL-20/Wnt signal that induces MAB-5/Hox expression (Whangbo and Kenyon, 1999) (Middelkoop et al., 2012). Indeed, MIG-21 itself is involved in this differential sensitivity to EGL-20/Wnt, positioning MIG-21 as a key regulator of differential responses in initial Q migrations as well as subsequent MAB-5-dependent Q descendant migrations.

While (Middelkoop et al., 2012) did not address posterior QR migration directly, their data (Figure 6A of Middelkoop et al., 2012) includes posteriorly-directed QR cells in *mig-21(u787)* mutants (~15-30%), with fewer in *unc-40(e1430)*; *mig-21(u787)* (~0-3%), consistent with our results. They also reported posterior AQR migration in *mig-21(u787)*, which was abolished in *unc-40(e1430); mig-21(u787)*, consistent with our results and with their finding that *unc-40(e1430); mig-21(u787)* mutants showed little or no *mab-5* expression due to nearly complete anterior QR and QL migration.

***unc-40; ptp-3* embryonic lethality.** In our genetic analyses, we found that *unc-40; ptp-3* double mutants resulted in embryonic lethality. We did not characterize this lethality here, but *ptp-3* has been shown previously to cause defects in embryonic cell movements in gastrulation resulting in low-penetrance embryonic lethality, and to act redundantly with other signaling molecules (e.g. VAB-

1/Ephrin) in this process (Harrington et al., 2002). Our results indicate that UNC-40 might have a role in gastrulation cell movements in parallel to PTP-3, resulting in embryonic lethality in the double mutant.

Our genetic analysis suggests that *unc-40(e1430)* retains some function and is a hypomorph. PQR migration defects were significantly weaker in *unc-40(e1430)* compared to *unc-40(n324)* and *unc-40(e271),* and an *n324/e1430 trans*-heterozygote was more severe than *unc-40(e1430)* and resembled *unc-40(n324)* and *unc-40(e271)* homozygotes. While there is no evidence of alternative splicing or alternative exon use in *unc-40*, it is possible that this happens at a low frequency that has not been detected molecularly, leading to functional transcripts in the *unc-40(e1430)* background.

PTP-3/LAR controls Q migration. The LAR receptor protein tyrosine phosphatase PTP-3 was previously implicated in Q migration (Ackley et al., 2005; Harrington et al., 2002). We found that *qid-5(mu245)* was a new allele of *ptp-3*. *mu245* was a premature stop codon early in the *ptp-3B* coding region (exon 4) that encodes an extracellular portion of the molecule (Figure 2.1). *mu245* also affects the *ptp-3A, D,* and E isoforms. However, these isoforms are not relevant to Q migration, as *ptp-3(ok244),* a deletion that affects these isoforms but not *ptp-3B*, caused no defects in QL, QR, AQR, or PQR migration. Thus, *ptp-3B* is the relevant isoform if Q migration. One caveat is that the shortest *ptp-3C* isoform is not affected by *mu245* or *ok244*, so it is possible that *ptp-3C* also contributes to Q migration.

ptp-3(mu245) mutants were significantly more severe than *ptp-3(mu256)* mutants in QL and QR migration defects, suggesting that *ptp-3(mu256)* is a hypomorph. *ptp-3(mu256)* is a single nucleotide insertion in the coding region for the first intracellular phosphatase domain (Ackley et al., 2005), and is predicted to cause frame shifts and premature stops in all known *ptp-3* isoforms, including the shortest *ptp-3C*. It is surprising that a frame shift mutation in a region shared by all isoforms might be a hypomorph. One explanation is that the *ptp-3(mu256)* transcript is subject to nonsense-mediated mRNA decay, affecting all isoforms

and functions of the locus. It is also conceivable that the *mu256* insertion is spliced out of some transcripts using cryptic splice sites, or that the intracellular phosphatase domains of PTP-3 are not required for its function in Q migration, and that despite a premature stop codon, some PTP-3 is made in *ptp-3(mu256)* that lacks the intracellular domains. Consistent with these latter possibilities, *ptp-3(mu256)* animals displayed some anti-PTP-3 immunoreactivity using an antiserum against the entire intracellular region, including the region before the *mu256* insertion (Ackley et al., 2005). In photoreceptor axon pathfinding in Drosophila, the catalytic activity of the dLAR phosphatase is not required, but the intracellular domains are still required to serve scaffolding functions (Hofmeyer and Treisman, 2009).

PTP-3 and MIG-21 might act in the same pathway in parallel to UNC-40. Genetic data presented here suggests that MIG-21 and PTP-3 might act in the same pathway in parallel to UNC-40. The *ptp-3(mu245)* phenotype resembled *mig-21(u787)* in severity QR migration defects compared to *unc-40(n324)* (*ptp-3* and *mig-21* had more severe QR and AQR defects than did *unc-40*), and *mig-21* and *ptp-3* behaved in a similar manner in genetic interactions with *unc-40*. In QL, *unc-40* enhanced both *mig-21* and *ptp-3,* but *ptp-3* did not enhance *mig-21.* Furthermore, *unc-40* reduced posterior QR migration in both *mig-21* and *ptp-3*, and QR posterior migration resembled *ptp-3* and *mig-21* alone in the *ptp-3; mig-21* double mutants. Finally, the triple mutant *ptp-3(mu245); mig-21(u787); unc-40(RNAi)* was not significantly different than the *ptp-3(mu245); unc-40(RNAi)* double mutant. Taken together, these data suggest that PTP-3 and MIG-21 might act together in a pathway in parallel to UNC-40.

UNC-40, PTP-3, and MIG-21 can act autonomously in the Q cells. We found that UNC-40::GFP expressed in the Q cells using the *egl-17* promoter rescued AQR and PQR migration defects of *unc-40(n324)* animals. Furthermore, *unc-40(RNAi)* and *mig-21(RNAi)* expressed by the *scm* promoter enhanced AQR and PQR migration defects similar to *unc-40* and *mig-21* alleles and was not sensitive

to *sid-1(pk3321)*. These results suggest that UNC-40 and MIG-21 act autonomously in the in the Q cells.

Rescue of *ptp*-3 mutants by expression of *ptp-3B* from the *egl-17* promoter active in the Q cells argues that *ptp-3* can act autonomously in the Q cells. However, expression in the Q cells and the seam cells by the *scm* promoter did not rescue. Possibly, the timing or levels of *ptp-3B* expression from the *scm* promoter were not conducive to *ptp-3* rescue. It is also possible transgenic PTP-3B expression on the neighboring seam cells might inhibit PTP-3B function in the Q cells, possibly through a homophilic interaction, suggesting a possible non-autonomous role of PTP-3B. The sensitivity of *scm* promoter driven *ptp-3* RNAi to *sid-1(pk3321)* also hints at a possible non-autonomous role of PTP-3. Thus, the *Pegl-17::ptp-3B* rescue experiments argue that *ptp-3* can act autonomously in the Q cells, but *ptp-3* might also have non-autonomous roles as well.

Most known roles of LAR have been shown to be or are presumed to be cell-autonomous (for example, see (Srinivasan et al., 2012; Wang et al., 2012)). Our studies indicate that PTP-3B can act autonomously in the Q cells, possibly as a receptor. However, our data hint that *ptp-3* might also have a non-autonomous role, possibly as a ligand. The transmembrane PTP-3 molecule could play a juxtacrine role, requiring cell-cell contact. It is also possible that the extracellular domain of PTP-3 is cleaved and serves as a diffusible signaling molecule. Indeed, the extracellular domain of mammalian LAR is shed in response to calcium ionophores, phorbol esters, and EGF receptor activity mediated by the alpha-secretase matrix metalloprotease ADAM-17/TACE (Aicher et al., 1997; Haapasalo et al., 2007; Ruhe et al., 2006). These studies show that ectodomain shedding is important for the regulation of the intracellular domain of LAR (an autonomous function), but it is possible that the cleaved ectodomain plays a non-autonomous signaling role.

We envision a mechanism in which UNC-40/DCC, PTP-3/LAR and MIG-21 act as receptors for an extracellular signal that controls Q migration, and that these molecules interact with each other distinctly in QR versus QL (Figure 2.10). Our genetic analysis suggests that PTP-3 and MIG-21 are in the same genetic

pathway in parallel to UNC-40. It is possible that these molecules interact physically as co-receptors in complexes that regulate responses to anterior-posterior guidance cues.

Many genes have been identified that control early Q neuroblast migrations, yet none encode a molecule that acts non-autonomously as a guidance signal. The transmembrane CUB-domain containing molecule MIG-13 non-autonomously guides Q descendants in the anterior-posterior axis, and is present on the commissures of motor axons in an anterior to posterior gradient along the animal (Sym et al., 1999), but MIG-13 does not affect early Q neuroblast migration. Further studies of genes affecting this process might reveal a signaling molecule that controls Q neuroblast migration via the parallel PTP-3/LAR and UNC-40/DCC pathways.

Figure 2.1

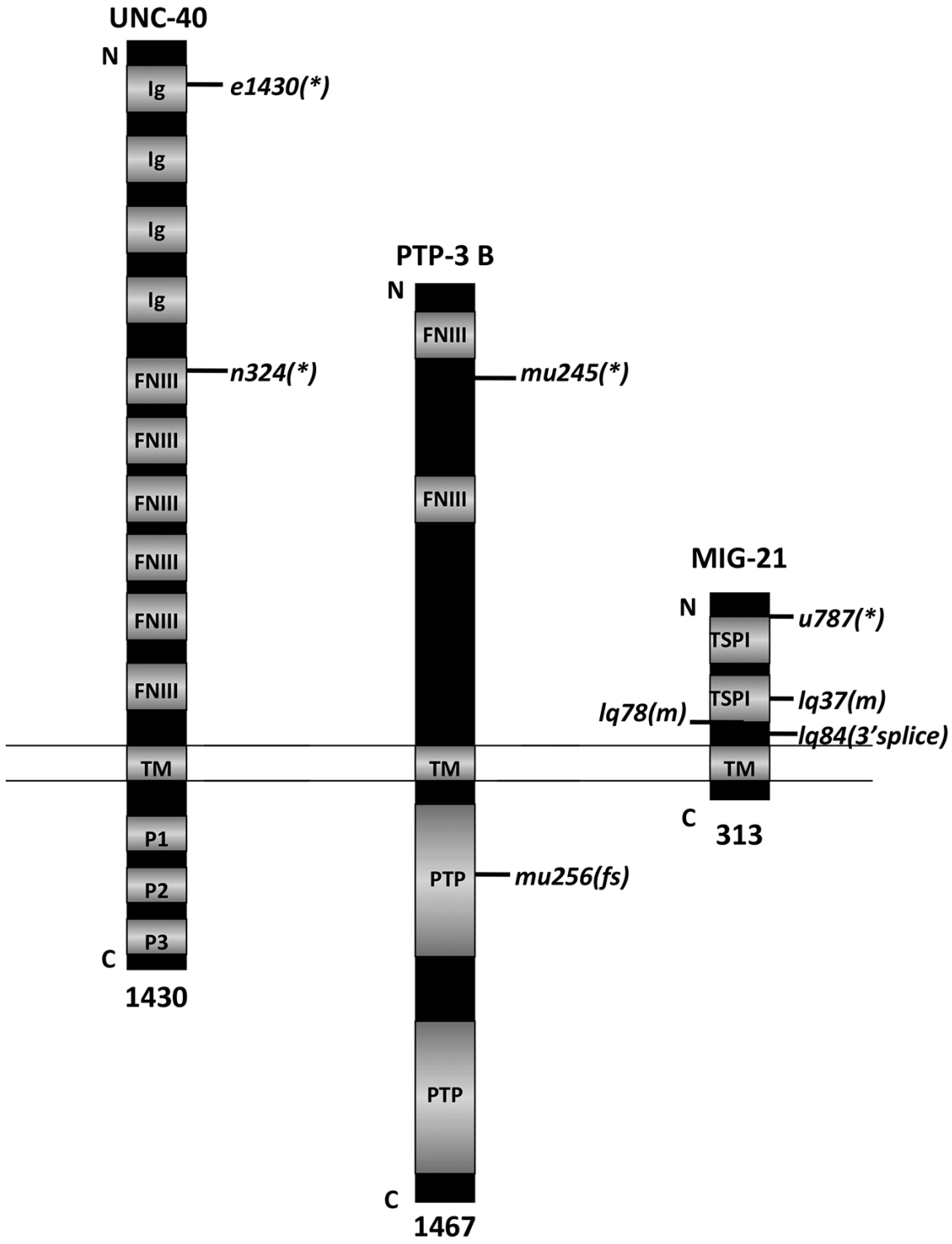
UNC-40
N
Ig
e1430(*)
Ig
Ig
Ig
FNIII
n324(*)
FNIII
FNIII
FNIII
FNIII
FNIII
TM
P1
P2
P3
C
1430
PTP-3 B
N
FNIII
mu245(*)
FNIII
TM
PTP
mu256(fs)
PTP
C
1467
MIG-21
N
u787(*)
TSPI
TSPI
lq37(m)
lq78(m)
lq84(3'splice)
TM
C
313

Figure. 2.1.Three transmembrane molecules affect Q neuroblast protrusion and migration. Diagrams of UNC-40/DCC, PTP-3B/LAR, and MIG-21 are shown. The relative positions of nucleotide lesions associated with each mutation used here are indicated. A "*" indicates a nonsense premature stop codon; an "m" indicates a missense mutation; and a "3' splice" indicates that the mutation affects the 3' splice site at that position in the transcript. Ig = Immunoglobulin I domain; FNIII = fibronectin type III domain; TM = transmembrane domain; P1, P2, P3 = conserved, proline-rich domains; PTP= protein tyrosine phosphatase domain; TSPI = thrombospondin type I domain.

Figure 2.2.

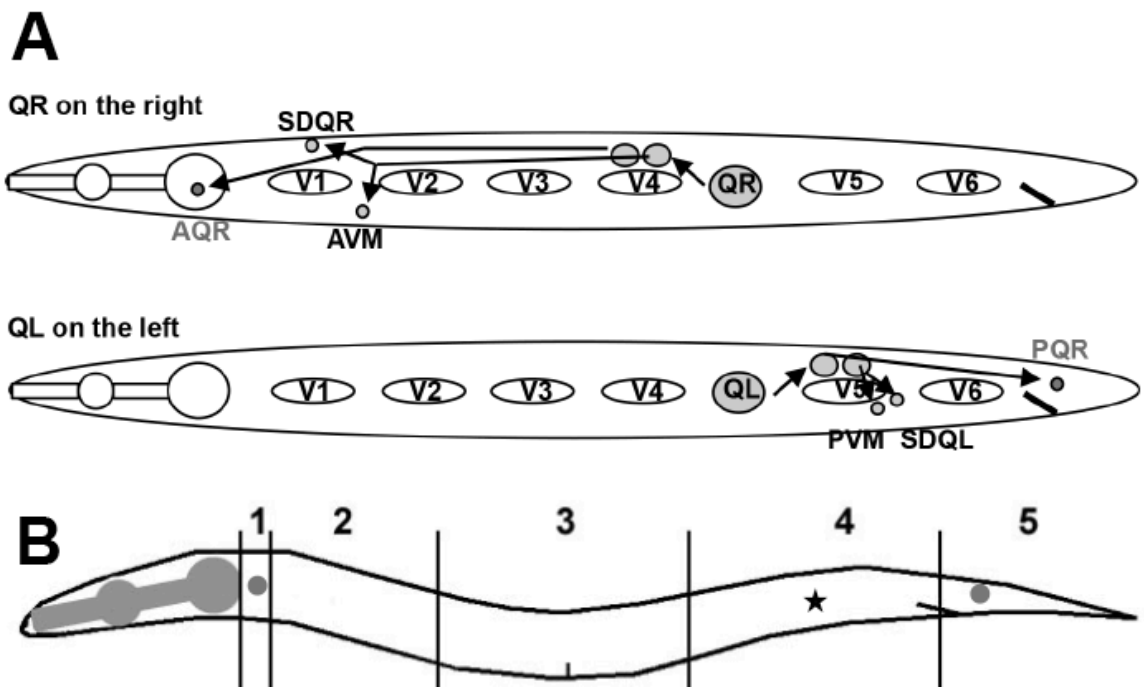
A
QR on the right
SDQR
V1
V2
V3
V4
QR
V5
V6
AQR
AVM
QL on the left
PQR
V1
V2
V3
V4
QL
V5
V6
PVM
SDQL
B
1
2
3
4
5

Figure 2.2.

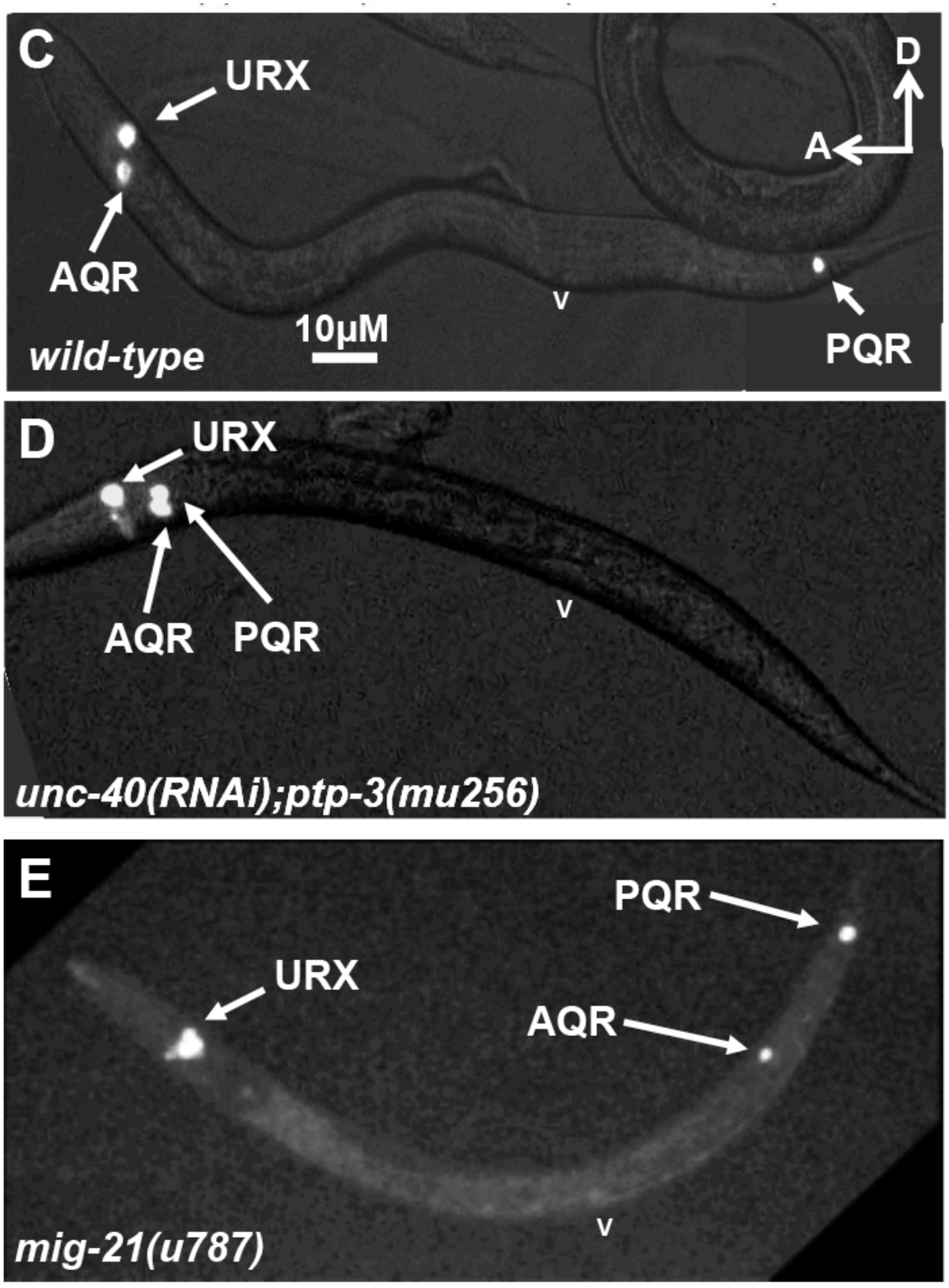
C
URX
D
A
AQR
V
10µM
wild-type
PQR
D
URX
AQR
PQR
V
unc-40(RNAi);ptp-3(mu256)
E
PQR
URX
AQR
V
mig-21(u787)

Figure 2.2. AQR and PQR migration in wild-type and mutants. A) A simplified diagram of QR and QL migrations and divisions that result in three neurons from each. QR on the right migrates anteriorly above V4 and divides, and the daughters continue anterior migrations and divisions to produce three neurons PQR, SDQR, and AVM. QL on the left migrates posteriorly above V5, divides, and, in response to MAB-5 expression, the daughters continue posterior migration and division to produce PQR, SDQL, and PVM. B) A diagram showing the scoring positions used in Figures 2.3, 2.7, 2.8 and 2.9 (see Materials and Methods). Position 1 is the normal final position of AQR near the anterior deirid ganglion, and position 5 is the normal final position of PQR behind the anus in the phasmid ganglion. The asterisk at position 4 represents the approximate birth place of the Q neuroblasts. Position 3 is proximate to the vulva, and position 2 is anterior to the vulva but still posterior to the anterior deirid ganglion. C-E) Fluorescent micrographs of animals expressing *cyan fluorescent protein (cfp)* from the *gcy-32* promoter in AQR, PQR and the URXL/R neurons. A "v" marks the position of the vulva. The scale bar in (C) represents 10μM. In all micrographs, anterior is to the left, and dorsal is up.

Figure 2.3.

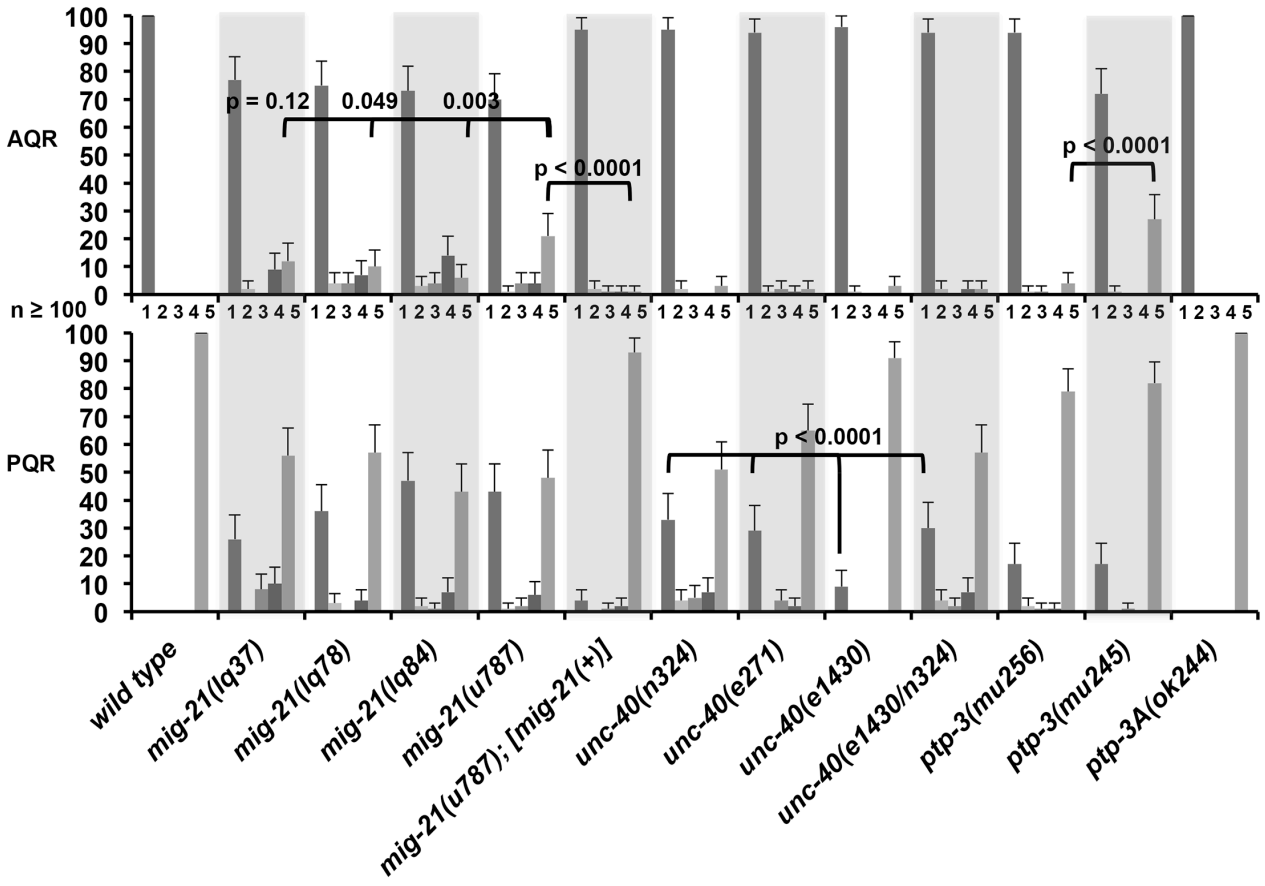
AQR
PQR
n ≥ 100
p = 0.12
0.049
0.003
p < 0.0001
p < 0.0001
p < 0.0001
1 2 3 4 5
wild type
mig-21(lq37)
mig-21(lq78)
mig-21(lq84)
mig-21(u787)
mig-21(u787); [mig-21(+)]
unc-40(n324)
unc-40(e271)
unc-40(e1430)
unc-40(e1430/n324)
ptp-3(mu256)
ptp-3(mu245)
ptp-3A(ok244)

Figure 2.3. AQR and PQR migration defects in single mutants. The X axis of the graph is the genotype, and the Y axis in the percentage of AQR or PQR neurons in each of the 5 positions (1 2 3 4 5) along the anterior-posterior as described in Figure 2 and Materials and Methods. Scale bars represent 2x standard error of the proportion, and significances of difference indicated were determined using the Fisher Exact test. At least 100 animals of each genotype were scored.

Figure 2.4.

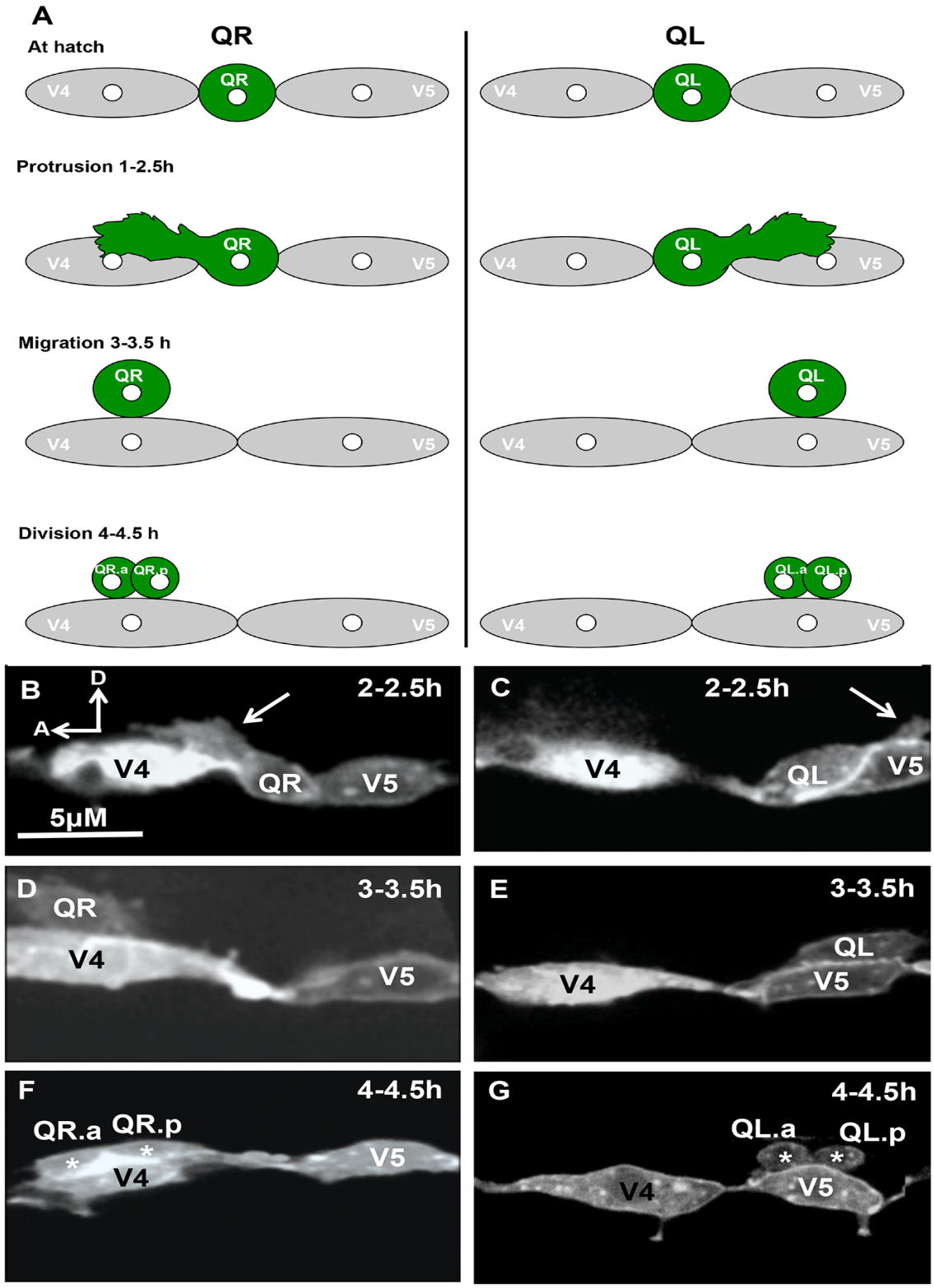
A
At hatch
QR
QL
V4
V5
Protrusion 1-2.5h
Migration 3-3.5 h
Division 4-4.5 h
QR.a
QR.p
QL.a
QL.p
B
D
A
2-2.5h
5µM
C
D
3-3.5h
E
F
4-4.5h
G
*

Figure 2.4. Q neuroblast protrusion and migration in wild-type. (A) A diagram of Q neuroblast protrusion and migration, with times after hatching indicated. (B-G) Micrographs of wild-type Q neuroblasts and seam cells V4 and V5 are shown at different stages scored (see Materials and methods). The *Pscm::gfp::caax* transgene *lqIs80* was used to visualize these cells. In all micrographs, anterior is to the left, and dorsal is up. (B, C) At 2-2.5 h post hatching, QR sent a protrusion anteriorly over V4, and QL posteriorly over V5 (arrows). (D,E) At3-3.5 h, QR had migrated atop V4, and QL had migrated atop V5. (F,G) At 4-4.5 h, QR had divided above V4, and QL atop V5 (daughter cells denoted by asterisks). The scale bar in (A) represents 5μM for each panel.

Figure 2.5.

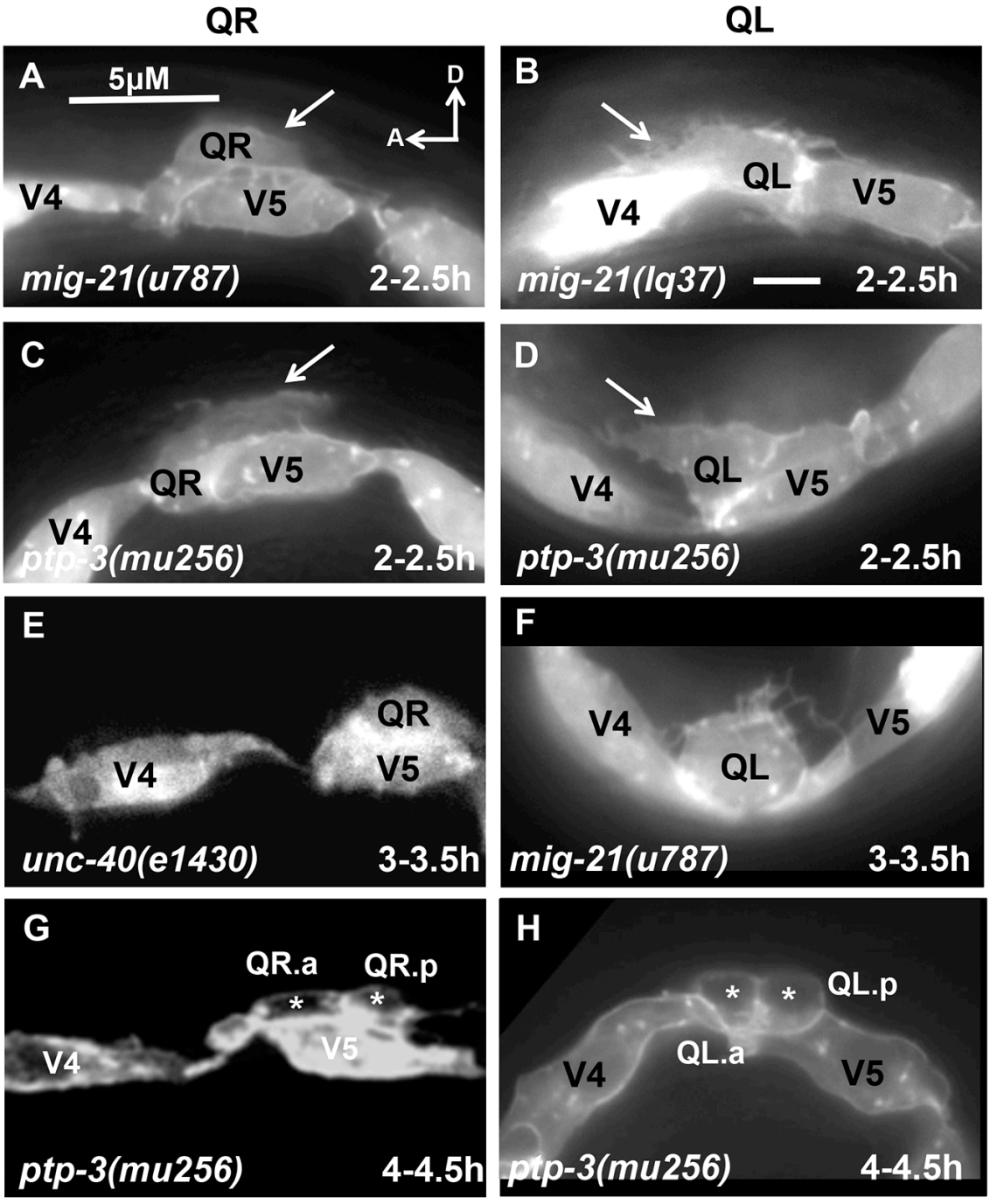
QR
QL
A
5µM
D
A
QR
V4
V5
mig-21(u787)
2-2.5h
B
QL
V4
V5
mig-21(lq37)
2-2.5h
C
QR
V5
V4
ptp-3(mu256)
2-2.5h
D
QL
V4
V5
ptp-3(mu256)
2-2.5h
E
QR
V4
V5
unc-40(e1430)
3-3.5h
F
V4
V5
QL
mig-21(u787)
3-3.5h
G
QR.a
QR.p
V4
V5
ptp-3(mu256)
4-4.5h
H
QL.p
QL.a
V4
V5
ptp-3(mu256)
4-4.5h

Figure 2.5. Q neuroblast polarization and migration in mutants. Images are as described in Figure 4, but in different mutant backgrounds. In all micrographs, anterior is to the left, and dorsal is up. (A-C) Images at 2-2.5 h post hatching. (A) A QR neuroblast protruded to the posterior over V5 in *mig-21(u787)* (arrow points to the protrusion). (B) A QL neuroblast protruded to the anterior over V4 in a *mig-21(lq37)* mutant (arrow). (C) A QR protruded posteriorly over V5 in a *ptp-3(mu256)* mutant. (D) A QL protruded anteriorly (arrow). (E-F) Images at 3-3.5 h post hatching. (E) A QR migrated posteriorly atop the V5 seam cell in an *unc-40(e1430)* mutant. (F) A QL failed to migrate and resided between V4 and V5 in *mig-21(u787)*. (G-H) Images at 4-4.5 h post hatching. (G) A QR had divided atop V5 in *ptp-3(mu256)* (daughter cells denoted by asterisks). (H) A QL divided between V4 and V5 seam cells in *ptp-3(mu256)*.

Figure 2.6.

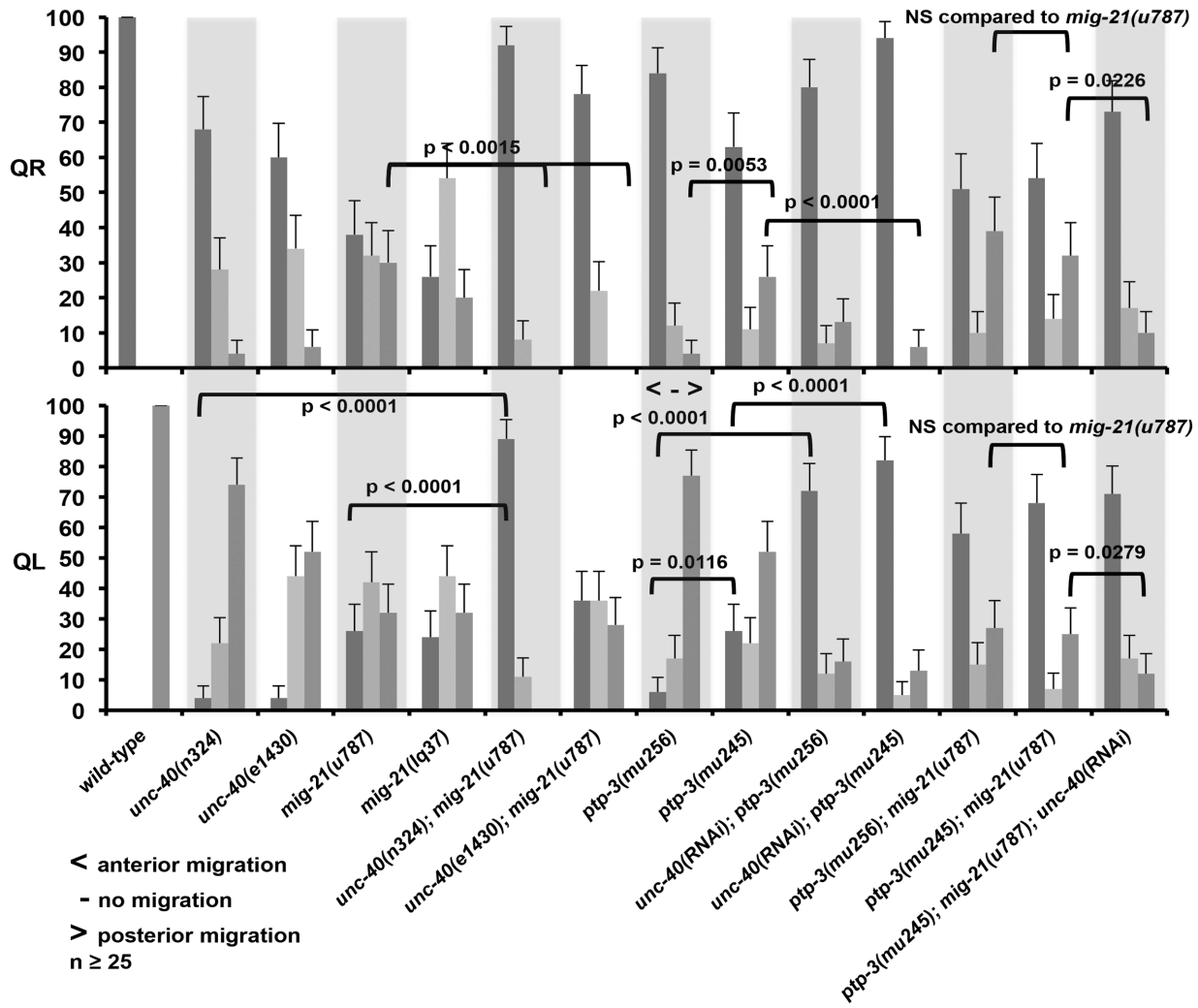
QR
QL
100
90
80
70
60
50
40
30
20
10
0
p < 0.0015
p = 0.0053
p < 0.0001
NS compared to mig-21(u787)
p = 0.0226
p < 0.0001
< - >
p < 0.0001
p < 0.0001
NS compared to mig-21(u787)
p < 0.0001
p = 0.0116
p = 0.0279
wild-type
unc-40(n324)
unc-40(e1430)
mig-21(u787)
mig-21(lq37)
unc-40(n324); mig-21(u787)
unc-40(e1430); mig-21(u787)
ptp-3(mu256)
ptp-3(mu245)
unc-40(RNAi); ptp-3(mu256)
unc-40(RNAi); ptp-3(mu245)
ptp-3(mu256); mig-21(u787)
ptp-3(mu245); mig-21(u787)
ptp-3(mu245); mig-21(u787); unc-40(RNAi)
< anterior migration
- no migration
> posterior migration
n ≥ 25

Figure 2.6. QR and QL migration defects. The graph plots genotype on the X axis against percent of QR and QL at 4-4.5 h post hatching that had divided above V4 (anterior migration; dark grey bars); between V4 and V5 (no migration; light grey bars); and above V5 (posterior migration; medium grey bars). The 2-2.5 h and 3-3.5 h data generally follow the trends seen with the 4-4.5 h division stage data shown here. *unc-40(RNAi)* represents the cell-specific *Pscm::unc-40(RNAi)* transgene. The error bars represent 2x standard error of the proportion, and significances of difference were calculated by Fisher Exact analysis. At least 25 animals were scored for each genotype.

Figure 2.7.

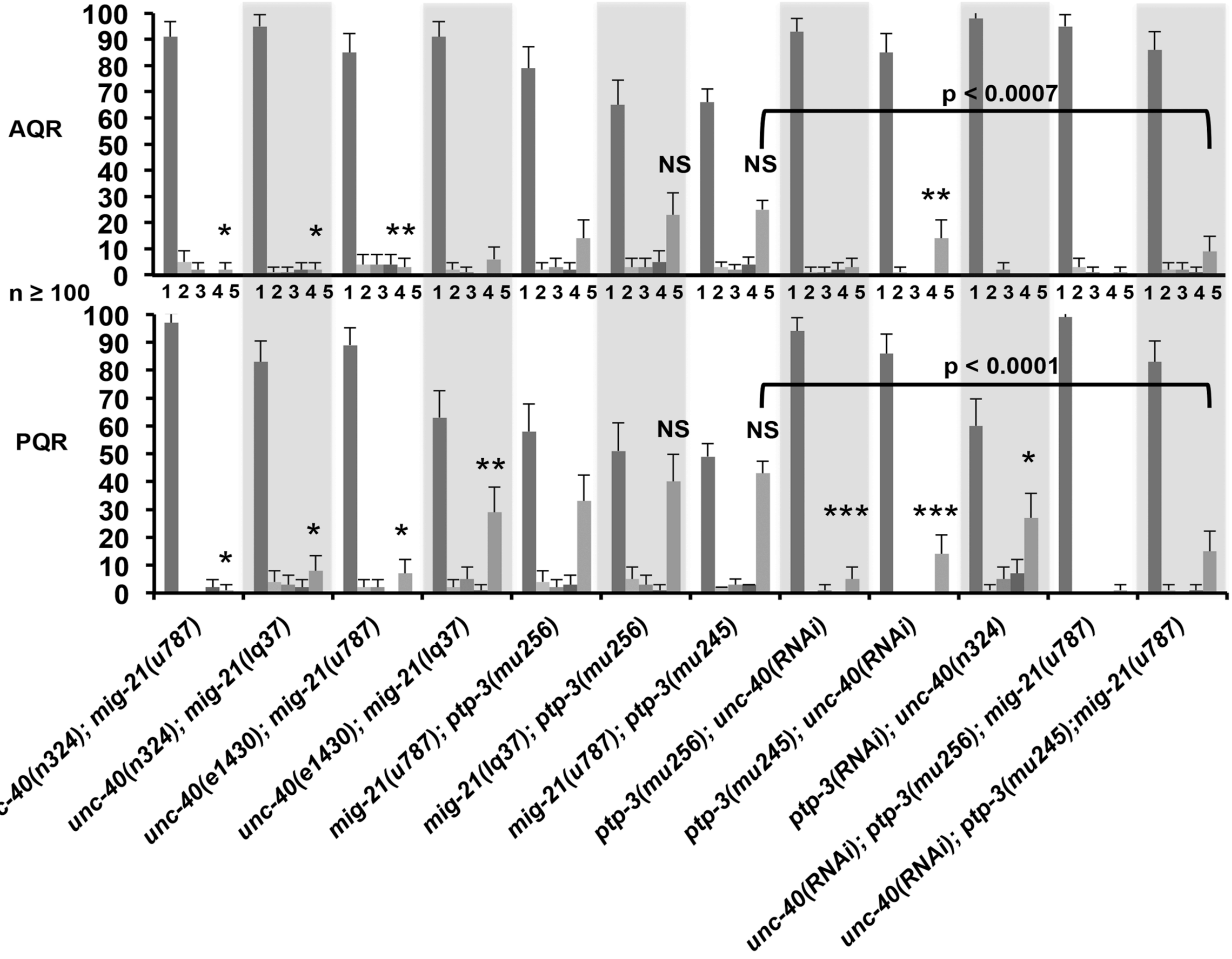
AQR
PQR
n ≥ 100
p < 0.0007
p < 0.0001
NS
*
**
***
unc-40(n324); mig-21(u787)
unc-40(n324); mig-21(lq37)
unc-40(e1430); mig-21(u787)
unc-40(e1430); mig-21(lq37)
mig-21(u787); ptp-3(mu256)
mig-21(lq37); ptp-3(mu256)
mig-21(u787); ptp-3(mu245)
ptp-3(mu256); unc-40(RNAi)
ptp-3(mu245); unc-40(RNAi)
ptp-3(RNAi); unc-40(n324)
unc-40(RNAi); ptp-3(mu256); mig-21(u787)
unc-40(RNAi); ptp-3(mu245);mig-21(u787)

Figure 2.7. AQR and PQR migration in double and triple mutants. Genotypes are listed on the X axis, and the percent of AQR and PQR in the 5 positions along the body axis are shown on the Y axis. The 5 positions (1 2 3 4 5) are described in materials and Methods and Figure 2. Asterisks denote statistical significance compared to single mutant genotypes displayed in Figure 3 as determined by Fisher Exact analysis. The table below describes the significance of each asterisk. Error bars represent 2x standard error of the proportion. At least 100 animals were scored for each genotype.

Figure 2.8.

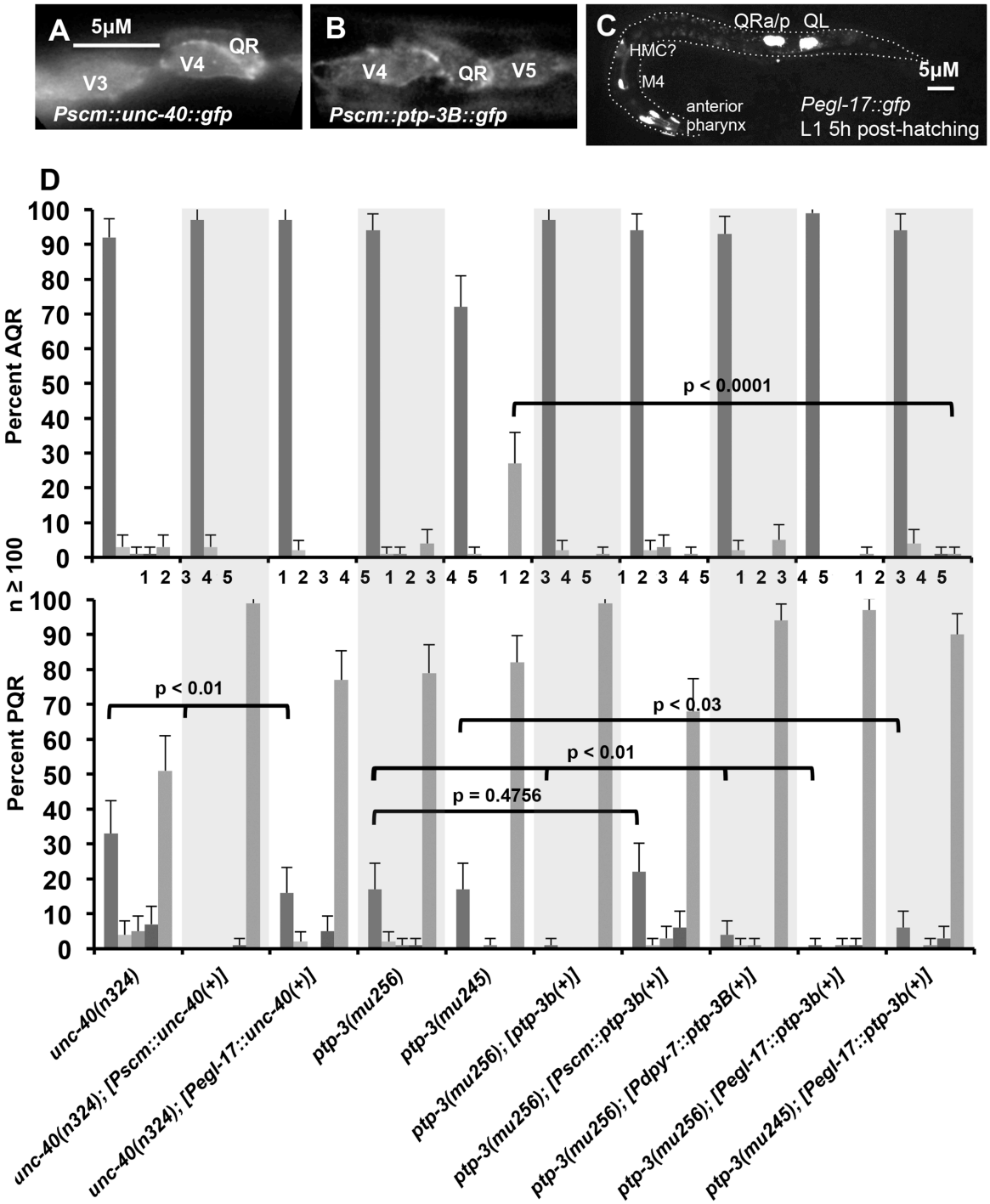
A
5µM
V3
V4
QR
Pscm::unc-40::gfp
B
V4
QR
V5
Pscm::ptp-3B::gfp
C
QRa/p
QL
HMC?
M4
anterior pharynx
5µM
Pegl-17::gfp
L1 5h post-hatching
D
Percent AQR
Percent PQR
n ≥ 100
p < 0.0001
p < 0.01
p < 0.03
p < 0.01
p = 0.4756
unc-40(n324)
unc-40(n324); [Pscm::unc-40(+)]
unc-40(n324); [Pegl-17::unc-40(+)]
ptp-3(mu256)
ptp-3(mu245)
ptp-3(mu256); [ptp-3b(+)]
ptp-3(mu256); [Pscm::ptp-3b(+)]
ptp-3(mu256); [Pdpy-7::ptp-3B(+)]
ptp-3(mu256); [Pegl-17::ptp-3b(+)]
ptp-3(mu245); [Pegl-17::ptp-3b(+)]

Figure 2.8. Rescue of AQR and PQR defects using cell-specific transgenes. In all micrographs, anterior is to the left, and dorsal is up. (A) A micrograph showing UNC-40::GFP expression from the *scm::unc-40::gfp* transgene (*lqIs151)* in seam cells (V3, V4, V5) and QR at 2-2.5h after hatching. UNC-40::GFP accumulated at the cell margins. The scale bar represents 5μM for A and B. (B) Expression of PTP-3B::gfp from the *scm::ptp-3B::gfp* transgene (*lqEx637*) in the seam cells V4 and V5 and QR at 2-2.5 h after hatching. PTP-B::gfp accumulated at cell margins similar to UNC-40::GFP. (C) *Pegl-17::gfp* expression from the *ayIs9* transgene in an early L1 larva 5 hours after hatching. The Q cells have migrated, and QR has divided. In the anterior, expression is observed in some anterior pharyngeal cells, the M4 pharyngeal neuron, and a cell whose position and morphology resemble the head mesodermal cell (HMC). The weak fluorescence along the length of the animal is autofluorescence from the gut. The dashed line indicates the approximate outline of the body of the animal. (D) A graph is shown relating genotypes on the X axis with the percent of AQR and PQR in the 5 positions as described in Materials and Methods and Figure 2. *[Pscm::unc-40(+)]* is the *Pscm promoter::unc-40::gfp* transgene *lqIs151*, shown in (A)*; [ptp-3B(+)]* is the full length *ptp-3B::gfp* under its own promoter (*juIs179)*, and *[Pscm::ptp-3B(+)]* is the *Pscm::ptp-3B::gfp* transgene (*lqEx637*) shown in (B) (see materials and Methods). Statistical significances of difference were determined by Fisher Exact analysis, and error bars represent 2x standard error of the proportion.

Figure 2.9.

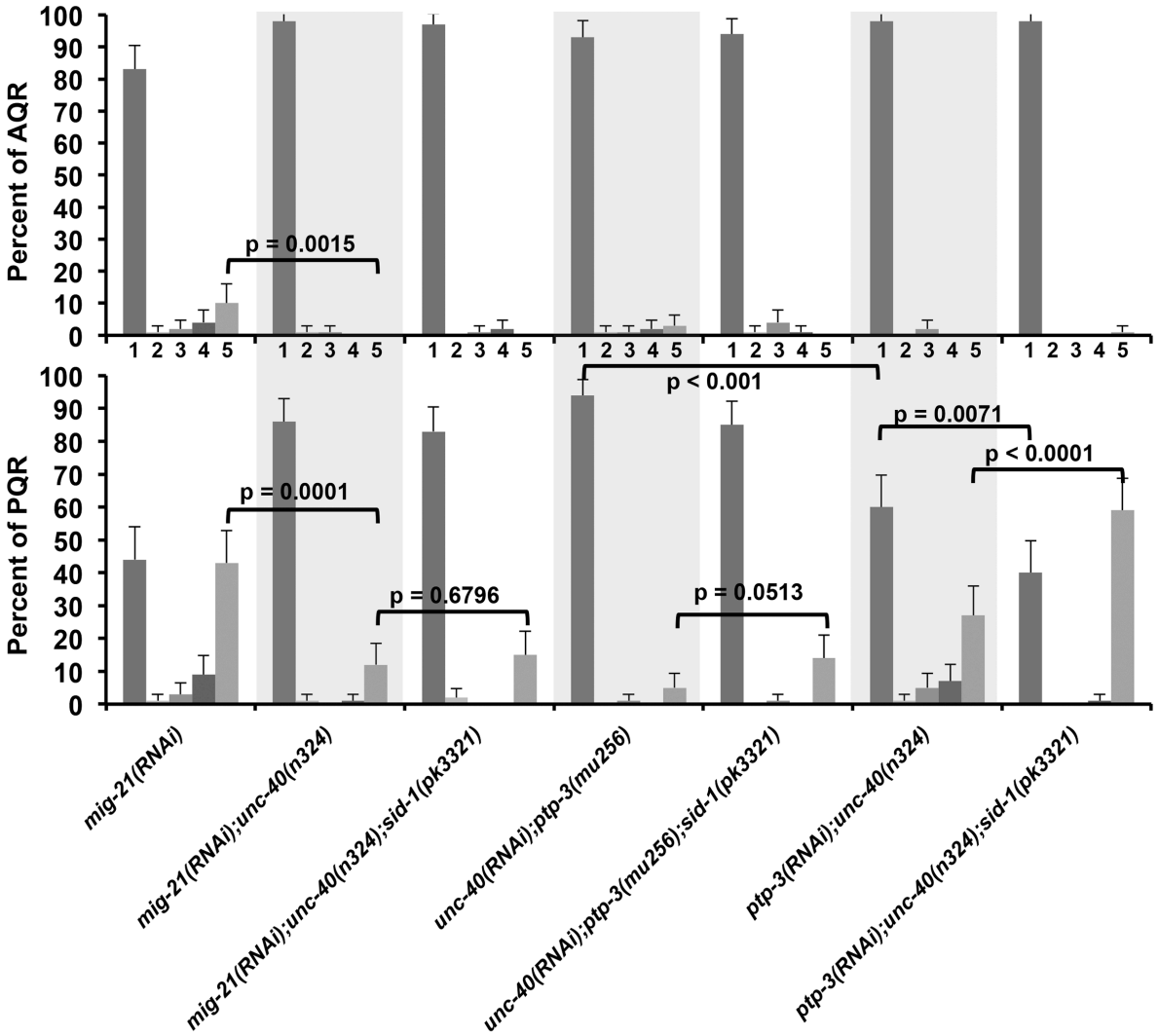
Percent of AQR
Percent of PQR
100
90
80
70
60
50
40
30
20
10
0
1 2 3 4 5
p = 0.0015
p = 0.0001
p = 0.6796
p < 0.001
p = 0.0513
p = 0.0071
p < 0.0001
mig-21(RNAi)
mig-21(RNAi);unc-40(n324)
mig-21(RNAi);unc-40(n324);sid-1(pk3321)
unc-40(RNAi);ptp-3(mu256)
unc-40(RNAi);ptp-3(mu256);sid-1(pk3321)
ptp-3(RNAi);unc-40(n324)
ptp-3(RNAi);unc-40(n324);sid-1(pk3321)

Figure 2.9. Cell autonomous RNAi of *mig-21, unc-40*, and *ptp-3*, and the effects of *sid-1(pk3321)*. The X axis shows genotypes analyzed, and the Y axis shows the percentage of AQR and PQR cells in each of the 5 positions as described in materials and Methods and Figure 2. *mig-21(RNAi)* represents the *scm::mig-21(RNAi)* transgene *lqEx661*; *unc-40(RNAi)* represents the *scm::unc-40(RNAi)* transgene *lqIs146*; and *ptp-3(RNAi)* represents the *scm::ptp-3(RNAi)* transgene *lqIs166* (see materials and Methods). Statistical significances of difference were determined by Fisher Exact analysis, and error bars represent 2x standard error of the proportion.

Figure 2.10.

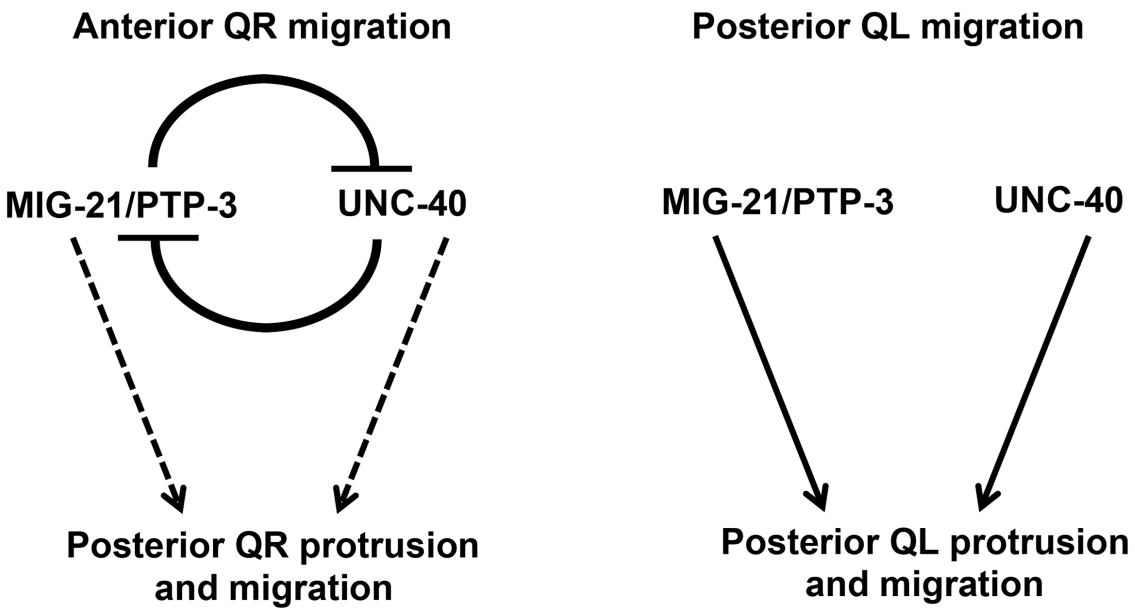
Anterior QR migration
MIG-21/PTP-3
UNC-40
Posterior QR protrusion
and migration
Posterior QL migration
MIG-21/PTP-3
UNC-40
Posterior QL protrusion
and migration

Figure 2.10. A model of MIG-21, UNC-40, and PTP-3 in Q neuroblast protrusion and migration. A) Genetic interactions indicate that MIG-21, UNC-40, and PTP-3 are all required for posterior migration. In QL, which normally protrudes and migrates posteriorly, UNC-40 acts in parallel to a pathway involving MIG-21 and PTP-3, as *unc-40* enhanced both *mig-21* and *ptp-3*, but *mig-21* and *ptp-3* did not significantly enhance each other. In QR, which normally protrudes and migrates anteriorly, UNC-40 and a pathway involving MIG-21 and PTP-3 mutually repress each other in QR posterior protrusion and migration, resulting in anterior protrusion and migration. Mutations in one pathway resulted in posterior QR protrusion and migration that was dependent on the function of the other.

Figure 2.S1.

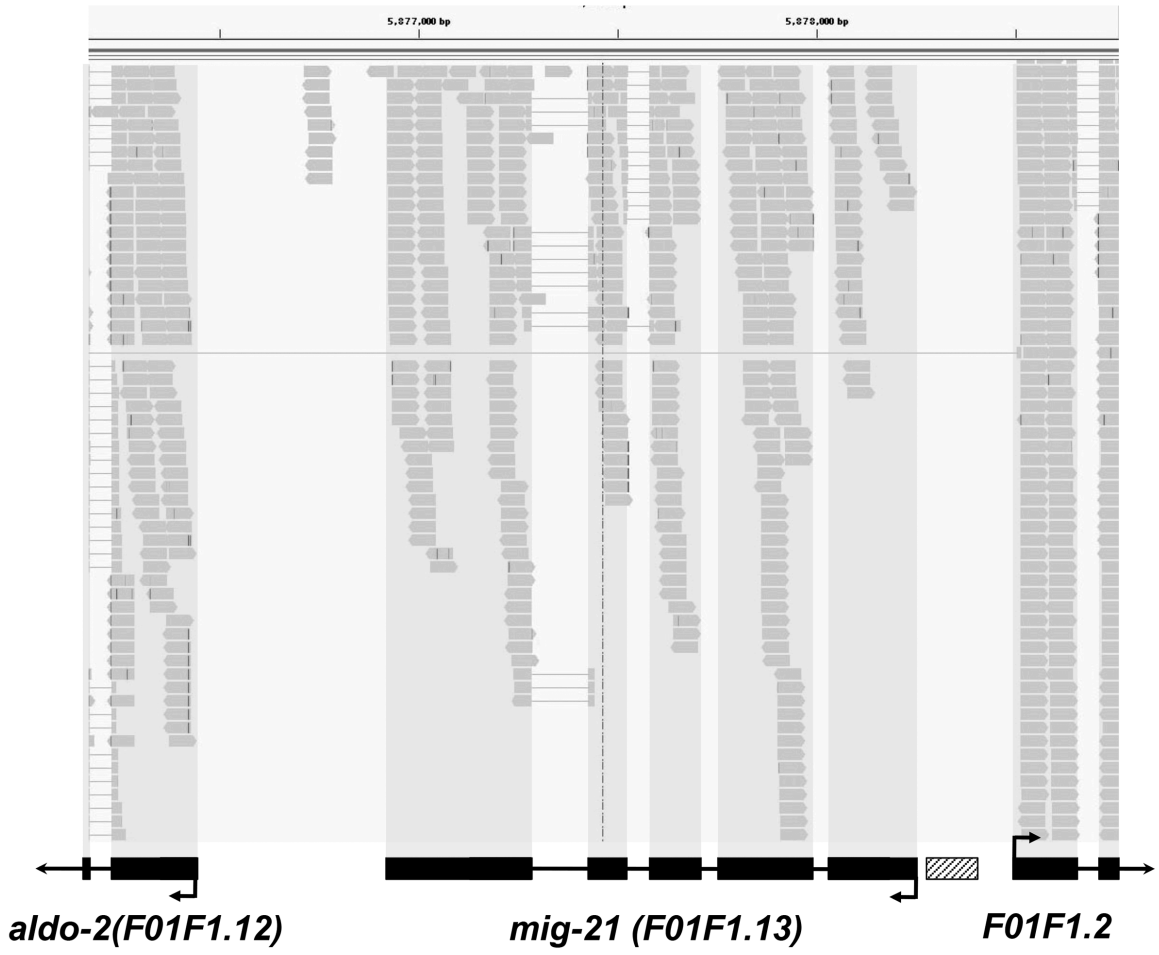

Figure 2.S1. **The *mig-21* locus as defined by RNA seq transcript sequencing.** Shown is output from the Integrated Genome Viewer 2.0.15 program which aligned RNA seq reads (grey bars) from L1 larvae at 5-5.5 h post hatching to the *C. elegans* genome. The *F01F1.13/mig-21* region is shown, as are the flanking genes *F01F1.12/aldo-1* and *F01F1.2*. Read polarity is indicated by a point at the end of each run, and thin lines between reads indicate that the read aligned across a putative intron. The hatched box represents the region of exon 1 predicted in Middelkoop et al., 2012 but that is not represented by reads in this RNA seq analysis.

Figure 2.S2.

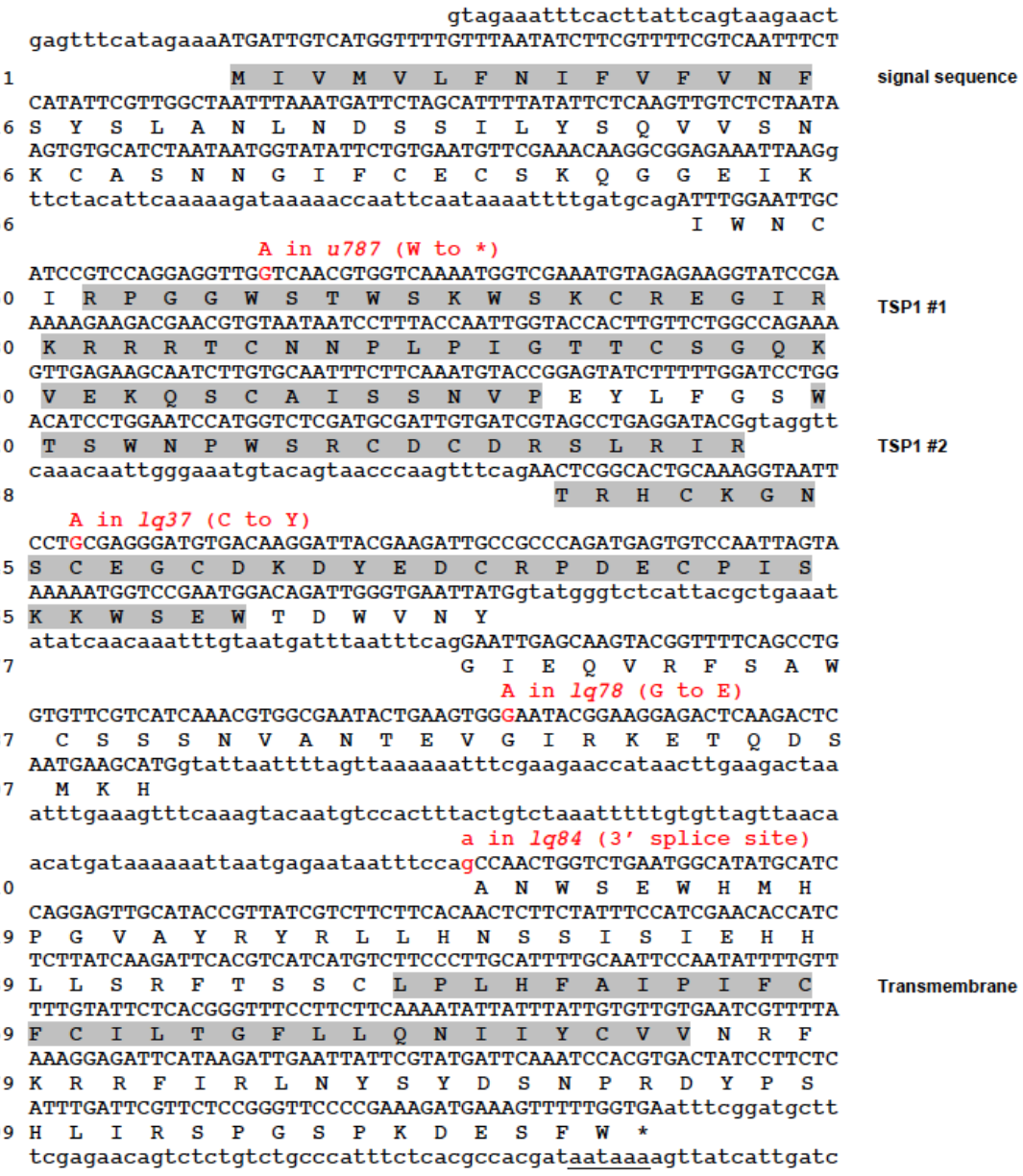
signal sequence
TSP1 #1
TSP1 #2
Transmembrane
A in u787 (W to *)
A in lq37 (C to Y)
A in lq78 (G to E)
a in lq84 (3' splice site)

Figure 2.S2. The *mig-21* coding region. The DNA sequence of the *mig-21* coding region as determined from cDNAs and transcript sequencing runs on Wormbase, and from our RNA seq analysis. The predicted 5' and 3' untranslated regions and introns are lowercase, and the open reading frame is upper case. A putative poly-A site in the 3' UTR is underlined. Nucleotide lesions associated with *mig-21* alleles are shown in red above the DNA sequence. The putative polypeptide encoded by *mig-21* is shown below the DNA sequence. A potential signal sequence, two potential thrombospondin type I domains, and a potential transmembrane domain and highlighted in grey.

Figure 2.S3.

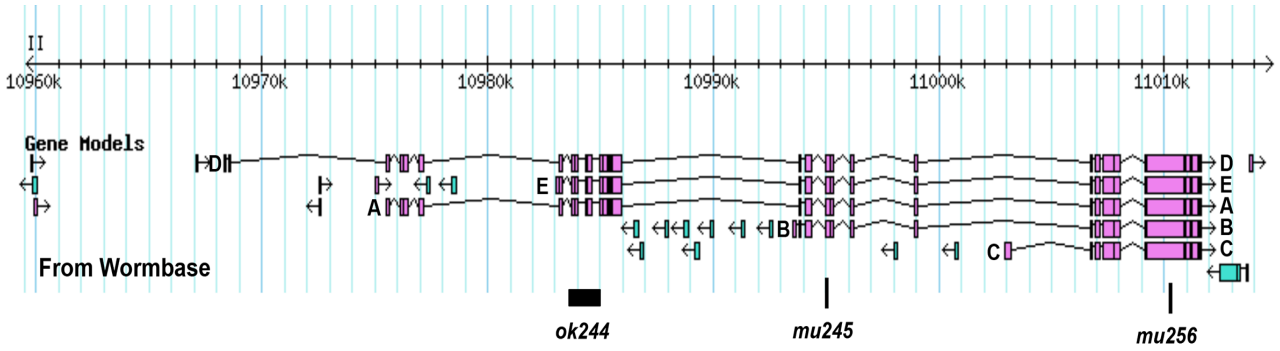

mu245: *ptp*-3B exon 4 A

ACAATCTATGGTTACGCGCACAAGGATATCCGGACTCATATGTCAAGGCGAAGACAGTCGACGGAACCGATCTATCAAC

mu256: *ptp*-3B exon 12 GA

CTGCCACATATGGAGATATCGAGGTGACACTGTTGGAAAGCGTTCATTTGGCTCATTATACGATGAGAACGATGCGATT

Figure 2.S3. The *ptp-3* locus and mutations. A screen shot from Wormbase 229 of the *ptp-3* locus with the A-E isoforms indicated. The sites of *ptp-3* mutations are shown, with the corresponding nucleotide changes above.

Chapter III

The Fat-like Cadherin Acts Cell-Non-Autonomously in Anterior-Posterior Neuroblast Migration

3.1 Abstract

Directed migration of neurons is critical in the normal and pathological development of the brain and central nervous system. In *C. elegans*, the bilateral Q neuroblasts, QR on the right and QL on the left, migrate anteriorly and posteriorly, respectively. Initial protrusion and migration of the Q neuroblasts is autonomously controlled by the transmembrane proteins UNC-40/DCC, PTP-3/LAR, and MIG-21. As QL migrates posteriorly, it encounters and EGL-20/Wnt signal that induces MAB-5/Hox expression that drives QL descendant posterior migration. QR migrates anteriorly away from EGL-20/Wnt and does not activate MAB-5/Hox, resulting in anterior QR descendant migration. A forward genetic screen for new mutations affecting initial Q migrations identified alleles of *cdh-4*, which caused defects in both QL and QR directional migration similar to *unc-40, ptp-3*, and *mig-21*. Previous studies showed that in QL, PTP-3/LAR and MIG-21 act in a pathway in parallel to UNC-40/DCC to drive posterior QL migration. Here we show genetic evidence that CDH-4 acts in the PTP-3/MIG-21 pathway in parallel to UNC-40/DCC to direct posterior QL migration. In QR, the PTP-3/MIG-21 and UNC-40/DCC pathways mutually inhibit each other, allowing anterior QR migration. We report here that CDH-4 acts in both the PTP-3/MIG-21 and UNC-40/DCC pathways in mutual inhibition in QR, and that CDH-4 acts cell-non-autonomously. Interaction of CDH-4 with UNC-40/DCC in QR but not QL represents an inherent left-right asymmetry in the Q cells, the nature of which is not understood. We conclude that CDH-4 might act as a permissive signal for each Q neuroblast to respond differently to anterior-posterior guidance information based upon inherent left-right asymmetries in the Q neuroblasts.

3.2 Introduction

Directed neuronal migration is of fundamental importance in nervous system development. The Q neuroblasts of *Caenorhabditis elegans* are an established and useful model for understanding the molecular mechanisms of directed neuronal migration. The Q neuroblasts are born embryonically in the posterior lateral region of the worm on the right (QR) and left side (QL), and are the sister cells of the V5 hypodermal seam cells (Chalfie and Sulston, 1981; Sulston and Horvitz, 1977). QR and its descendants migrate anteriorly, and QL and descendants migrate posteriorly. Q migration can be divided into two steps, the first of which involves the protrusion and migration of the Q cells, QR to the anterior over the V4 hypodermal seam cell and QL to the posterior over V5 (Chapman et al., 2008; Honigberg and Kenyon, 2000). The Q cells then undergo their first division. The second stage of migration is regulated by EGL-20/Wnt signaling and the Hox molecule MAB-5 (Chalfie et al., 1983; Eisenmann, 2005; Harris et al., 1996; Herman, 2001; Kenyon, 1986; Korswagen et al., 2000; Salser and Kenyon, 1992; Whangbo and Kenyon, 1999). As QL migrates to the posterior, it encounters an EGL-20/Wnt signal from posterior cells, which through canonical Wnt signaling, activates expression of MAB-5/Hox in QL. QR migrates anteriorly away from the EGL-20/Wnt signal and does not activate MAB-5/Hox. MAB-5/Hox is a determinant for further posterior migration of QL descendants. QR continues anterior migration because it does not express MAB-5/Hox.

Initial Q neuroblast protrusion and migration resembles neuroblast migration in the developing vertebrate central nervous system, which extend leading processes followed by nuclear translocation in a saltatory fashion (reviewed in (Solecki et al., 2006)). At 1-2.5 h after hatching to L1 larvae, QR extends a protrusion anteriorly over V4, and QL posteriorly over V5. At 3-3.5 h post-hatching, the cell bodies follow the protrusions and migrate over the respective seam cells. At 4-4.5 h post hatching, the Q cells divide.

Clues about the molecules that control initial Q neuroblast directed protrusion and migration were first provided by (Honigberg and Kenyon, 2000),

who showed that the Immunoglobulin-superfamily receptor UNC-40, similar to vertebrate Deleted in Colorectal Cancer, DCC, was required for directed protrusion and migration. Subsequent work delineated a group of transmembrane molecules that interact genetically in regulating Q directional migration, including UNC-40/DCC, the LAR receptor protein tyrosine phosphatase PTP-3, and the small thrombospondin type I-repeat containing protein MIG-21 (Honigberg and Kenyon, 2000; Middelkoop et al., 2012; Sundararajan and Lundquist, 2012). Mutations in all three genes cause misdirected QL and QR migrations. In QL, UNC-40/DCC acts redundantly in parallel to MIG-21 and PTP-3 in posterior QL migration (Middelkoop et al., 2012; Sundararajan and Lundquist, 2012). These molecules interact distinctly in QR, as genetic analysis indicates that UNC-40 and PTP-3/MIG-21 mutually inhibit each other's roles in posterior migration, allowing anterior migration of QR (Sundararajan and Lundquist, 2012). Finally, cell autonomy experiments indicate that UNC-40/DCC, PTP-3/LAR, and MIG-21 act autonomously in the Q cells (Sundararajan and Lundquist, 2012), possibly as receptors for extracellular guidance information. Other molecules have been identified that act in cytoplasmic signaling involving Q cell migrations, including the DPY-19 C-mannosyltransferase that glycosylates thrombospondin repeat proteins including MIG-21 (Buettner et al., 2013; Honigberg and Kenyon, 2000), the MIG-15 NIK-family kinase (Chapman et al., 2008), the Rac GTPases CED-10 and MIG-2, and the GTP exchange factors UNC-73/Trio and PIX-1/PIX (Dyer et al., 2010). These molecules might act downstream of receptor signals to regulate cellular and or cytoskeletal polarity in initial Q migrations.

To identify genes that interact with *unc-40*, *ptp-3* and *mig-21* in in QR and QL migration, we performed a forward genetic screen for mutations that disrupted both QR and QL directional migration. We isolated three novel mutations in *cdh-4* gene, which encodes a cadherin repeat-containing transmembrane protein most similar to the Fat family of cadherins (Ackley, 2013; Najarro et al., 2012; Schmitz et al., 2008). In *C. elegans*, CDH-4 has been implicated in axon development and cell migration, including migration of Q cell

descendants (Najarro et al., 2012; Schmitz et al., 2008). In *Drosophila*, Fat is thought to coordinate cellular asymmetry generated by the core planar cell polarity pathway components with tissue and organismal polarity in a non-autonomous fashion, and to be distributed asymmetrically across imaginal disc primordia in response to Wnt signaling (Cho and Irvine, 2004; Loveless and Hardin, 2012; Matakatsu and Blair, 2004; Rawls et al., 2002; Strutt and Strutt, 2002, 2005; Tanoue and Takeichi, 2004; Yang et al., 2002).

In *C. elegans*, initial Q cell migration is independent of EGL-20/Wnt and MAB-5/Hox (Chapman et al., 2008), although the initial migration can influence the expression of MAB-5 in the Q descendants (Middelkoop et al., 2012) Furthermore, CDH-4 acts independently of MAB-5/Hox in Q descendant migration (Schmitz et al., 2008). Consistent with Wnt-independence of initial Q migrations and of CDH-4 function, we found that the triple *Wnt* mutant *egl-20 cwn-2; cwn*-1 displayed severe Q descendant migration defects but no initial directional migration defects. To determine if CDH-4 acts with the previously-defined signaling system of UNC-40/DCC, PTP-3/LAR and MIG-21 in directing early Q neuroblast migration, we analyzed double and triple mutants. In QL migration, CDH-4 acted genetically in the PTP-3/LAR pathway in parallel to UNC-40/DCC in posterior migration. In QR migration, CDH-4 acted genetically in both the PTP-3/LAR and UNC-40/DCC pathways in mutual inhibition of posterior migration. Mosaic analysis indicated that CDH-4 acts cell-non-autonomously to control QR and QL migration, possibly providing extracellular information to the Q cells about migration. Our results suggest a differential genetic interaction of CDH-4 with UNC-40/DCC in QL versus QR, acting in parallel in QL and acting with both PTP-3/LAR and UNC-40/DCC in QR in mutual inhibition. The nature of this inherent left-right asymmetry in the Q cells is unknown, but QL and QR display other left-right asymmetries, such as sensitivity to the EGL-20/Wnt signal and to MAB-5/Hox (Middelkoop et al., 2012; Whangbo and Kenyon, 1999). Possibly, an as-yet unidentified molecule that is expressed in QR but not QL mediates CDH-4 interaction with UNC-40/DCC in QR but not QL, thus

establishing the mutual inhibition mechanism between PTP-3/LAR and UNC-40/DCC that allows anterior migration of QR.

2.3 Materials and Methods

***C. elegans* genetics and microscopy**. Experiments were performed at 20° C using standard *C. elegans* techniques (Sulston and Brenner, 1974). The following mutations and transgenics were used: LGI *unc-40(n324), smg-1(e1228), smg-2(e2008)*; LGII *ptp-3(mu256), cwn-1(ok546)*; LGIII *mig-21(u787)*, *cdh-4(lq56)*, *cdh-4(lq83)*, *cdh-4(lq97), cdh-4(rh310)*, *cdh-4(ok1323)*, *cdh-4(hd40)*; LGIV *egl-20(n585)*, *cwn-2(ok895)*, *lqIs80[Pscm::gfp::caax]*; LGV *lqIs58[Pgcy-32::cfp]*. Chromosomal locations for the following transgenes were not assigned: *lqIs146[Pscm::unc-40(RNAi)]*, *lqIs166[Pscm::ptp-3(RNAi)]*, *lqIs249[Pegl-17::mCherry].* Extrachromosomal arrays used were *lhEx397[unc-119; cdh-4(+)::gfp fosmid]*, and *lqEx755[Pgcy-32::yfp; cdh-4::gfp fosmid]*. The extrachromosomal arrays were built using standard gonadal microinjection techniques and were integrated into the genome using UV-TMP techniques (Mello and Fire, 1995). The *cdh-4::gfp* fosmid clone 77167333417072 A06 was obtained from the TransgeneOme project (Sarov et al., 2012). *cdh-4* and *smg-1* feeding RNAi was conducted using the standard RNAi by feeding protocol with bacterial stocks form the “Ahringer” library (Source Bioscience, UK) (Kamath and Ahringer, 2003).

Micrographs were obtained using a Leica DM550 compound microscope with filters for GFP, YFP, CFP, and mCherry and a Qimaging Retiga camera. The micrographs in Figure 3.5 were obtained using a Nikon laser scanning confocal microscope.

Imaging and scoring Q neuroblast defects. Previously described larval synchronization techniques were used (Chapman et al., 2008) (Sundararajan and Lundquist, 2012). Adult and larval animals were washed from plates using M9 buffer. Eggs remained adhered to the agar surface of the plates. Newly-hatched L1 larvae were collected every 30 minutes by washing the plates with M9 and placing the larvae onto fresh NGM plates. These larvae were then visualized at 2, 3 and 4 hours post hatching using a the *Pscm*::*gfp::caax* transgene *lqIs80*. All the wild-type larvae visualized at 2 hours post

synchronization (2-2.5 h timepoint) displayed defined anterior QR protrusions over the seam cell V4 and defined posterior QL protrusions over the seam cell V5. At 3 hours post synchronization (the 3-3.5 h timepoint), QR had migrated anteriorly on V4 and QL posteriorly on V5. At 4 hours post synchronization (4-4.5 h timepoint) QR had divided on V4 and QL on V5. Defects in mutant backgrounds were scored for direction of protrusion, migration and division. QR that protruded, migrated and divided posteriorly on V5 were scored as defective. QL that protruded, migrated and divided anteriorly on V4 were scored as defective. Cells also failed to migrate in *cdh-4* and other mutants, but only directional migration defects were scored and included in Figures 3.3 and 3.4. At least 25 cells were scored for all stages, but only the 4-4.5 h division stage is included in Figures 3.3 and 3.4, as the position of division correlates with defects in protrusion and migration (Sundararajan and Lundquist, 2012). Statistical differences between genotypes were determined by Fisher's exact test.

Scoring and analysis of AQR and PQR defects in Table 1 and Figure 3.7. Previously described quantification methods were used (Sundararajan and Lundquist, 2012) (Chapman et al., 2008). The *gcy-32*::*cfp* transgene *lqIs58* was used to visualize the positions of AQR and PQR in L4 larval animals, well after AQR and PQR undergo their migrations in L1 larvae. The final positions of AQR and PQR were binned into five positions along the body of the worm. Position 1 is the wild-type position of AQR in the anterior deirid ganglion just posterior to the pharyngeal bulb. Position 2 represents the region posterior to the pharyngeal bulb and just anterior to the vulva. Position 3 represents the region around the vulva. Position 4 represents the region posterior to the vulva and anterior to posterior deirid, where the Q cells are born and begin their migrations. Position 5 is the wild-type position of PQR, behind the anus in the phasmid ganglion. To best represent the defects in direction of migration, only the percentage of PQR in position 1 and the percentage of AQR in position 5 were included in Figure 3.7, but Table 1 shows each position. At least 100 worms were scored for each mutant background and all comparisons were done using Fisher's exact test.

Mosaic analysis. The *cdh-4(+)::gfp* fosmid transgene *lqEx755* rescued the defects in AQR and PQR migration observed in a *cdh-4(lq56)* background (Table 3.1 and 3.7). A *Pgcy-32*::*yfp* construct was included with the *cdh-4(+)* extra chromosomal array to visualize the presence and absence of *cdh-4(+)* in AQR, PQR, and URX L/R. During mitotic divisions, extrachromosomal arrays are spontaneously lost from some daughter cells, resulting in genetically mosaic animals. Animals with losses in AQR and PQR were identified by lack of *Pgcy-32::*yfp expression in these cells (Figure 3.6). The strain also carried the stably-integrated *Pgcy-32::cfp* transgene *lqIs58* to mark the positions of AQR in all animals, including those that lost the rescuing *cdh-4(+)* array in AQR and PQR. Animals that lost the rescuing *cdh-4(+)* array in AQR, but retained it in PQR and the URX neurons were scored for AQR position; and those that lost the rescuing *cdh-4(+)* array in PQR, but retained it in AQR and the URX neurons were scored for PQR position (Figure 3.7).

3.4 Results

cdh-4 mutations were identified in a screen for neuronal migration defects

Our earlier work showed that the transmembrane molecules UNC-40/DCC, PTP-3/LAR and MIG-21 act cell-autonomously in a genetic pathway directing anterior-posterior Q neuroblast migrations (Sundararajan and Lundquist, 2012). To identify new genes that could function with *unc-40, ptp-3* and *mig-21*, we performed an ethyl methansulfonate forward genetic screen for new mutations affecting Q migrations (see Materials and Methods), using the positions of Q descendant neurons AQR and PQR. AQR and PQR are descendants of QR and QL, respectively, and make the longest anterior and posterior migrations of Q descendants (Sulston and Horvitz, 1977; White et al., 1986). AQR migrates anteriorly to a position near the anterior deirid just behind the posterior pharyngeal bulb, and PQR migrates into the phasmid ganglion posterior to the anus. Directional migrations of AQR and PQR are disrupted when earlier Q migrations are defective, and defects in AQR and PQR migrations serve as a proxy for earlier defects in Q neuroblast migrations. We focused on new mutations that affected both AQR and PQR directional migration, as do *unc-40, ptp-3*, and *mig-21*. The new mutations *lq56*, *lq83,* and *lq97* were identified (Table 3.1). *lq56* and *lq83* were mapped to linkage group III by single nucleotide polymorphism (snp) mapping against the CB4856 Hawaiian background (Davis et al., 2005). The strains were then subject to whole genome sequencing (see Methods) to identify potential mutations. *lq97* was mapped to LGIII and sequenced using the CloudMap strategy (see Materials and Methods) (Minevich et al., 2012). Each of the three strains carried a novel premature stop codon in the *cdh-4* gene on LGIII (Figure 3.1A). The lesions were confirmed by polymerase chain reaction of the genomic region and Sanger sequencing.

CDH-4 is a member of the Cadherin superfamily most similar to Fat, a transmembrane molecule with multiple extracellular cadherin repeats, EGF-like repeats, and a laminin G domain (Figure 3.1B) (Schmitz et al., 2008). *lq83* was in the second exon, *lq56* was in the eighth exon that codes for the sixth cadherin

repeat, and *lq97* was in penultimate exon eighteen, introducing a premature stop thirty codons upstream of the region coding for the transmembrane domain (Figure 3.1A,B). *lq56* and *lq83* failed to complement each other and the previously identified *cdh-4(hd40)* mutation for AQR and PQR migration (data not shown), and a fosmid transgene harboring a wild-type *cdh-4(+)* gene rescued AQR and PQR migration defects of *lq56* animals (Table 3.1).

Previous studies showed that CDH-4 is required for migration of the Q descendants AVM/PVM and SDQL/R (Schmitz et al., 2008). We found that AQR often migrated posteriorly and PQR often migrated anteriorly in *cdh-4* mutants, including in the previously-characterized alleles *rh310, ok1323*, and *hd40*, and the new alleles *lq56, lq83*, and *lq97* (Table 3.1). The AQR migration defects of *lq97* were significantly less severe than *lq56, lq83, rh310, ok1323,* and *hd40* (Table 3.1), indicating that the *lq97* allele might retain some *cdh-4* function. That the *lq97* premature stop is in the second-to-the-last exon, it is possible that some *lq97* transcripts escape nonsense mediated mRNA decay (Popp and Maquat, 2013) and produce a truncated CDH-4 protein with a signal sequence but no transmembrane domain or cytoplasmic region. This putative truncated protein would be expected to be secreted, and might retain some function, resulting in the less-severe *lq97* phenotype. Double mutants of *lq97* with *smg-1(e1228)* (Grimson et al., 2004) and *smg-2(e2008)* (Johns et al., 2007) mRNA surveillance mutants were lethal, suggesting that in the absence of nonsense-mediated decay, a truncated CDH-4 is produced that results in lethality. *smg-1* feeding RNAi slightly but significantly suppressed PQR migration defects of *lq97* (Table 3.1). Together, these results suggest that *cdh-4(lq97)* might produce a truncated, secreted version of CDH-4 that is functional.

CDH-4 is required for anterior-posterior Q neuroblast migrations

We showed previously that defects in Q descendent AQR and PQR migrations can be due to defects in initial QR and QL protrusions and migrations (Chapman et al., 2008; Dyer et al., 2010; Sundararajan and Lundquist, 2012). We next analyzed the early Q neuroblast migrations in the putative null *cdh-4*

(lq56) and *cdh-4(lq83)* using the *scm::GFP::CAAX* reporter to observe QR and QL migration as described previously (Chapman et al., 2008). In *wild-type*, at 1-2.5 h post hatching, QR and QL extend protrusions anteriorly and posteriorly over seam cells V4 and V5, respectively (Figure 3.2A,E). At 3-3.5 h post hatching, the cell bodies follow the protrusions and migrate over the seam cells. At 4-4.5 h post hatching, the Q cells divide on top of their respective seam cells to produce two daughter cells (Figure 3.2B,F) (Chapman et al., 2008; Dyer et al., 2010; Ou and Vale, 2009; Sundararajan and Lundquist, 2012). In *cdh-4* mutants, we observed directional migration defects and failures to migrate of both QR and QL. Figure 3.2C shows a QR that has migrated posteriorly over V5 at 3-3.5h, and figure 3.2D shows a QR that has divided over V5 at 4-4.5h. Figure 3.2G shows a QL that protruded anteriorly over V4 at 1-2.5 h, and Figure 3.2H a QL that has divided between V4 and V5, but in contact with the anterior V4.

We quantified the extent of QR and QL migration defects by determining the cell position upon division at 4-4.5 h (Figures 3.3 and 3.4). Defects observed at this stage were similar in percentage to defects at the protrusion and migration stages (data not shown) (Sundararajan and Lundquist, 2012). In wild type, no migration defects were observed in QR and QL (Figure 3.3A and 3.4A). In putative null *cdh-4(lq56* and *lq83)* mutants, 42% and 27% of QLs migrated anteriorly and divided over V4 (Figure 3.3A), and 72% and 73% of QRs migrated posteriorly and divided over V5 (Figure 3.4A). These results suggest that CDH-4 is required for directional migration of both QR to the anterior and QL to the posterior. QR posterior migration was greater than 50% in each mutant, suggesting that QR migration was not randomized. Rather, this result suggests that CDH-4 might alter QR's response to A-P guidance information.

cdh-4(lq97) showed significantly reduced AQR migration defects compared to *lq56* and *lq83* (Table 3.1). Early QL and QR migrations were both significantly less severe in *lq97* compared to *lq56* and *lq83* (Figure 3.3A and 3.4A), further indicating that *lq97* might retain function, possibly via the production of a truncated, secreted form of CDH-4.

Fat-like cadherins have been implicated in acting in parallel to Wnt signaling in planar cell polarity (Cho and Irvine, 2004; Loveless and Hardin, 2012; Matakatsu and Blair, 2004; Rawls et al., 2002; Strutt and Strutt, 2002; Tanoue and Takeichi, 2004; Yang et al., 2002). EGL-20/Wnt, which controls Q descendant migrations including PQR to the posterior, showed no early Q migration defects (Chapman et al., 2008). The five *C. elegans* Wnts act in a complex and redundant fashion in guiding Q descendants (Zinovyeva et al., 2008). The triple mutant *cwn-1; egl-20 cwn-2* displayed extensive defects in the migrations of AQR and PQR (Table 3.1) but showed no apparent defects in early QL or QR migrations (n = 10; data not shown). While we cannot rule out a role of Wnt in early Q protrusion and migration, these results are consistent with a Wnt-independent role of CDH-4 in early Q protrusion and migration.

CDH-4 acts genetically in the PTP-3/LAR pathway, in parallel to UNC-40/DCC, in posterior QL migration.

Previous studies revealed that UNC-40/DCC, PTP-3/LAR, and MIG-21 each stimulated posterior migration of QL and QR, and that distinct interactions between these molecules in QL versus QR governed posterior versus anterior migration (Sundararajan and Lundquist, 2012). In QL, UNC-40 acts redundantly with PTP-3 and MIG-21 to control posterior QL migration, and in QR, UNC-40 and PTP-3/MIG-21 mutually repress each other's posterior migration function to allow anterior migration. We sought to determine how CDH-4 acts with these molecules in Q cell migration.

We first focused on interactions of *cdh-4* with *unc-40, ptp-3* and *mig-21* in QL posterior migration. Double mutants of *unc-40* with *ptp-3* or *mig-21* showed synergistic defects in QL posterior migration (Sundararajan and Lundquist, 2012). *unc-40(n324)* mutants alone displayed 4% QL migration defects wherein QL migrated anteriorly and divided over V4 (Fig 3.3A). *unc-40; cdh-4* double mutants were lethal, so we reduced *unc-40* function using expression of *unc-40* RNAi from the *scm* promoter expressed in the seam cells and Q cells as described previously (Sundararajan and Lundquist, 2012). *unc-40(RNAi)*

showed no defects alone, but *cdh-4; unc-40(RNAi)* double mutants displayed a significant increase in the percentage of anterior QL compared to *cdh-4* alone (Figure 3.3A). This result indicates that CDH-4 acts in parallel to UNC-40/DCC in posterior QL migration, similar to PTP-3 and MIG-21 (Sundararajan and Lundquist, 2012).

We used *ptp-3(RNAi)* to reduce *ptp-3* gene function, as double mutants of *cdh-4* with the null *ptp-3(mu245)* allele were inviable. The previously-described *scm::ptp-3(RNAi)* transgene was used in these studies, which enhanced QL defects of *unc-40* mutants (Sundararajan and Lundquist, 2012). We found that QL defects in *cdh-4; ptp-3(RNAi)* double mutants did not differ significantly from *cdh-4* single mutants (Figure 3.3B). The double mutant of *cdh-4(lq56)* with the hypomorphic *ptp-3(mu256)* allele (Sundararajan and Lundquist, 2012) was also no more severe than *cdh-4(lq56)* alone. These data suggest that PTP-3 and CDH-4 might act in the same pathway in parallel to UNC-40 to direct posterior QL migration. Consistent with this idea, the triple mutant *cdh-4(feedingRNAi); unc-40(RNAi); ptp-3(mu256)* showed no enhancement relative to *unc-40; ptp-3* and *cdh-4; unc-40* double mutants (Figure 3.3A). While *cdh-4* RNAi by feeding alone had no effect, it did significantly enhance PQR migration defects of *unc-40(n324)* ($p < 0.0001$) (Table 3.1), suggesting that *cdh-4* gene function is reduced by feeding RNAi.

The small transmembrane thrombospondin repeat containing protein MIG-21 acts in the PTP-3 pathway in parallel to UNC-40 in posterior QL migration (Middelkoop et al., 2012; Sundararajan and Lundquist, 2012). Due to close proximity on LGIII and similarity in Q cell phenotype, we were unable to construct *mig-21; cdh-4* double mutants. *cdh-4* RNAi by feeding did not modify the *mig-21(u787)* QL phenotype (Figure 3.3B). The consistent lack of enhancement between *cdh-4* and *ptp-3*/*mig-21* support the idea that CDH-4 acts in the PTP-3/MIG-21 pathway, in parallel to UNC-40, in posterior QL migration. While our double and triple mutant analysis using RNAi was consistent with CDH-4 acting in the PTP-3 pathway in parallel to UNC-40, it is also possible that RNAi did not

effectively reduce gene function in *ptp-3* double mutants and that CDH-4 defines a third pathway in parallel to both UNC-40 and PTP-3.

CDH-4 acts genetically in both the UNC-40/DCC and PTP-3/LAR pathways in QR anterior migration

unc-40, ptp-3 and *mig-21* mutations each displayed QRs that migrated to the posterior over V5 (Sundararajan and Lundquist, 2012). In *unc-40; ptp-3* and *unc-40; mig-21* double mutants, this aberrant posterior migration was reduced, suggesting a mutual inhibition between UNC-40 and PTP-3/MIG-21 in QR that allows anterior migration (Sundararajan and Lundquist, 2012). In other words, in the absence of PTP-3, UNC-40 is free to drive posterior migration, and *vice versa*.

cdh-4 mutants each displayed over 70% of QRs migrating posteriorly and dividing over V5, significantly more severe than *unc-40, ptp-3*, and *mig-21* mutants (Figure 4.4A). *unc-40(RNAi)* significantly reduced posterior QR migration of *cdh-4(lq56* and *lq83)* (Figure 4.4A), as it did with *ptp-3* (Sundararajan and Lundquist, 2012). Double mutant combinations with *ptp-3* and *cdh-4* showed reduced posterior QR compared to *cdh-4* alone, but only one was significant at the $p < 0.05$ level (the *ptp-3(RNAi); cdh-4(lq83)* double) (Figure 4.4B). *cdh-4(RNAi)* did not significantly modify the QR defects of *mig-21(u787)* (Figure 4.4B). CDH-4 was clearly involved in inhibition of UNC-40 in QR, as *unc-40(RNAi)* suppressed posterior QR migration in *cdh-4* mutants. CDH-4 might also act in inhibition of PTP-3, as *ptp-3; cdh-4* doubles showed consistent reductions in posterior QR, only one of which was significant at $p < 0.05$. These data are consistent with CDH-4 acting in both the PTP-3/LAR and UNC-40/DCC pathways to facilitate a mutual inhibition between them to allow anterior QR migration. The triple *unc-40(RNAi); ptp-3(mu256); cdh-4(feeding RNAi)* showed reduced posterior QR, but was not significantly different compared to *unc-40(RNAi) ptp-3(mu256)* alone. It is possible that posterior QR defects in *unc-40(RNAi) ptp-3(mu256)* are already too low to detect any significant enhancement. However, this result is consistent with CDH-4 acting in both the

UNC-40/DCC and PTP-3/LAR pathways in QR. This model accounts for why the QR defects of *cdh-4* mutants are significantly stronger than *unc-40* and *ptp-3,* as in *cdh-4* mutants, both UNC-40 and PTP-3 would be free to drive posterior migration. *cdh-4; unc-40* and *cdh-4; ptp-3* double mutants have significantly more posterior QR than the *unc-40; ptp-3* double mutant, suggesting that CDH-4 is not the only molecule that acts with UNC-40 and PTP-3 in mutual inhibition.

cdh-4::gfp is expressed in Q cells and surrounding cells

A recombineered version of a fosmid clone containing the full-length *cdh-4* genomic locus and surrounding region with *gfp* fused in frame at the *cdh-4* 3' end was obtained from the TransgeneOme project (Sarov et al., 2012). This transgene is predicted to drive expression of CDH-4::GFP under its endogenous promoter and regulatory regions. Expression of *cdh-4::gfp* was observed in many cells at the time of Q cell polarization and migration in early L1 larvae (1-4.5h post hatching), including hypodermal seam cells and P cells (Figure 3.5). *cdh-4::gfp* expression was also observed in the Q cells, as noted by overlapping expression with *egl-17::mCherry*, expression of which is limited to the Q cells in the posterior of early L1 animals (Branda and Stern, 2000; Cordes et al., 2006; Sundararajan and Lundquist, 2012). Thus *cdh-4::gfp* is expressed in the Q cells but also in neighboring hypodermal cells. CDH-4::GFP accumulated throughout the cell bodies and margins, incuding the nucleus. This accumulation could reflect endogenous localization of CDH-4, or could be an artifact of transgenic expression, possibly overexpression. However, *cdh-4::gfp* rescued the Q migration defects of *cdh-4* mutants, indicating that some functional CDH-4::GFP is expressed from the transgene.

CDH-4 acts non-cell autonomously in Q migrations

To test the functional requirement of *cdh-4* in the Q cells, we performed a mosaic analysis using the *cdh-4::gfp* fosmid transgene and a strategy used previously to demonstrate autonomy of function of *mig-15/NIK* kinase in the Q cells (Chapman et al., 2008) (see Materials and Methods). A stably-integrated *gcy-32::cfp*

transgene was used to score the positions of AQR and PQR, and an unstable extrachromosomal array containing rescuing *cdh-4::gfp* and *gcy-32::yfp* was used to generate genetic mosaics of *cdh-4(+)* activity in the *cdh-4(lq56)* mutant (Figure 3.6A). The *cdh-4::gfp* extrachromosomal array rescued AQR and PQR defects in *cdh-4(lq56)* mutants, indicating that it supplies *cdh-4(+)* activity (Figure 3.7). We next screened for mosaic animals in which the *cdh-4::gfp* extrachromosomal array was specifically lost in either AQR or PQR but retained in the other and in the URX neurons using *gcy-32::cfp* expression (Figure 3.6). The positions of AQR or PQR that lost the array were then determined by *gcy-32::yfp*. In such mosaic animals, AQR and PQR migration defects were not significantly different from non-mosiac, rescued animals (Figure 3.7). These results indicate that *cdh-4* is not required in AQR and PQR for their proper migration. A similar strategy with *mig-15/NIK* showed opposite results, that loss of the rescuing array in AQR and PQR led to migration defects, indicating autonomy of function (Chapman et al., 2008). These results suggest that CDH-4 acts non-autonomously in directing AQR and PQR migrations. These results do not indicate which tissues require *cdh-4(+)* for AQR and PQR migration, but *cdh-4::gfp* is expressed broadly, including in hypodermal cells neighboring the Q cells (Figure 3.5).

2.5 Discussion

Fat-like cadherins have been implicated extensively in cooperating with Wnt signaling and PCP core pathway components to generate tissue polarity (reviewed in (Thomas and Strutt, 2012)). Here we show that the Fat-like cadherin CDH-4 in *C. elegans* is required for anterior-posterior protrusion and migration of the Q neuroblasts. In *cdh-4* mutants, QR often migrated posteriorly, and QL anteriorly. Greater than 50% of QR cells migrated in the wrong direction posteriorly in *cdh-4* mutants, indicating that migration direction is not randomized in *cdh-4* mutants, but rather that CDH-4 might change the direction of migration of Q cells in response to similar guidance information. Wnts control the anterior-posterior migration of Q cell descendants. EGL-20/Wnt activates expression of MAB-5/Hox in QL and descendants to cause posterior migration (Chapman et al., 2008; Eisenmann, 2005; Harris et al., 1996; Harterink et al., 2011; Herman, 2001; Kenyon, 1986; Maloof et al., 1999; Salser and Kenyon, 1992), and the five *C. elegans* Wnts display complex interactions in anterior-posterior migration of Q descendants (Zinovyeva et al., 2008). However, EGL-20/Wnt is not required for Q neuroblast initial migrations (Chapman et al., 2008), and despite having severe defects in AQR and PQR migration, the Wnt triple mutant *egl-20 cwn-2; cwn-1* had no defects in initial Q migrations. These results are consistent with early Q cell migration and thus CDH-4 function in early Q migration being Wnt-independent.

We found that *cdh-4; unc-40* and *cdh-4; ptp-3* double mutants were inviable. *cdh-4* mutants show some embryonic lethality coupled with variable failures in elongation and hypodermal organization (Schmitz et al., 2008). *ptp-3* mutants when combined with *vab-1*/EphR display defects in embryonic morphogenesis (Harrington et al., 2002), and *ptp-3; unc-40* double mutants are lethal (Sundararajan and Lundquist, 2012). Possibly, UNC-40/DCC, PTP-3/LAR, and CDH-4 all act in parallel to control aspects of embryonic morphogenesis and gastrulation.

CDH-4 acts in parallel to UNC-40, in the PTP-3/LAR pathway, in posterior QL migration. Previous work showed that UNC-40/DCC, PTP-3/LAR and MIG-21 are each required for posterior migration (Honigberg and Kenyon, 2000; Middelkoop et al., 2012; Sundararajan and Lundquist, 2012). In QL, MIG-21 and PTP-3 function in the same genetic pathway redundantly with UNC-40 to direct posterior migration (Sundararajan and Lundquist, 2012). In QL, *cdh-4* mutations enhanced *unc-40/DCC* but not *ptp-3/LAR* or *mig-21,* suggesting that CDH-4 acts in the PTP-3/LAR pathway (Figure 3.3). CDH-4 acted non-autonomously (Figures 3.6 and 3.7), while UNC-40/DCC and PTP-3/LAR were required autonomously (Sundararajan and Lundquist, 2012). One model is that CDH-4 acts as an extracellular cue that directs posterior QL migration via PTP-3/LAR (Figure 3.8). This model implies that an unidentified, possibly redundant, cue would act through UNC-40/DCC. This cue is unlikely to be the canonical UNC-40/DCC ligand UNC-6/Netrin, as *unc-6* mutants have no effect on anterior-posterior Q migrations (Honigberg and Kenyon, 2000). It is also possible that RNAi reduction of gene function was ineffective in *cdh-4(RNAi); ptp-3* double mutants, and that CDH-4 defines a third pathway in parallel to both UNC-40 and PTP-3.

CDH-4 acts in both the UNC-40/DCC and PTP-3/LAR pathways in QR, and possibly facilitates mutual inhibition. Previous results indicate that UNC-40/DCC and PTP-3 interact differently in QR versus QL. In QR, UNC-40/DCC and PTP-3/LAR mutually inhibit each others' roles in posterior migration, resulting in anterior migration (Sundararajan and Lundquist, 2012). *cdh-4* mutants displayed greater than 70% posterior QR migration, a significantly higher defect than *unc-40* and *ptp-3* (Figure 3.4). *unc-40(RNAi)* reduced posterior QR migration in *cdh-4* (Figure 3.4), suggesting that when CDH-4 is absent, UNC-40 drives posterior QR migration and that CDH-4 normally inhibits UNC-40. *ptp-3* loss also reduced posterior QR migration in *cdh-4* mutants. This effect was not as dramatic as with *unc-40*, but three different double mutant combinations showed reduced posterior QR, one of which was significant. Thus, CDH-4 might

also normally inhibit PTP-3/LAR. The triple *unc-40(RNAi); ptp-3(mu256); cdh-4(feeding RNAi)* showed reduced posterior QR, but was not significantly different compared to *unc-40(RNAi) ptp-3(mu256)* alone. It is possible that posterior QR defects in *unc-40(RNAi) ptp-3(mu256)* are already too low to detect any significant enhancement. However, this result is consistent with CDH-4 acting in both the UNC-40/DCC and PTP-3/LAR pathways in QR, explaining why QR defects are so much more severe in *cdh-4* mutants versus *unc-40* and *ptp-3* (i.e. both UNC-40 and PTP-3 drive posterior QR in the absence of CDH-4) (Figure 3.8).

Our results are consistent with a model in which CDH-4 facilitates the mutual inhibition of UNC-40/DCC and PTP/LAR in QR by interacting with both pathways in a non-autonomous manner (Figure 3.8). However, CDH-4 does not act in the UNC-40/DCC pathway in QL. This model requires that a QR-specific function, such as a co-receptor or a cytoplasmic molecule, mediates interaction of CDH-4 with the UNC-40 pathway in QR and not QL, and thus facilitates mutual inhibition in QR but not QL. QL and QR have inherent differences, such as response to EGL-20/Wnt and MAB-5/Hox. QL is more sensitive to both than QR. The conserved transmembrane protein MIG-13 specifically affects QR descendant migrations (Sym et al., 1999; Wang et al., 2013). However, MIG-13 does not affect initial QR migration (Sym et al., 1999). Instead, MIG-13 expression is activated specifically in QR descendants by the Hox transcription factors LIN-39 and MAB-5 after initial QR migration (Wang et al., 2013). A molecule that mediates CDH-4/UNC-40 interaction in QR and not QL to mediate early migration has not yet been identified.

CDH-4 acts non-autonomously. UNC-40/DCC and PTP-3/LAR are required in the Q cells to guide their migrations (Sundararajan and Lundquist, 2012). In contrast, mosaic analysis of *cdh-4* suggests that it acts non-autonomously to guide Q migrations. Loss of *cdh-4(+)* activity in either AQR or PQR had no effect on their migrations (Figures 3.6 and 3.7), suggesting that *cdh-4* is required in other cells that retained the *cdh-4(+)* activity in the mosaic animals. Our

experiments could not determine which cells these were, but *cdh-4(+)::gfp* is expressed in cells neighboring the Q cells, such as the hypodermal seam cells and the hypodermal P cells (Figure 3.5). In QL, our data support a model in which CDH-4 might be a cue that directs posterior QL migrations via PTP-3/LAR (Figure 3.8). In QR, our data suggest CDH-4 that facilitates mutual inhibition of UNC-40/DCC and PTP-3/LAR because of an inherent left-right asymmetry in QR versus QL (Figure 3.8). This inherent asymmetry would allow CDH-4 to interact with the UNC-40/DCC pathway in QR but not QL, thus inhibiting both UNC-40/DCC and PTP-3/LAR and allowing anterior migration. This is similar to the role of Fat in planar cell polarity, which acts non-autonomously to orient cells polarized by the core PCP pathway to the tissue or organismal axis.

Despite non-autonomous function in determining direction of migration in QR and QL, *cdh-4::gfp* is expressed in the Q cells. Possibly, CDH-4 has a role in the Q cells that does not involve direction of migration, such as cell adhesion. Indeed, *cdh-4* mutants display defects in attachment of the pharynx to the hypodermis, suggestive of a defect in cell adhesion (Schmitz et al., 2008).

A non-autonomous role of CDH-4 is supported by the *lq97* mutation, which is in the second to the last exon but is still 894 bp upstream of the endogenous stop codon and is thus likely subject to nonsense-mediated mRNA decay. It is possible that a fraction of the mRNA escapes nonsense mediated decay and produces a CDH-4 molecule that lacks a transmembrane domain and is potentially secreted. AQR migration defects of *cdh-4(lq97)* were significantly less severe than other *cdh-4* alleles (Table 3.1), and *smg-1* RNAi slightly suppressed PQR migration defects, indicating that a potentially secreted form of CDH-4 in *cdh-4(lq97)* mutants retains some function. That this secreted version retains function in AQR migration supports a non-autonomous role.

CDH-4::GFP showed no apparent asymmetric distribution in the anterior-posterior axis, suggesting that it might act as a permissive cue for migration, rather than a directional cue. Possibly, CDH-4 modifies the response of the Q cells to the same anterior-posterior guidance information. That QR migration is not randomized in *cdh-4* mutants but rather skewed toward the posterior is

consistent with a permissive role of CDH-4 in distinguishing the responses of QR and QL to similar anterior-posterior guidance information. The *Fat* gene in humans has been associated with neuropsychiatric disorders such as bipolar disorder and schizophrenia (Abou Jamra et al., 2008; Jung and Jun, 2013; Light et al., 2007; Redies et al., 2012). Mechanisms described here might be relevant in vertebrate central nervous system development and neuropsychiatric disorders.

Figure 3.1.

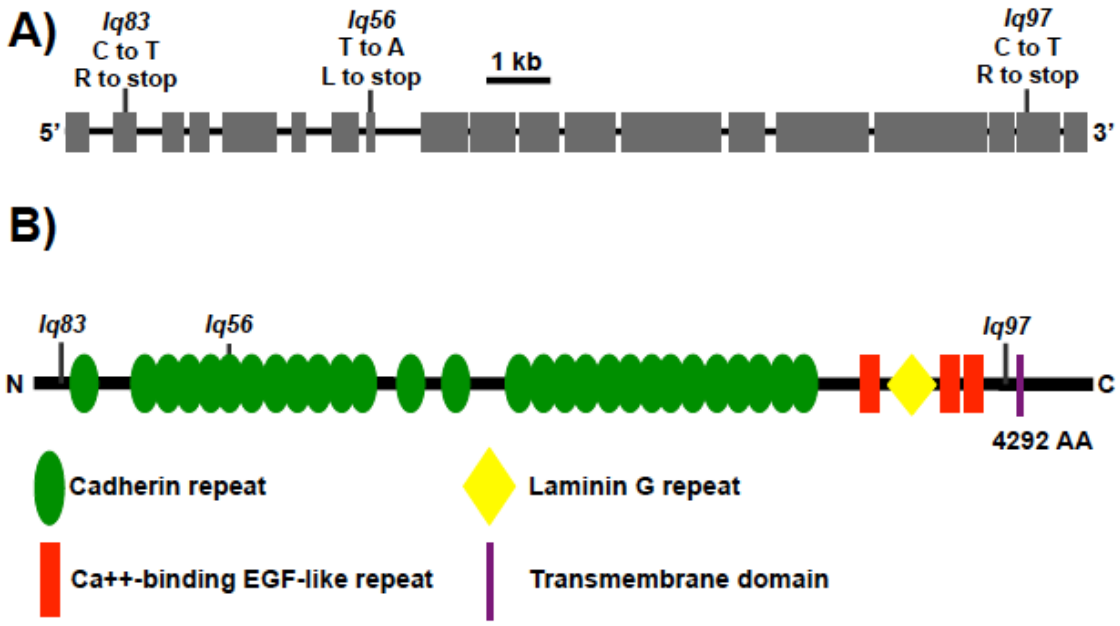
A)
lq83
C to T
R to stop
lq56
T to A
L to stop
1 kb
lq97
C to T
R to stop
5'
3'
B)
lq83
lq56
lq97
N
C
4292 AA
Cadherin repeat
Laminin G repeat
Ca++-binding EGF-like repeat
Transmembrane domain

Figure 3.1. CDH-4 is a Fat-like cadherin. A) A diagram representing the genomic region of the *cdh-4A* isoform. Exons are indicated by boxes, and introns by lines. Positions of the lesions are marked and the corresponding nucleotide changes are noted. *lq56* was a T to A transversion resulting in a leucine to stop (TTG to TAG) at LGII position 4525658 in Wormbase WS240. *lq83* was a C to T transition resulting in an arginine to stop (CGA to TGA) at position 4521154. *lq97* was C to T transition resulting in an arginine to stop (CGA to TGA) at position 4535721. B) A diagram of the 4292 residue CDH-4A polypeptide. The position of the stop codons introduced by *lq56*, *lq83,* and *lq97* are indicated.

Figure 3.2.

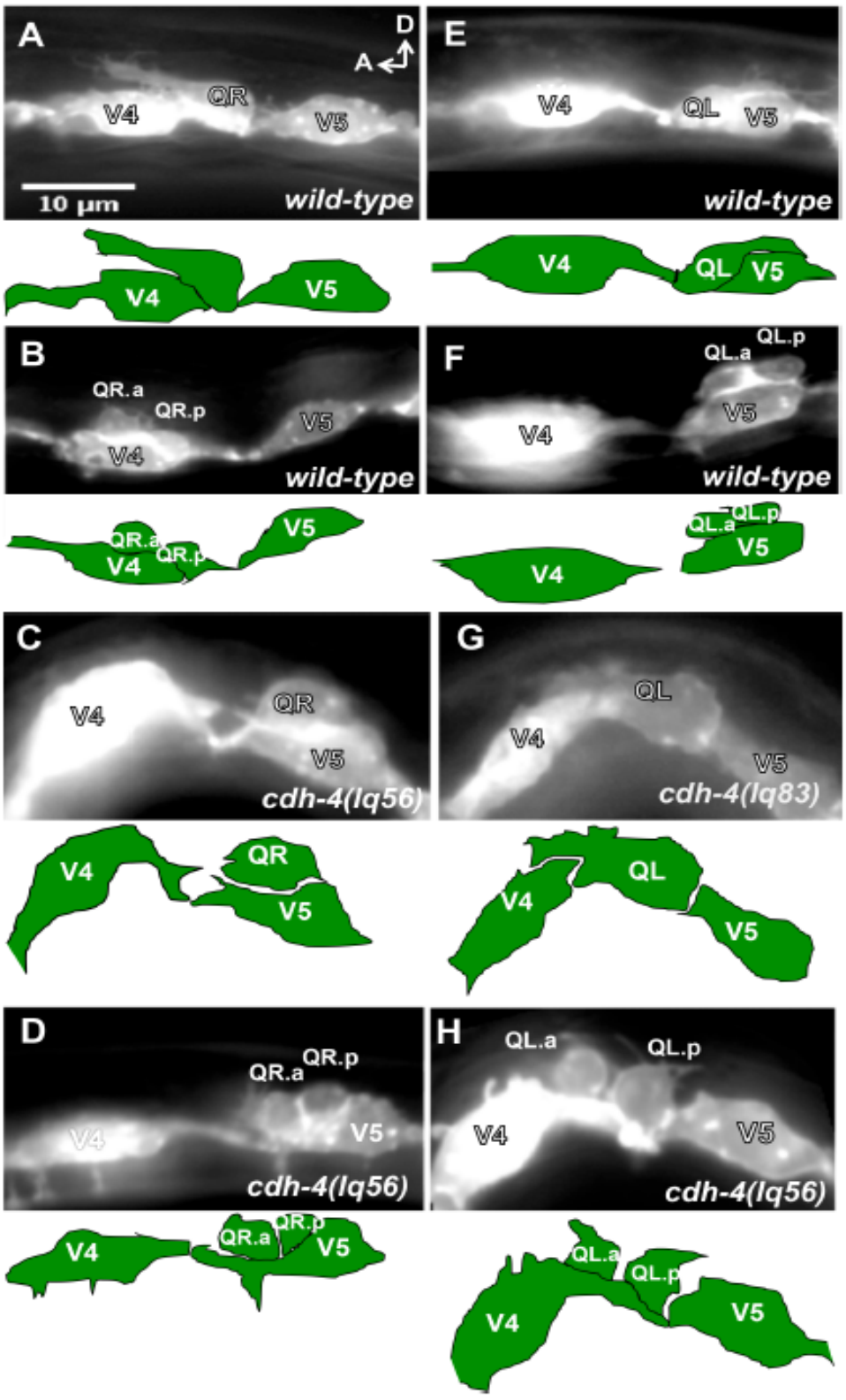
A
D
A
QR
V4
V5
10 µm
wild-type
V4
V5
E
V4
QL
V5
wild-type
V4
QL
V5
B
QR.a
QR.p
V5
V4
wild-type
QR.a
QR.p
V5
V4
F
QL.a
QL.p
V5
V4
wild-type
QL.a
QL.p
V5
V4
C
V4
QR
V5
cdh-4(lq56)
V4
QR
V5
G
QL
V4
V5
cdh-4(lq83)
V4
QL
V5
D
QR.a
QR.p
V4
V5
cdh-4(lq56)
V4
QR.a
QR.p
V5
H
QL.a
QL.p
V4
V5
cdh-4(lq56)
V4
QL.a
QL.p
V5

Figure 3.2. Q neuroblast migration defects in *cdh-4* mutants. Micrographs of animals with *scm::myr::gfp* expression in the Q cells and seam cells. Anterior is left, and dorsal is up. The tracing below each micrograph indicates the position of the Q cells and seam cells. (A-D) QR migration in wild-type and *cdh-4*. A) A QR of a wild-type L1 animal at 2-2.5h post-hatch protruded anteriorly over V4. B) A wild-type QR at 4-4.5 h post-hatch divided over V4. C) A *cdh-4(lq56)* mutant QR migrated posteriorly over V5 at 3-3.5 h post-hatch. D) A *cdh-4(lq56)* mutant QR divided over V5 at 4-4.5 h post-hatch. (E-H) QL migration in wild-type and *cdh-4.* E) A wild-type QL at 2-1.5 h post-hatch protruded posteriorly over V5. F) A wild-type QL at 4-4.5 h post-hatch divided over V5. G) A *cdh-4(lq83)* QL at 2-2.5 h post-hatch protruded anteriorly over V4. H) A *cdh-4(lq56)* mutant QL divided over V4 at 4-4.5 h post-hatch.

Figure 3.3A.

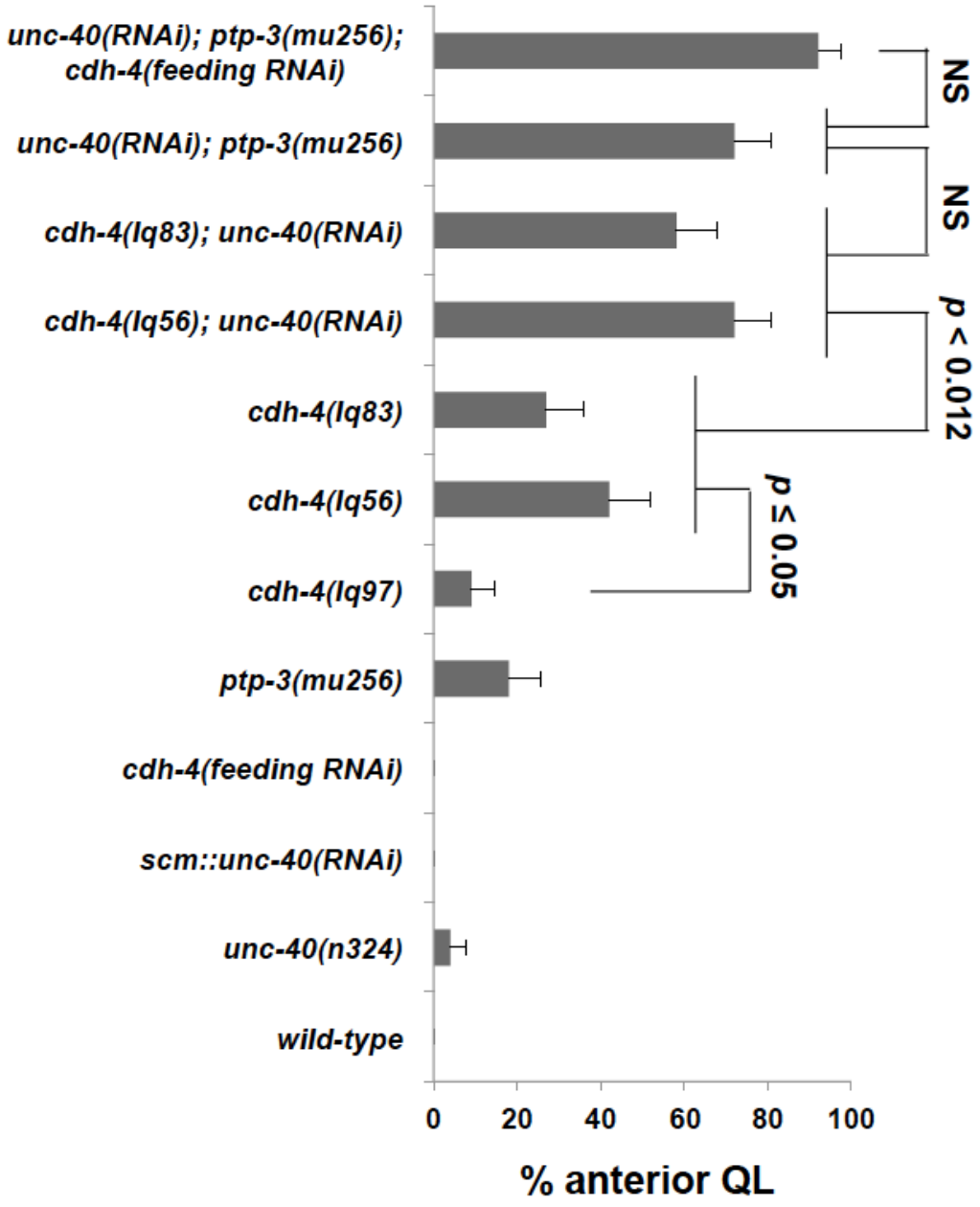
unc-40(RNAi); ptp-3(mu256); cdh-4(feeding RNAi)
unc-40(RNAi); ptp-3(mu256)
cdh-4(lq83); unc-40(RNAi)
cdh-4(lq56); unc-40(RNAi)
cdh-4(lq83)
cdh-4(lq56)
cdh-4(lq97)
ptp-3(mu256)
cdh-4(feeding RNAi)
scm::unc-40(RNAi)
unc-40(n324)
wild-type
NS
NS
p < 0.012
p ≤ 0.05
0
20
40
60
80
100
% anterior QL

Figure 3.3B.

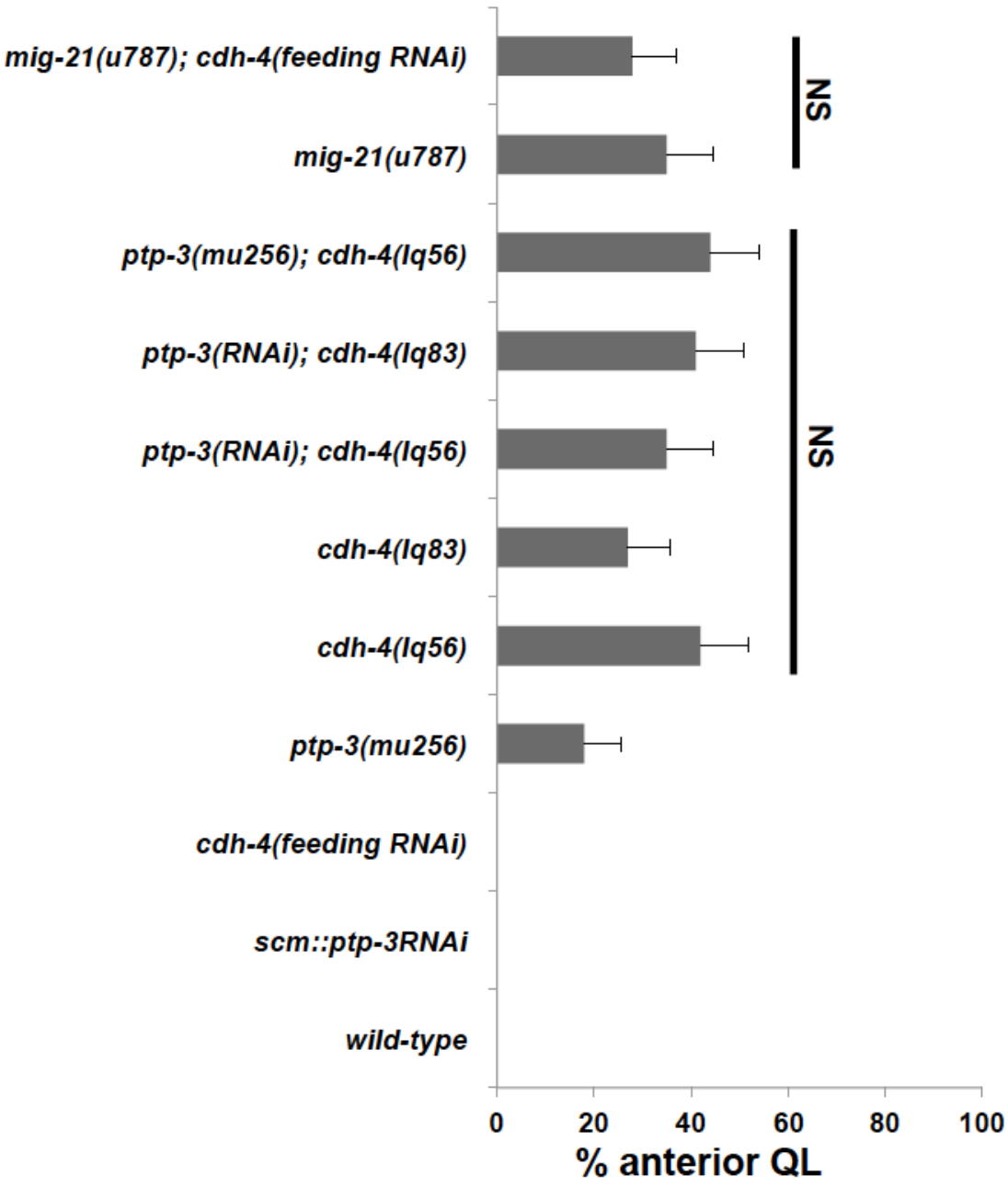
mig-21(u787); cdh-4(feeding RNAi)
mig-21(u787)
ptp-3(mu256); cdh-4(lq56)
ptp-3(RNAi); cdh-4(lq83)
ptp-3(RNAi); cdh-4(lq56)
cdh-4(lq83)
cdh-4(lq56)
ptp-3(mu256)
cdh-4(feeding RNAi)
scm::ptp-3RNAi
wild-type
SN
SN
0
20
40
60
80
100
% anterior QL

Figure 3.3. Quantification of QL migration in *cdh-4* mutants. Graphs represent the division stage of early QL neuroblast migrations at 4-4.5 hours post hatching. Genotype is the Y-axis, and the percentage of defective anterior QL migration and division is the X-axis. Migration was scored as defective if QL migration was reversed and it divided while in contact with the anterior V4 seam cell. Failure to migrate, resulting in division between the seam cells, was also observed in *cdh-4* mutants but is not included in the graphs. *unc-40(RNAi)* and *ptp-3(RNAi)* represent the *Pscm::unc-40(RNAi)* and *Pscm::ptp-3(RNAi)* transgenes (Sundararajan *et al*., 2012), and *cdh-4* RNAi by feeding is indicated (see Materials and Methods). The error bars represent two times the standard error of proportion, and the statistical difference between the genotypes were determined by Fisher's Exact test. Twenty-five animals or more were scored for each genotype. A) *cdh-4* double mutants with *unc-40*. B) *cdh-4* double mutants with *ptp-3* and *mig-21*.

Figure 3.4A

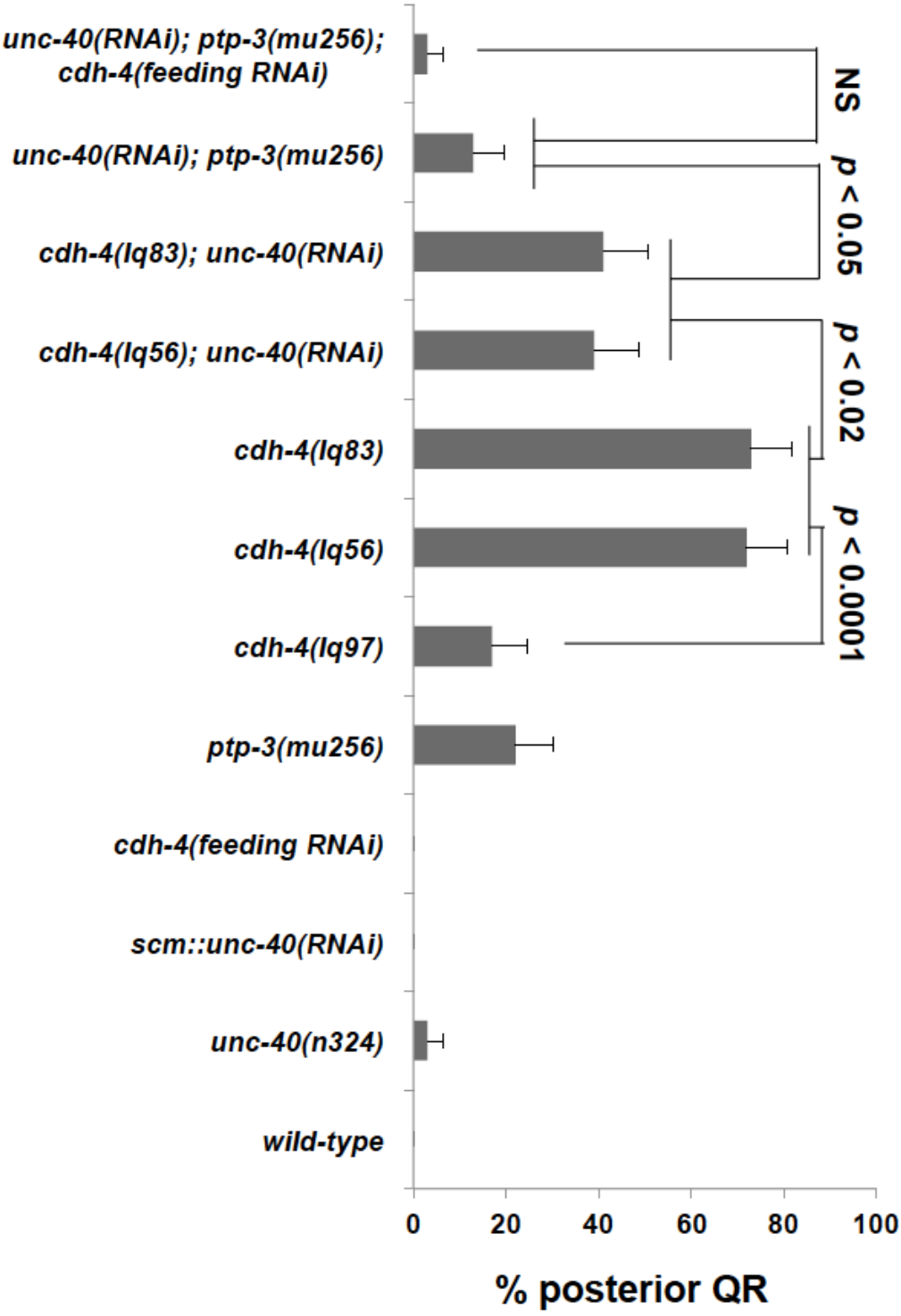
unc-40(RNAi); ptp-3(mu256); cdh-4(feeding RNAi)
unc-40(RNAi); ptp-3(mu256)
cdh-4(lq83); unc-40(RNAi)
cdh-4(lq56); unc-40(RNAi)
cdh-4(lq83)
cdh-4(lq56)
cdh-4(lq97)
ptp-3(mu256)
cdh-4(feeding RNAi)
scm::unc-40(RNAi)
unc-40(n324)
wild-type
NS
p < 0.05
p < 0.02
p < 0.0001
0
20
40
60
80
100
% posterior QR

Figure 3.4B

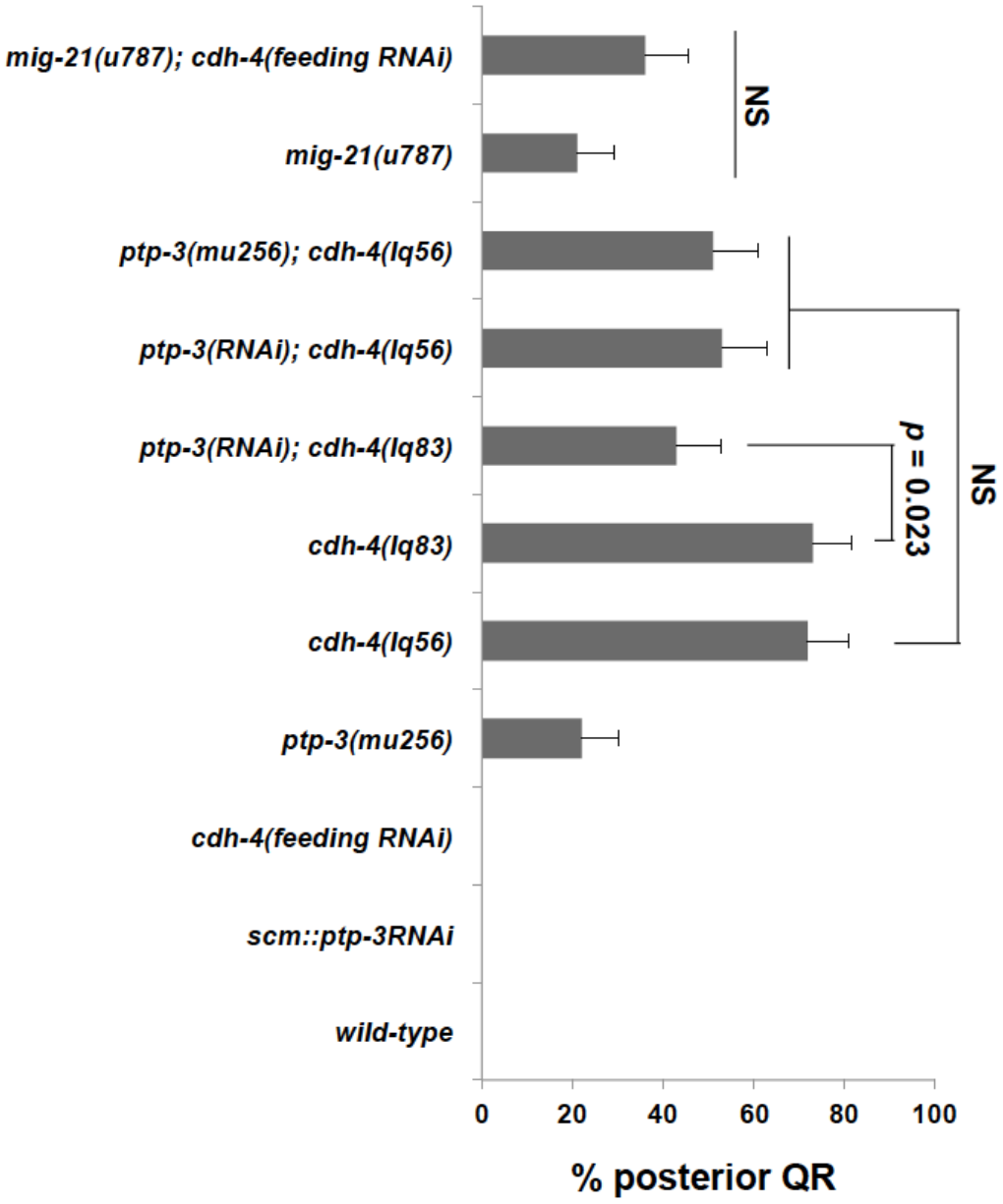
mig-21(u787); cdh-4(feeding RNAi)
mig-21(u787)
ptp-3(mu256); cdh-4(lq56)
ptp-3(RNAi); cdh-4(lq56)
ptp-3(RNAi); cdh-4(lq83)
cdh-4(lq83)
cdh-4(lq56)
ptp-3(mu256)
cdh-4(feeding RNAi)
scm::ptp-3RNAi
wild-type
NS
p = 0.023
NS
0
20
40
60
80
100
% posterior QR

Figure 3.4. Quantification of QR migration in *cdh-4* mutants. Graphs represent the division stage of early QR neuroblast migrations at 4-4.5 hours post hatching. Genotype is the Y-axis, and the percentage of defective posterior QR migration and division is the X-axis. Migration was scored as defective if QR migration was reversed and it divided while in contact with the posterior V5 seam cell. Failure to migrate, resulting in division between the seam cells, was also observed in *cdh-4* mutants but is not included in the graphs. *unc-40RNAi* and *ptp-3(RNAi)* represent the *Pscm::unc-40(RNAi)* and *Pscm::ptp-3(RNAi)* transgenes (Sundararajan *et al*., 2012), and *cdh-4* RNAi by feeding is indicated (see Materials and Methods). The error bars represent two times the standard error of proportion, and the statistical difference between the genotypes were determined by Fisher's Exact test. Twenty-five animals or more were scored for each genotype. A) *cdh-4* double mutants with *unc-40*. B) *cdh-4* double mutants with *ptp-3* and *mig-21*.

Figure 3.5.

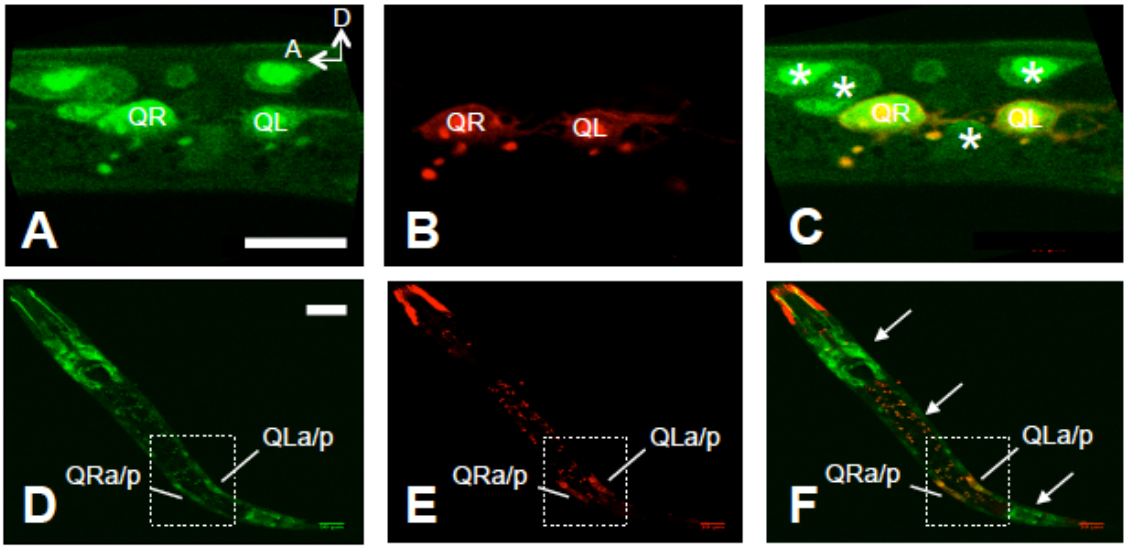

Figure 3.5. Expression of *cdh-4::gfp* in the Q cells and neighboring cells. Images are micrographs of L1 animals with transgenic expression of the *cdh-4::gfp* recombineered fosmid (green) and the *Pegl-17::mCherry* transgene expressed in the Q neuroblasts (red). The scale bar in A represents 10μm for A-C, and in C for C-E. A) *cdh-4::gfp* expression in the Q cells an L1 animal 3-3.5 h post-hatch. Neighboring cells expressing *cdh-4::gfp* can also be seen (asterisks in C). B) The same animal in A showing *Pegl-17::mCherry* expression in the Q cells. C) A merge of images in A and B. (C-E) A lower magnification image of expression in an L1 animal at 4-4.5 h post-hatch with the same parameters as A-C. *cdh-4::gfp* is expressed along the length of the animal (arrows in F), including in the Q cells, which have divided.

Figure 3.6.

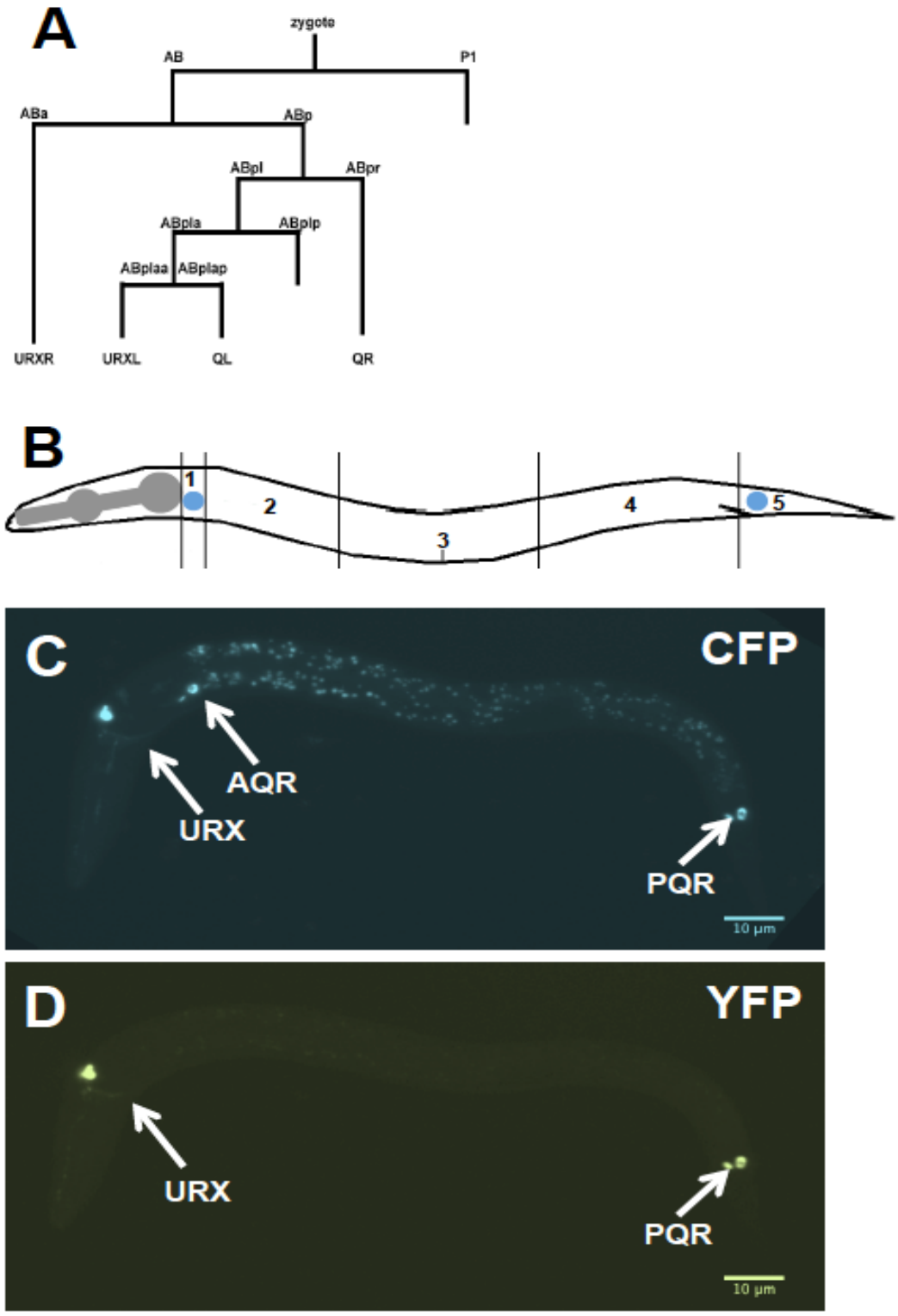
A
zygote
AB
P1
ABa
ABp
ABpl
ABpr
ABpla
ABplp
ABplaa
ABplap
URXR
URXL
QL
QR
B
1
2
3
4
5
C
CFP
AQR
URX
PQR
10 µm
D
YFP
URX
PQR
10 µm

Figure 3.6. Mosaic analysis of *cdh-4* function. A) A simplified representation of the *C. elegans* cell lineage showing the origins of all *Pgcy-32::gfp*-expressing cells (AQR, PQR, URX L/R). Not all cell divisions are shown. B) A diagram of an animal subdivided into five segments along its body is shown. The wild-type positions of AQR (QR descendent) and PQR (QL descendent) are indicated in the diagram in positions 1 and 5 respectively. C-D) Micrographs of an early L2 larval animal with stably-integrated *Pgcy-32::cfp* expression to mark the positions of AQR and PQR, as well as an unstable extrachromosomal array with rescuing *cdh-4::gfp* and *Pgcy-32::yfp* to identify genetic mosaics of this array in AQR and PQR. C) *Pgcy-32::cfp* expression shows that AQR is in its normal position 1, and PQR is in its normal position 5. D) *Pgcy-32::*yfp expression shows that the rescuing *cdh-4::gfp* array has been lost in AQR, but retained in PQR and the URX neurons. Despite loss of the array in AQR, it has migrated normally as judged by *Pgcy-32::cfp* expression in C.

Figure 3.7.

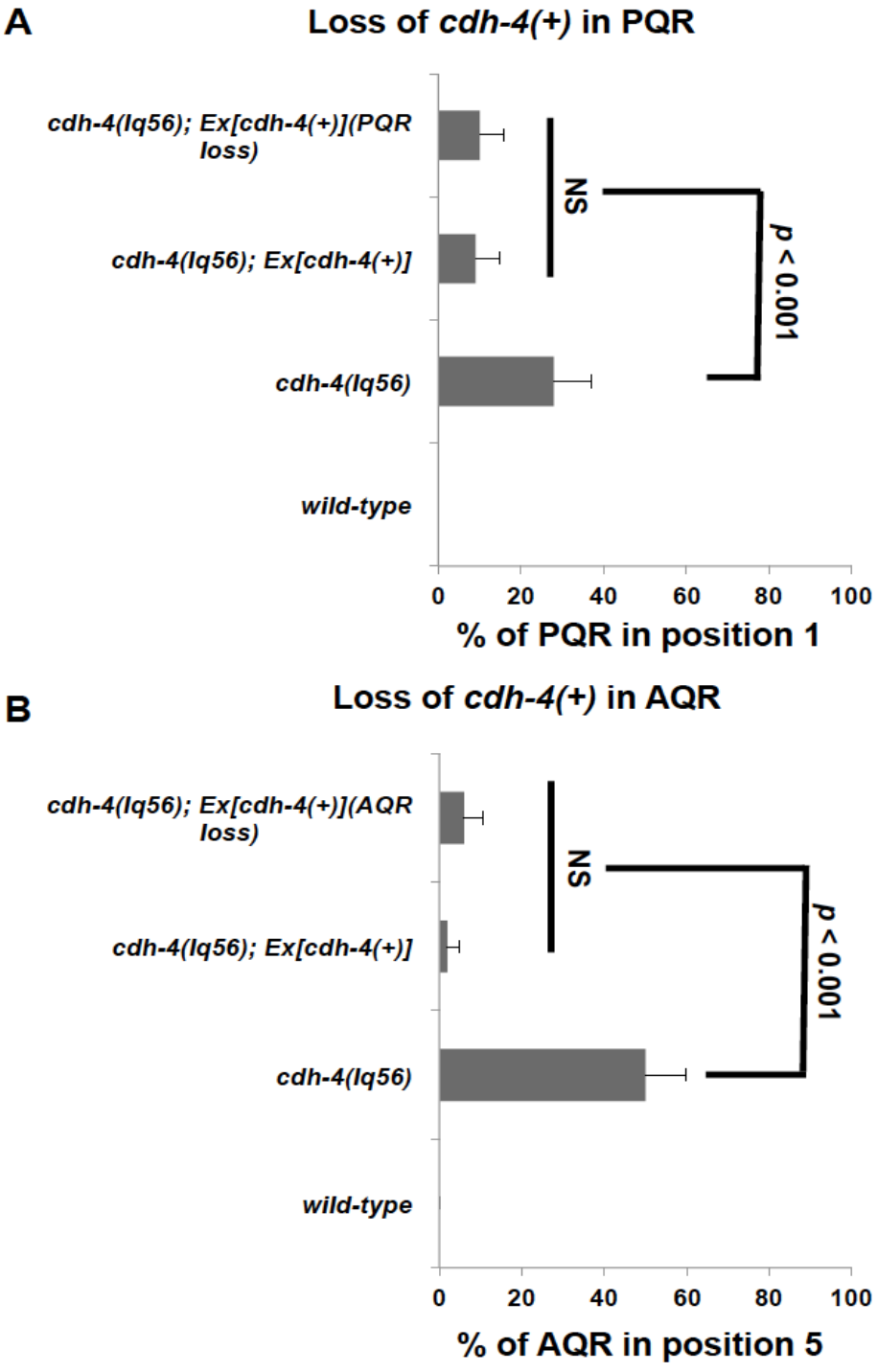
A
Loss of cdh-4(+) in PQR
cdh-4(lq56); Ex[cdh-4(+)](PQR loss)
cdh-4(lq56); Ex[cdh-4(+)]
cdh-4(lq56)
wild-type
NS
p < 0.001
0
20
40
60
80
100
% of PQR in position 1
B
Loss of cdh-4(+) in AQR
cdh-4(lq56); Ex[cdh-4(+)](AQR loss)
cdh-4(lq56); Ex[cdh-4(+)]
cdh-4(lq56)
wild-type
NS
p < 0.001
0
20
40
60
80
100
% of AQR in position 5

Figure 3.7. Quantification of AQR and PQR migration in *cdh-4* genetic mosaics. Graphs plot the percentage of AQR or PQR migration defects (Y-axis) in different genotypes (X-axis). Error bars represent 2x SEP, and at least 100 animals of each genotype were scored. Statistical significance was determined by Fisher's exact test. A) PQR migration defects in animals that lost the rescuing *cdh-4::gfp* array in PQR (PQR loss) but retained the array in AQR and URX L/R. Animals with and without the array in PQR showed reduced defects compared to *cdh-4(lq56)* alone that were not significantly different from one another. B) AQR migration defects in animals that lost the array in AQR (AQR loss) but retained it in PQR and URX L/R. Animals with and without the array in AQR showed reduced defects compared to *cdh-4(lq56)* alone that were not significantly different from one another.

Figure 3.8.

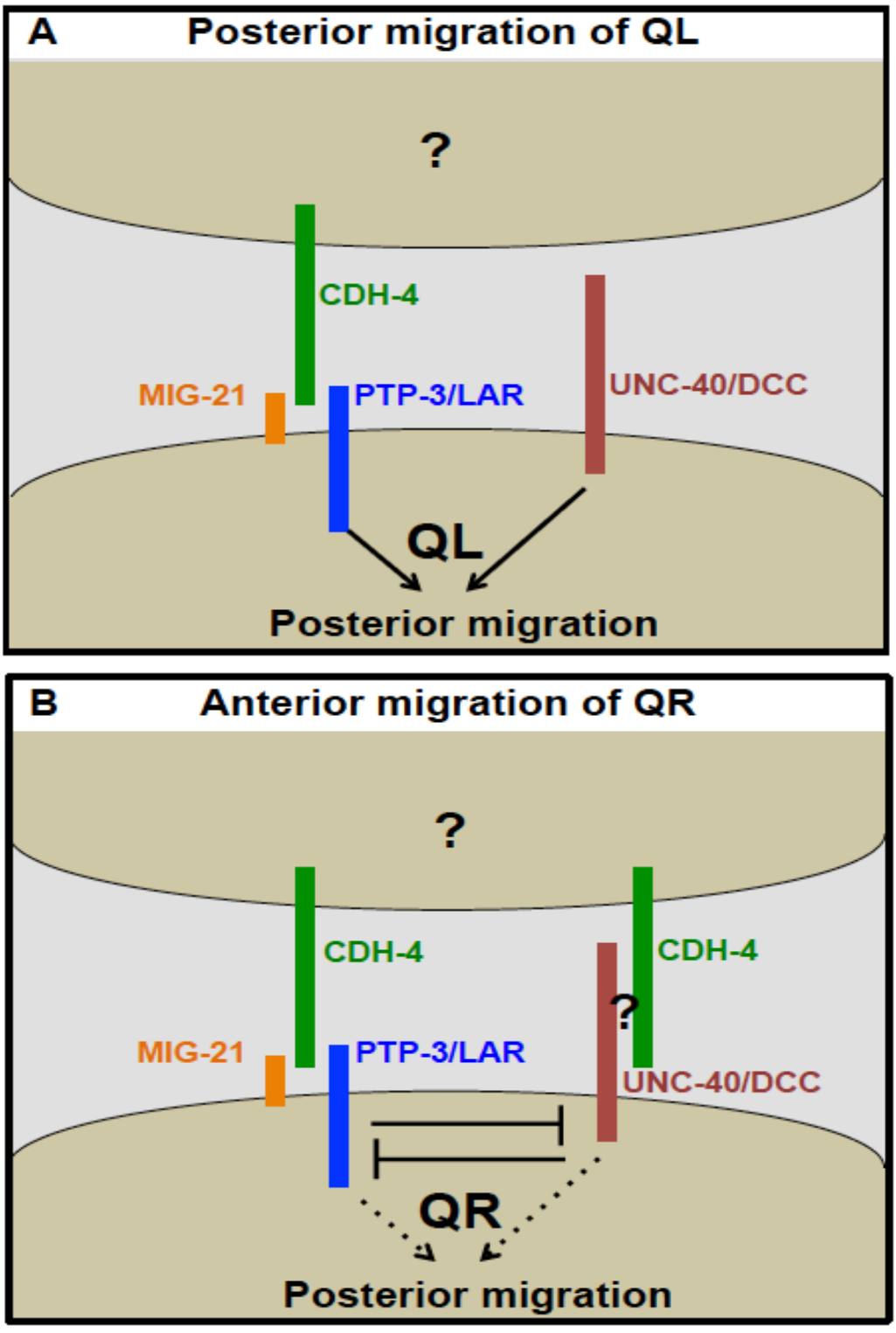
A
Posterior migration of QL
?
CDH-4
MIG-21
PTP-3/LAR
UNC-40/DCC
QL
Posterior migration
B
Anterior migration of QR
?
CDH-4
CDH-4
?
MIG-21
PTP-3/LAR
UNC-40/DCC
QR
Posterior migration

Figure 3.8. A model of CDH-4 genetic interaction with UNC-40/DCC, PTP-3/LAR, and MIG-21 that is consistent with data described in this work. A) CDH-4 acts non-autonomously with PTP-3/LAR and MIG-21 in parallel to UNC-40/DCC in directing posterior QL migration. Grouping of molecules does not imply physical interaction in this model, rather action in the same genetic pathway. The non-autonomous cellular source of CDH-4 is unknown (?). B) CDH-4 acts in both the PTP-3/LAR and UNC-40/DCC pathways in QR in mutual inhibition, allowing anterior QR migration. The QR-specific factor that mediates UNC-40/DCC function with PTP-3/LAR in QR but not QL is unknown (?).

Table 1. The Fat-like cadherin CDH-4 controls AQR and PQR migration.

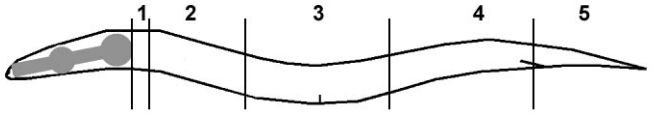

	AQR position (%)						PQR position (%)					
Genotype	1	2	3	4	5	N	1	2	3	4	5	N
wild-type	100	0	0	0	0	100	0	0	0	0	100	100
cdh-4(lq56)	39	3	2	7	49	100	28	3	4	4	60	100
cdh-4(lq56); Ex[cdh-4(+)]	90*	0	1	0	9	100	2*	0	1	1	96	100
cdh-4(lq83)	48	2	0	3	47	100	23	0	0	2	75	100
cdh-4(lq97)	80**	3	1	0	16	205	19	2	1	1	77	205
cdh-4(lq97); smg-1(RNAi)	82	3	1	0	14	200	13	1	1	1	84***	200
cdh-4(rh310)	50	1	1	2	46	100	19	0	0	2	79	100
cdh-4(ok1323)	45	0	2	1	52	100	24	0	1	0	75	100
cdh-4(hd40)	42	1	1	2	54	100	20	0	0	1	80	100
cdh-4(RNAi)	100	0	0	0	0	100	0	0	0	0	100	100
unc-40(n324)	96	1	0	0	3	76	32	3	8	6	51	76
unc-40(n324); cdh-4(RNAi)	99	0	0	1	0	100	76	4	2	5	13****	100
egl-20(n585) cwn-2(ok895); cwn-1(ok546)	39	49	10	2	0	100	3	16	19	25	37	100

* $p < 0.0001$ compared to other *cdh-4(lq56).*
** $p < 0.001$ compared to other *cdh-4* alleles *lq56, lq83, rh310, ok1323,* and *hd40*.
*** $p = 0.0416$ compared to *cdh-4(lq97)* alone.
**** $p < 0.0001$ compared to *unc-40(n324)* alone.

Chapter IV

SDN-1 and MIG-13 constitute an anterior guidance system for migration of QR descendants and might function downstream of MAB-5.

4.1 Abstract

Determining the downstream effectors in a pathway directing anterior-posterior migration is essential to understanding the inherent left-right asymmetry existent in the Q neuroblasts. The role of MAB-5/Hox in directing posterior migration of QL descendants has been well established. However, the anterior guidance system required for migration of QR descendants has not been well characterized. Previous studies have implicated MIG-13, a single pass transmembrane protein, in anterior QR descendant migration. Mutations in *mig-13* affect the extent and to a lesser degree the direction of AQR migration. Posterior expression of MIG-13 is restricted by MAB-5/Hox, making it an ideal anterior guidance gene. Both *mig-13* and *mab-5* contribute to the inherent left-right asymmetries in Q descendants. Heparan sulfate proteoglycans have been implicated in various aspects of cell migration. *C. elegans* have several heparan sulfate proteoglycans that have a known role in nervous system development. To understand the role of heparan sulfate proteoglycan in Q neuroblast migration, we quantified Q descendant migration in *unc-52/Perlecan*, *lon-2*, *gpn-1/Glypican* and *sdn-1/Syndecan* background. In a *sdn-1* mutant background, we observed significant AQR defects i.e., both extent and direction of migration. However, we did not observe any defects in any of the other heparan sulfate proteoglycan mutant backgrounds that could be explained by potential redundancy amongst the genes. We wanted to see if SDN-1 could be functioning with MIG-13 in directing anterior guidance of AQR. *sdn-1; mig-13* double mutants exhibit a significant increase in the percentage of AQR defects suggesting that SDN-1 and MIG-13 might function redundantly to direct anterior AQR migration. Now we wanted to see if SDN-1 could function to direct early QR migrations. However, *sdn-1* mutants do not exhibit any defects in early Q neuroblast migrations implying that SDN-1 does not play a role in early Q neuroblast migrations. It could also mean that SDN-1 could be functioning redundantly with the other heparan sulfate proteoglycans to direct early Q neuroblast migrations. Previous work has shown that the HS side chains of

SDN-1 are modified by the C5 epimerase HSE-5. Mutations in *hse-5* cause defects in early QR and QL migrations. Also, *sdn-1; hse-5* double mutants showed a significant increase in the percentage of mis-migrated AQR suggesting that HSE-5 might function in a separate pathway to direct anterior QR and AQR migrations and might function redundantly with SDN-1 to direct anterior AQR migration. In sum, we have started to characterize the role of heparan sulfate proteoglycans in Q descendant migrations and tease apart the role of genes that contribute to their anterior guidance.

4.2 Introduction

Directed neuronal migration is an essential part of nervous system development. We use the Q neuroblasts, QR and QL, as system to study neuronal cell migration. The Q neuroblasts are born in the posterior lateral region of the worm (Chalfie and Sulston, 1981; Sulston and Horvitz, 1977). QR, at about 1-2.5 hours post hatching, sends out defined anterior protrusions over the seam cell V4. Almost simultaneously, QL protrudes posterior over the seam cell V5. At about 3-3.5 hours post hatching QR and QL follow their protrusions and migrate on top of the seam cells V4 and V5 respectively (Chapman et al., 2008; Honigberg and Kenyon, 2000). At 4-4.5 hours post hatching, the cells divide to produce two daughters each (Figure 2.4). The daughter cells of QR and QL undergo further directional migration, divisions and cell death to give rise to three neurons each. The QR descendants SDQR, AVM and AQR migrate anterior with AQR migrating the farthest to near the pharyngeal bulb (Figure 2.2A,B). The QL descendants SDQL, PVM and PQR migrate posterior with PQR migrating the farthest to behind the anus to the posterior deirid (Chapman et al., 2008; Sulston and Horvitz, 1977; White et al., 1986). The directional migration of early QR and QL is directed by transmembrane proteins UNC-40/DCC, PTP-3/LAR, MIG-21 and CDH-4/Fat (Honigberg and Kenyon, 2000; Middelkoop et al., 2012; Sundararajan and Lundquist, 2012). In both QR and QL, UNC-40/DCC and PTP-3/MIG-21 act in parallel pathways directing posterior migration (Sundararajan and Lundquist, 2012). In QR, CDH-4/Fat functions in both UNC-40 and PTP-3/MIG-21 pathways and facilitates mutual inhibition between the posterior directing pathways to cause anterior QR migration. In QL, CDH-4/Fat functions with PTP-3/MIG-21 redundantly with UNC-40 to direct posterior QL migrations (Figure 3.8). QL undergoes its initial migration and division into an EGL-20/Wnt gradient (Honigberg and Kenyon, 2000). EGL-20 turns on MAB-5/Hox cell autonomously in the QL daughter cells to direct them posterior (Chalfie, 1993; Eisenmann, 2005; Harris et al., 1996; Herman, 2001; Kenyon, 1986; Korswagen et al., 2000; Salser and Kenyon, 1992; Whangbo and Kenyon, 1999). However,

QR migrates away from the EGL-20/Wnt signal and all its descendants migrate anterior since MAB-5/Hox is not expressed (Figure 1.1).

Previous work has shown that the EGL-20 directed MAB-5 is not required to direct early anterior- posterior migrations (Chapman et al., 2008). Nevertheless, it is necessary and sufficient to direct posterior QL descendant migrations. In a *mab-5* loss-of-function background, QR and QL undergo wild-type early migrations, however the QL descendants migrate anterior i.e., both AQR and PQR are located near the pharyngeal bulb that is the wild-type position of AQR. In a *mab-5* gain-of-function background, both QR and QL descendants migrate posterior i.e., both AQR and PQR are located at the wild-type position of PQR (Chalfie, 1993; Chapman et al., 2008; Kenyon, 1986).

The anterior QR descendants migrate away from the EGL-20/Wnt signal and hence MAB-5/Hox is never expressed in them and they migrate anterior (Kenyon, 1986). However, the genes required to direct anterior QR descendant migrations has not been characterized very well. Despite the definite correlation between the genes that affect early QR and QL migration and descendant migration, all the genes involved in descendant migrations are not required early on, for example MAB-5 is required to direct posterior QL descendant migrations but is not required for early anterior-posterior migrations (Chapman et al., 2008). *mig-13* was isolated in a forward genetic screen performed to isolate novel mutations that disrupt Q descendant migrations (Sym et al., 1999). Mutations in *mig-13* disrupt the extent and direction of QR descendant migrations suggesting that MIG-13 is required for anterior QR descendant migrations (Sym et al., 1999; Wang et al., 2013). MIG-13 is a single pass transmembrane protein with CUB domains and LDL receptor repeats (Sym et al., 1999). It is expressed primarily in the anterior region of the worm and its expression is controlled by transcription factors, MAB-5/Hox and LIN-39 (Sym et al., 1999; Wang et al., 2013). LIN-39 promotes the anterior expression of MIG-13 in QR descendant neurons (Wang et al., 2013). However, MAB-5/Hox inhibits the posterior expression of both LIN-39 and MIG-13 in the QL descendants (Wang et al., 2013). Hence, previous work

has shown a definite control between the molecules that direct posterior and anterior Q descendant migrations.

We wanted to identify and characterize the role of other genes that functioned in this process. Previous work has implicated Heparan sulfate proteoglycans (HSPG) in cell migration (Hudson et al., 2006; Merz et al., 2003; Rhiner et al., 2005; Schwabiuk et al., 2009; Wang et al., 2012). HSPGs have long chains of differentially modified sugar side chains that play different roles in nervous system development (Hudson et al., 2006; Johnson et al., 2006; Minniti et al., 2004; Rhiner et al., 2005; Wang et al., 2012) (Bulow et al., 2002). We tested the role of the HSPGs coded by the *C. elegans* genome in Q descendant migrations. Our observations showed that SDN-1/Syndecan was the only *C. elegans* HSPG that had an effect on QR descendant migration i.e., AQR migration.

SDN-1/Syndecan is the only Syndecan in the *C. elegans* genome (Rhiner et al., 2005). SDN-1 is a transmembrane protein with heparan sulfate side chains attached to the extracellular domains and intracellular PDZ domains (Bernfield et al., 1999; Esko and Selleck, 2002; Lindahl et al., 1998). SDN-1 is necessary for the migration of different neuronal cell types such as the HSN, ALM and CAN neurons and is expressed extensively in the nervous system (Rhiner et al., 2005). In a *sdn-1* mutant background, we observed AQR not being able to migrate all the way anterior to its wild-type position but stopping along its migratory path. We also saw AQR migrate posterior from its birthplace to the wild-type position of PQR. These results suggest that SDN-1 is required for proper anterior AQR migration However, *sdn-1* mutants did not display any defects in early Q neuroblast migrations suggesting that if SDN-1 had any role in directing early Q neuroblast migrations, it is minimal or SDN-1 is acting redundantly with other HSPGs. To understand whether *sdn-1* could be functioning with *mig-13* to direct anterior QR descendant migration, we built *sdn-1; mig-13* double mutants. The double mutant analyses showed that SDN-1 and MIG-13 act in parallel pathways to direct anterior AQR migrations. Then, we wanted to see if SDN-1 interacted with MAB-5/Hox in a genetically similar fashion

as MIG-13. So we analyzed both AQR and PQR defects in a *mab-5; sdn-1* loss of function and *mab-5* gain of function; *sdn-1* mutant backgrounds. In a mab-5 loss of function background PQR can no longer migrate posterior and hence migrates anterior probably due to the effect of SDN-1 and MIG-13 pathways. In a *sdn-1; mab-5* loss of function background, the anterior migratory pattern of PQR resembles that of AQR in a *sdn-1* mutant background, suggesting that PQR cannot complete its anterior migrations due to the absence of a SDN-1 signal. This result suggests that SDN-1 and MAB-5 function in the same pathway. To confirm the order of genes in the pathway, we tested the effect of *mab-5* gain of function; *sdn-1* loss of function mutants. In a *mab-5* gain of function background, MAB-5 is ectopically expressed in the AQR and directs it posterior. When the SDN-1 signal is lost in a MAB-5 gain of function background, the percentage of AQR defects resemble that observed in a *sdn-1* mutant background alone. This suggests that SDN-1 functions downstream of MAB-5 and MAB-5 negatively regulates SDN-1's role in posterior migration.

HSPGs are normally modified with the aid of epimerases and sulfotransferases depending on its functional context (Lindahl et al., 1998; Rhiner et al., 2005). We isolated a mutation in *hse-5* in a screen performed to identify mutations that disrupted both QR and QL migrations. HSE-5 is a C-5 epimerase that is known to modify HSPGs (Lindahl et al., 1998; Rhiner et al., 2005). We wanted to see if *hse-5* could be interacting with *sdn-1* and modify it specific for its anterior AQR directing function. So we analyzed *hse-5; sdn-1* double mutants and quantified a significant increase in the percentage of AQR and PQR defects when compared to the single mutants alone. This suggests that HSE-5 is not modifying SDN-1 directly but is possibly modifying another HSPG acting redundant to SDN-1. Also, mutations in *hse-5* affect the early Q neuroblast migration that is not seen in a *sdn-1* mutant background suggesting that HSE-5 might have SDN-1 independent functions in the Q neuroblasts.

The Q cells that are born in the left-right region of the worm display some inherent asymmetries like the sensitivity of QL descendants to the EGL-20 derived MAB-5 signal. However, we are still in the process of identifying genes

that contribute to this left-right asymmetry. So far, our results suggest that SDN-1 and MIG-13 also contribute to this asymmetry by specifically directing anterior guidance of QR descendants. Through our genetic analysis, we hope to understand how these genes interact with one another. We have uncovered interactions between the posterior signaling system MAB-5 and the anterior guidance system SDN-1 and MIG-13, where MAB-5 regulates the response of cells to SDN-1 and MIG-13. Together, our results suggest that the left-right asymmetry in these cells is due to a combination of intersecting signaling pathways that we are just beginning to uncover.

4.3. Materials and Methods

***C. elegans* genetics.** All experiments were conducted at 20° C using standard *C. elegans* techniques (Sulston and Hodgkin, 1988). The following strains and transgenes were used: LGIII *hse-5(ok2463)*, *hse-5(lq49)*, *hse-5(tm472)*, *mab-5(e1239), mab-5(gk670), mab-5(e1751);* LG IV *lqIs80[Pscm::gfp::caax];* LGV *lqIs58[Pgcy-32::cfp];* LGX *sdn-1(zh20), sdn-1(ok244), mig-13(mu225).* The chromosomal locations for the following transgene was not assigned: *[Pscm::SDN-1cDNA].* Transgenes were constructed using the standard gonadal microinjection techniques to produce extra-chromosomal arrays (Mello and Fire, 1995).

Plasmids. The plasmid injected used to produce the rescue construct *scm::SDN-1cDNA* was a gift from Dr. Martin Hudson (Kennesaw state university). It contains the entire SDN-1 cDNA in a pCR8/TOPO/GW vector backbone. We have built a *scm*::SDN-1cDNA plasmid (pEL769) which is specific to the seam and Q cells.

Scoring AQR and PQR defects. Previously described quantification techniques were used (Chapman et al., 2008; Sundararajan and Lundquist, 2012). The *gcy-32:: cfp* transgene expressed in the URX, AQR and PQR neurons is used to visualize and score the final positions of AQR and PQR. The position of AQR and PQR are scored in five positions along the body of the worm (Figure 4.1A). Position 1 is the wild type position of AQR in the anterior deirid just posterior to the pharyngeal bulb. Position 2 represents the region posterior to the pharyngeal bulb and anterior to the vulva. Position 3 represents the region around the vulva. Position 4 represents the region posterior to the vulva to the posterior deird. The Q cells are born and undergo their intial polarizations and migrations in this position. Position 5 represents the region behind the anus in the phasmid ganglion, which is the wild-type position of PQR. AQR and PQR were scored and analyzed in L4 larval animals, which is after AQR and PQR undergo their final

migrations. At least 100 animals were scored for each genotype and statistical significance was determined using the Fischer Exact Test.

Scoring early QR and QL defects. Previously described larval synchronization techniques were used (Chapman et al., 2008; Dyer et al., 2010; Sundararajan and Lundquist, 2012). All adult and larval worms were washed from plates using M9 buffer when the eggs remain adhered to the plates. These eggs were allowed to hatch and the larvae were collected every half an hour. So all the larvae were collected between 0-0.5 hours after hatching. The larvae were then staged and visualized at 2-2.5, 3-3.5 and 4-4.5 hours post hatching using the *Pscm::gfp::caax* transgene. The wild-type larvae were visualized at 2-2.5 hours post hatching and they exhibited defined anterior QR protrusions and posterior QL protrusions. These protrusions extended over the seam cells V4 and V5 respectively. At about 3-3.5 hours post hatching QR and QL follow the protrusions and migrate on top of the seam cells. QR migrates anterior on the seam cell V4 and QL migrates posterior on the seam cell V5. The larvae visualized at 4-4.5 hours post hatching showed QR and QL undergoing their first round of division. QR divides on V4 and QL divides on V5. Defects in direction of protrusion, migration and division stages were scored for all the genotypes. QR that protruded, migrated and divided posterior on the seam cell V5 were scored as defective. QL that protruded, migrated and divided anterior on the seam cell V4 were scored as defective. However, the defects observed in QR and QL at 4-4.5 hours post hatching were represented in Figure 4.4. Previous work has shown that the defects seen in protrusion and migration stages do not differ significantly from the division stage. At least 25 cells were scored for each genotype and statistical significance was determined using the Fischer Exact Test.

4.4 Results

SDN-1 and MIG-13 are required for anterior QR descendant migration:

Previous work characterized MIG-13 in anterior QR descendant migration (Sym et al., 1999; Wang et al., 2013). In a *mig-13(mu225)* (Figure 4.1A) mutant background, we observed about 45% of AQR failed to reach its wild-type position (Figure 4.1C). AQR and PQR are descendants of QR and QL respectively, and migrate the farthest from their birthplace. AQR migrates anterior to the anterior deirid near the pharyngeal bulb and PQR migrates posterior into the phasmid ganglion behind the anus. To understand anterior guidance further, we wanted to identify new genes that direct anterior AQR migration. Heparan sulfate proteoglycans have a well-characterized role in axon pathfinding and cell migrations (Hudson et al., 2006; Minniti et al., 2004; Rhiner et al., 2005; Schwabiuk et al., 2009). We wanted to analyze the effect of all the *C. elegans* HSPGs in AQR and PQR migrations. Our observations showed that mutations in *glp-2/Glypican*, *lon-2* and *unc-52/Perlecan* did not affect AQR (Figure 4.1B) or PQR migrations (data not shown). However, mutations in *sdn-1/Syndecan* affect the extent and direction of AQR migration. In a *sdn-1* mutant background, AQR does not migrate all the way to its wild-type position in about 21% of the animals and it migrates posterior to the wild-type position of PQR in about 3% of the animals suggesting that SDN-1 is required for proper anterior AQR migration (Figure 4.1C). However, we observed that mutations in *sdn-1* did not disrupt PQR migration (data not shown).

The two well characterized mutant alleles of *sdn-1*, *zh20* and *ok244* (Rhiner et al., 2005) are large deletions that affect exons 1-5 and exons 2 and 3 respectively (Figure 4.1A). *zh20* is a characterized null mutant but *ok244* is thought to function as a hypomorph (Rhiner et al., 2005). However, for all our observed phenotypes we saw similar trend in the percentage of defects in both the mutant backgrounds. In sum, we have identified a new gene that has a role in the anterior guidance of AQR.

SDN-1 and MIG-13 function redundantly in directing anterior AQR migration:

Our work has shown that mutations in *mig-13* and *sdn-1* affect anterior AQR migration (Figure 4.1C). Thus, MIG-13 and SDN-1 are required for anterior AQR migration. However, they do not seem to be required for PQR migration, as mutations in *sdn-1* and *mig-13* do not disrupt the direction or extent of PQR migrations (data not shown). To understand how these genes interact to direct anterior AQR migration, we built double mutants. In a *sdn-1; mig-13* double mutant we observed a significant decrease ($p < 0.0001$) in the percentage of AQR (24%) that migrate to the wild-type position when compared to each of the single mutants (~75%) (Figure 4.2A). This suggests that MIG-13 and SDN-1 are functioning redundantly to direct anterior AQR migration.

As we mentioned earlier single mutations in *sdn-1* and *mig-13* do not disrupt PQR migrations. However, in a *sdn-1; mig-13* double mutant background we observed 14% of PQR displaced from its wild type position (Figure 4.2B). This result suggests that MIG-13 and SDN-1 could be required redundantly to direct posterior PQR migrations. Previous work has shown that MIG-13 is required autonomously in QR descendants to direct their anterior migration (Wang et al., 2013). However, its role in posterior PQR migration has not been identified. It is possible this is a non-autonomous role of MIG-13 as MIG-13 is expressed in the motor neuronal cells suck as DD4 and DA9 (Sym et al., 1999). DD4 is close to the birthplace of the Q cells and DA9 is close to the final position of PQR. It is possible that in the absence of both SDN-1 and MIG-13 signals, PQR loses some of its posterior migratory potential and remains at its birthplace and in some cases even migrates anterior.

MIG-13 functions downstream of MAB-5 in directing PQR migrations:

Previous work has shown that MAB-5/Hox restricts MIG-13 expression to the anterior and central regions of the worm (Sym et al., 1999; Wang et al., 2013). In a *mab-5* loss of function background, MIG-13 is ectopically expressed

in the posterior of the worm, and in a *mab-5* gain of function background (Hedgecock et al., 1987), MIG-13 is expressed exclusively in the anterior regions of the worm (Sym et al., 1999). MAB-5/Hox expression is cell autonomously required to direct posterior QL descendant migration (Kenyon, 1986). In a *mab-5* loss-of-function background, both AQR and PQR migrate anterior to the wild-type AQR position (Figure 4.3). In a *mig-13; mab-5* double mutant background, the trend of defects in AQR is similar to that of *mig-13* and the percentage of defects is not significantly different from that observed in a *mig-13* background alone (Figure 4.3). This result is not surprising, as MAB-5 does not have a role in directing anterior AQR migration and hence the defects in a *mig-13; mab-5* double mutant background resembles that of *mig-13* alone (Figure 4.3A). In a *mig-13; mab-5* double mutant background there is a significant suppression ($p < 0.0001$) in the percentage of anterior migrating PQR when compared to a *mab-5* loss of function background alone (Figure 4.3A). These results show that in the absence of MAB-5, the deficits in PQR migration are both in direction and extent. This suggests that MAB-5 functions upstream of MIG-13 inhibiting its posterior expression. In a *mab-5* loss of function background, MIG-13 is free to be expressed in the posterior region of the worm and direct anterior PQR migration. However, in a *mig-13; mab-5* double mutant background, the anterior PQR migration is disrupted (Figure 4.3B).

SDN-1 functions downstream of MAB-5 in directing PQR migrations:

Now, we wanted to see if SDN-1 could function in a similar manner downstream of MAB-5. In AQR, *mab-5; sdn-1* double mutants showed a trend in defects that are not dissimilar to that observed in a *sdn-1* mutant background (Figure 4.3A). This suggests that the genetic relationship between MAB-5 and SDN-1 is similar to that between MAB-5 and MIG-13 i.e., since MAB-5 does not function in directing AQR migration, the absence of *sdn-1* disrupts anterior AQR migration. In a *mab-5* gain of function background, MAB-5 is ectopically expressed in AQR, which directs AQR posterior to the wild type position of PQR. In a *mab-5* gain of function; *sdn-1* loss of function double mutant background,

there is a significant decrease in the percentage of posterior migrating AQR observed in a *mab-5* gain of function background (Figure 4.3A). This result suggests that SDN-1 functions genetically downstream of MAB-5, and MAB-5 normally restrict the function SDN-1 in posterior migration. In PQR, *mab-5; sdn-1* loss of function double mutants showed a significant decrease in anterior PQR migration when compared to *mab-5* loss of function mutants alone (Figure 4.3B). And, in a *mab-5* gain of function; *sdn-1* loss of function double mutant background, there is a significant percentage of PQR migrating anterior when compared to *mab-5* gain of function and a *sdn-1* loss of function background alone (Figure 4.3B). The anterior PQR migration observed in a *mab-5* gain of function; *sdn-1* background resembles that observed in a *sdn-1; mig-13* double mutant (Figure 4.2B). It is possible that MIG-13 is required non-cell autonomously to direct posterior PQR migration along with SDN-1 and in a *mab-5* gain of function background MIG-13 is completely suppressed in the posterior region essentially functioning as a *mig-13* loss of function scenario. Hence, in a *mab-5* gain of function; *sdn-1* loss of function background, PQR migrates anterior as the posterior environment resemble that of a *sdn-1; mig-13* double mutant background (Figure 4.2B). In sum, the above results shows that SDN-1 functions downstream of MAB-5, and MAB-5 inhibits the posterior function of SDN-1.

HSE-5 could be functioning redundant with SDN-1 in directing anterior AQR migration:

HSE-5 is a C-5 epimerase that has been shown to modify the HS side chains of HSPGs depending on the cellular context (Lindahl et al., 1998; Rhiner et al., 2005). Previous work has shown that in axon pathfinding and cell migration HSE-5 functions possibly with other HSPGs redundantly with SDN-1 (Rhiner et al., 2005). We isolated a novel mutation *lq49* of *hse-5* in an EMS (ethyl methyl sulfonate) screen performed to identify new mutations in genes required for AQR and PQR migrations. Mutations in *hse-5* including *lq49* and previously characterized null mutations *ok2463* and *tm472* disrupted the direction and extent of both AQR and PQR migrations (Figure 4.5). This indicates that HSE-5

is required for directional AQR and PQR migrations. Also, mutations in *hse-5* disrupt early QR and QL migrations. In a *hse-5* mutant background, QR migrates posterior (~30%) and QL migrates anterior (~5%) (Figure 4.4). As we mentioned earlier, mutations in *sdn-1* do not disrupt the direction of early QR and QL migrations (Figure 4.4). Hence, it is possible that HSE-5 has SDN-1 independent roles in directing early QR and QL migrations. To understand whether *hse-5* and *sdn-1* could work together in directing AQR and PQR migrations, we built *hse-5; sdn-1* double mutants and looked at the final positions of AQR and PQR (Figure 4.5). In a *hse-5; sdn-1* double mutant background, we observed a significant increase in the percentage of migration defects in both AQR and PQR when compared to the single *hse-5* and *sdn-1* mutant backgrounds (Figure 4.5). Our results suggest that HSE-5 and SDN-1 function in redundant pathways to direct Q descendant i.e., AQR and PQR migrations. It is possible that HSE-5 modulates another HSPG in a redundant pathway to SDN-1 in AQR and PQR. Our results also show that HSE-5 could possibly be performing functions distinctly different from that of SDN-1 alone.

SDN-1 could be functioning cell autonomously to direct AQR migrations:

Our results so far have implicated SDN-1 in directing AQR migration. It is also possible that SDN-1 functions redundantly with other genes in directing PQR migrations. To test whether SDN-1 is required in the Q cells to direct their migrations, we carried out functional analyses using a construct built with a cell specific promoter (*Pscm*) driving SDN-1 cDNA. We built the cell specific construct in a *sdn-1* mutant background. We observed that the cell specific construct was capable of significantly rescuing the AQR migration defects seen in a *sdn-1* mutant background (Figure 4.6). This result strongly suggests that SDN-1 is required in the Q cells to direct their migrations. We also saw that the transgene disrupted PQR migration in a *sdn-1* mutant background. This could be explained by a possible over expression artifact of the rescuing transgene.

In sum, we have shown that SDN-1 is required cell autonomously to direct anterior AQR migrations and it possibly functions downstream of MAB-5/Hox with

MAB-5 regulating its posterior function. SDN-1 acts redundantly with MIG-13 and possibly HSE-5 to direct anterior AQR migrations. SDN-1 could also be functioning in some capacity to direct posterior QL descendant migrations possibly redundantly with other HSPGs and MIG-13.

4.5 Discussion:

Heparan sulfate proteoglycans (HSPGs) have been implicated considerably in nervous system development (Bulow et al., 2002; Hudson et al., 2006; Johnson et al., 2006; Minniti et al., 2004; Rhiner et al., 2005; Schwabiuk et al., 2009). The two classes of HSPGs, the Syndecans and Glypicans, are known to regulate cell migration and axon pathfinding in the nervous system (Hudson et al., 2006; Rhiner et al., 2005). In *C. elegans*, SDN-1 is the only Syndecan encoded by the genome (Rhiner et al., 2005). Previous work has shown that SDN-1 is required to direct neuronal cell migration including HSN, CAN and ALM neurons (Rhiner et al., 2005). It is also required for proper axon pathfinding (Rhiner et al., 2005). Heparan sulfate proteoglycans have heparan side chains that require modifications in a function dependent manner (Lindahl et al., 1998). SDN-1 interacts with HS modifying genes in a functional context dependent manner (Lindahl et al., 1998; Rhiner et al., 2005). HSE-5, a C-5 epimerase is thought to function independent of SDN-1 possibly modulating a different HSPG in a parallel pathway to SDN-1 (Rhiner et al., 2005). Here we show that SDN-1 is required for proper extent and direction of migration of QR descendant AQR, and HSE-5 functions redundantly with SDN-1 possibly modulating a different HSPG in a parallel pathway. *sdn-1* mutants show extensive defects in anterior QR descendant migration (Figure 4.1C), both extent and direction of migration and the percentage of defects is significantly enhanced in *hse-5; sdn-1* double mutants (Figure 4.5).

We also show that the posterior function of SDN-1 is negatively regulated by MAB-5/Hox. Wnts are required posterior QL descendent migration (Chalfie, 1993; Eisenmann, 2005; Harris et al., 1996; Herman, 2001; Kenyon, 1986; Whangbo and Kenyon, 1999). EGL-20/Wnt activates MAB-5/Hox expression in the QL descendants (PQR) to cause posterior migration (Kenyon, 1986; Maloof et al., 1999; Whangbo and Kenyon, 1999). We observed a significant suppression of anterior PQR migration in a *mab-5; sdn-1* double mutant background. Also, *sdn-1* mutants significantly suppress the posterior AQR

migration seen in a *mab-5* gain of function background suggesting that SDN-1 functions downstream of MAB-5/Hox, and MAB-5 possibly inhibits the posterior function of SDN-1 (Figure 4.3). Our results also show that SDN-1 functions redundantly with MIG-13, a transmembrane protein that has been implicated in anterior QR descendant migrations. Posterior expression of MIG-13 is restricted by MAB-5/Hox to keep its expression primarily in the anterior and central regions of the worm.

SDN-1/Syndecan acts in parallel to MIG-13 to direct anterior QR descendent migrations: Previous work showed that SDN-1 is required to direct neuronal cell migrations (Hudson et al., 2006; Rhiner et al., 2005; Schwabiuk et al., 2009). Mutations in *sdn-1* caused defects in proper positioning of AQR in its wild type position near the pharyngeal bulb (Figure 4.1C). Another gene shown to be required for proper AQR positioning is *mig-13* (Sym et al., 1999; Wang et al., 2013). Our results show that *sdn-1* and *mig-13* possibly function in parallel genetic pathways to direct proper anterior AQR migrations. *sdn-1; mig-13* double mutants show a significant increase in the percentage of AQR migration defects that include defects in direction and extent of migration, when compared to the single mutants alone (Figure 4.2). Previous work showed that MIG-13 acts cell autonomously to direct anterior QR descendant migration (Wang et al., 2013). However, other work also showed that MIG-13 might have some non-cell autonomous roles in Q descendant migrations (Sym et al., 1999). SDN-1 seems to function cell autonomously to direct anterior QR descendant migration (Figure 4.6). Thus, we propose a model in which MIG-13 and SDN-1 possibly function cell autonomously in parallel genetic pathways as an anterior guidance system to direct QR descendant migration. However, in a *mig-13; sdn-1* double mutant background, we observed a significant percentage of PQR migrating anterior despite no anterior PQR migration in a *mig-13* or *sdn-1* single mutant background. This result suggests that MIG-13 and SDN-1 could have role in directing posterior PQR migration. The posterior PQR migration could be an effect of the non-autonomous role of MIG-13.

MAB-5/Hox regulates the role of SDN-1 in posterior migration: Wnts have been extensively implicated in directing posterior QL descendant migrations (Chalfie, 1993; Eisenmann, 2005; Harris et al., 1996; Harterink et al., 2011; Kenyon, 1986; Korswagen et al., 2000; Whangbo and Kenyon, 1999). However, they are not required for early QL posterior migration (Chapman et al., 2008). EGL-20/Wnt turns on MAB-5 in the QL descendants after the QL neuroblast undergoes its first division to produce two daughter cells. MAB-5 is necessary and sufficient to direct posterior QL descendant migration, contributing to the inherent left-right asymmetry of the QR and QL descendants. Previous work has shown that the posterior expression of MIG-13 is controlled by MAB-5/Hox, and MIG-13 is genetically placed downstream of MAB-5/Hox (Sym et al., 1999; Wang et al., 2013). We wanted to see if SDN-1 has a similar genetic interaction to MAB-5. Our results showed that mutations in *sdn-1* suppress the anterior PQR migration seen in a *mab-5* loss of function background. In a *mab-5* loss of function background QL undergoes an initial wild-type posterior migration but QL descendants no longer have a posterior migratory signal and hence migrate anterior. In the absence of MAB-5, SDN-1 is free to direct anterior PQR migration, suggesting that MAB-5 normally inhibits SDN-1 in PQR to drive its migration posterior. Mutations in *sdn-1* also suppress the posterior AQR migration seen in a *mab-5* gain of function background placing SDN-1 downstream of MAB-5 in a genetic pathway. A *sdn-1; mab-5* gain of function background also caused PQR to migrate anterior (Figure 4.3). This result could be explained by a possible non-autonomous role MIG-13 could have in directing posterior PQR migration. In a *mab-5* gain of function background MIG-13 is expressed exclusively in the anterior regions of the worm, simulating a *mig-13* loss of function background in the posterior region, thus causing PQR to migrate anterior as observed in a *sdn-1; mig-13* double mutant background.

SDN-1 functions independent of HSE-5 directed modifications in anterior AQR migration: Previous work has shown that HSPGs undergo HS side chain modifications in a cellular context dependent manner (Lindahl et al., 1998; Rhiner

et al., 2005). We isolated mutations in *hse-5* in a screen performed to identify novel mutations in genes that affect Q descendant i.e., AQR and PQR migrations. HSE-5 is a C-5 epimerase that is known to modify HS side chains of HSPGs (Lindahl et al., 1998). So we wanted to check whether *hse-5* could be functioning with *sdn-1* in directing anterior QR descendant migrations. We analyzed *sdn-1; hse-5* double mutants and observed a significant increase in the percentage of AQR and PQR migration defects when compared to the single mutants suggesting that HSE-5 and SDN-1 function in parallel pathways to direct Q descendant migration (Figure 4.5). Mutations in *hse-5* disrupt the direction of early QR and QL as well as QR and QL descendant migrations. Mutations in *sdn-1* do not disrupt early QR and QL migrations, and *hse-5; sdn-1* double mutants do not significantly differ from the early QR and QL defects seen in a *hse-5* single mutant (Figure 4.4). These results suggest that HSE-5 might have SDN-1 independent roles in Q neuroblast migrations in addition to the redundant function in AQR migration.

SDN-1 acts cell autonomously: MIG-13 is required in the Q cells to direct its migration. To understand whether SDN-1 was also required in the Q cells to direct their migrations, we used a cell specific promoter *scm* that is expressed in the seam cells and the Q cells. The cell specific construct *scm*:: SDN-1 is capable of rescuing defects seen in a *sdn-1* mutant background (Figure 4.6). This result suggests that SDN-1 is acting cell autonomously to direct anterior QR descendant migrations.

In sum, we are beginning to understand the nature of signaling pathways required to direct anterior versus posterior Q descendant migrations. Our results so far show that the genes that contribute toward the inherent left-right asymmetry between QR and QL interact in distinct genetic pathways. The genes, *sdn-1* and *mig-13,* that are required to direct anterior migrations are regulated by *mab-5* that directs posterior migration. It is interesting to understand how these signaling pathways intersect despite their opposing roles (anterior versus posterior) in migration. These studies will be a step toward understanding the

complexity of genetic pathways directing neuronal cell migration in a vertebrate system.

Figure 4.1.

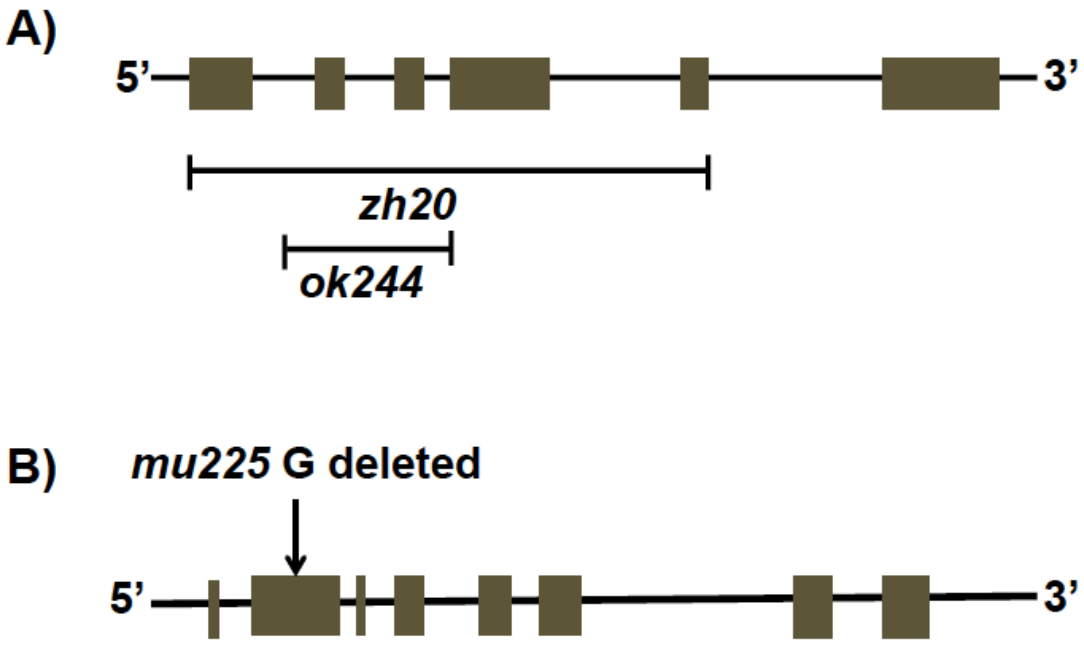

Figure 4.1.

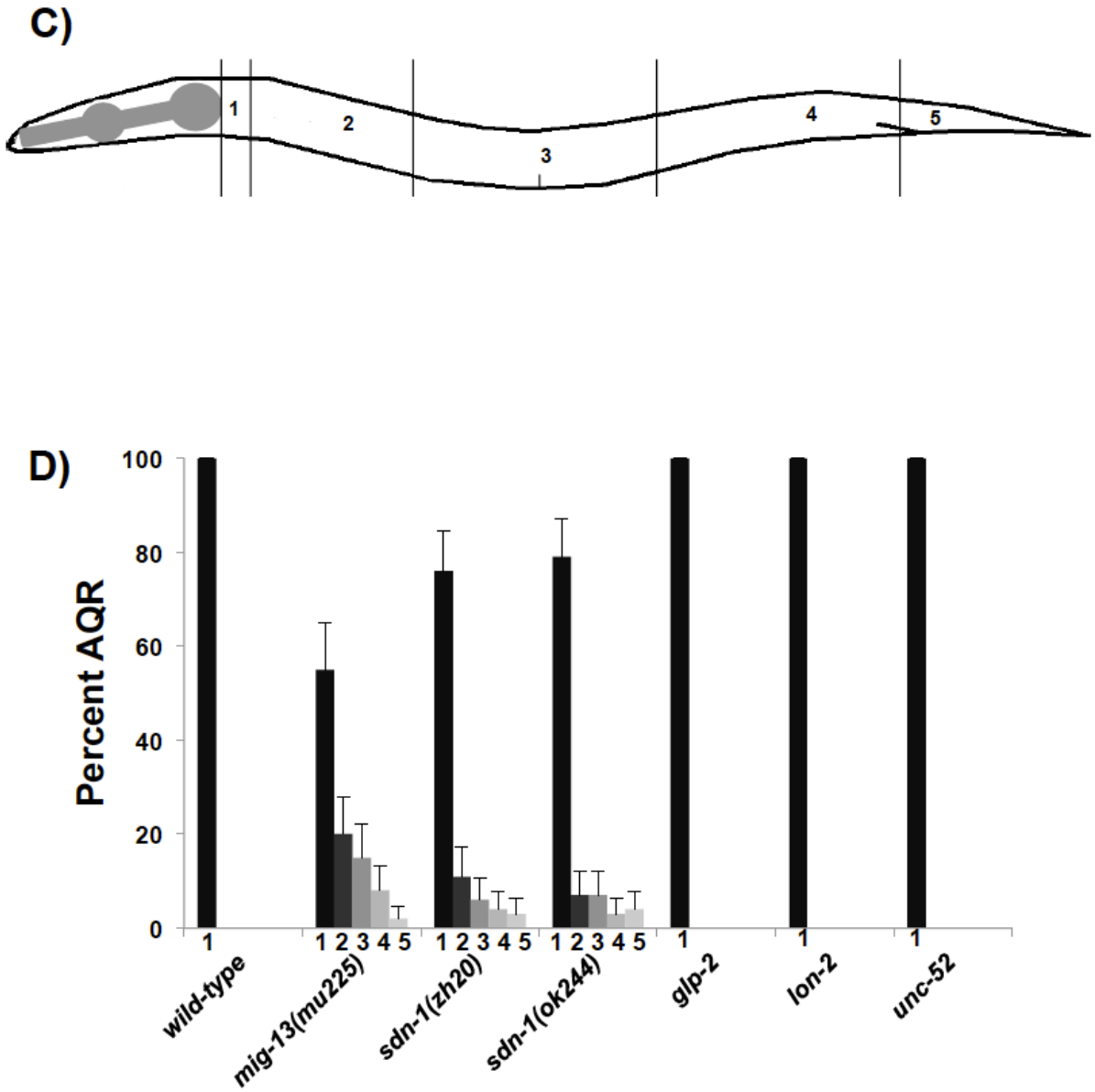
C)
1
2
3
4
5
D)
Percent AQR
100
80
60
40
20
0
1
1 2 3 4 5
1 2 3 4 5
1 2 3 4 5
1
1
1
wild-type
mig-13(mu225)
sdn-1(zh20)
sdn-1(ok244)
glp-2
lon-2
unc-52

Figure 4.1. AQR migration defects in single mutants: A) A diagram that represents the genomic region of *sdn-1* with its exons indicated by boxes and introns by lines connecting the boxes. Positions of deletions are marked for both the alleles. *zh20* is a deletions that spans across 5 exons and *ok244* spans across 2 exons. B) A diagram that represents the genomic region of *mig-13* with its exons indicated by boxes and introns by lines. Position of the lesion *mu225* is indicated with information that the mutation is a deletion of G nucleotide that encodes for a premature stop. C) A diagram represents the scoring positions used in figure 4.1B, 4.2, 4.3, 4.4, 4.5, 4.6 and 4.7.). Position 1 is the normal final position of AQR near the anterior deirid ganglion, and position 5 is the normal final position of PQR behind the anus in the phasmid ganglion. The position 4 represents the approximate birthplace of the Q neuroblasts. Position 3 is proximate to the vulva, and position 2 is anterior to the vulva but still posterior to the anterior deirid ganglion. D) The X-axis of the graph represents genotypes and the Y-axis represents the percentage of AQR neurons in each of the 5 positions (1 2 3 4 5) along the anterior-posterior as described in Figure 4.1A. Scale bars represent 2x standard error of the proportion, and significances of difference indicated were determined using the Fisher Exact test. At least 100 animals of each genotype were scored.

Figure 4.2.

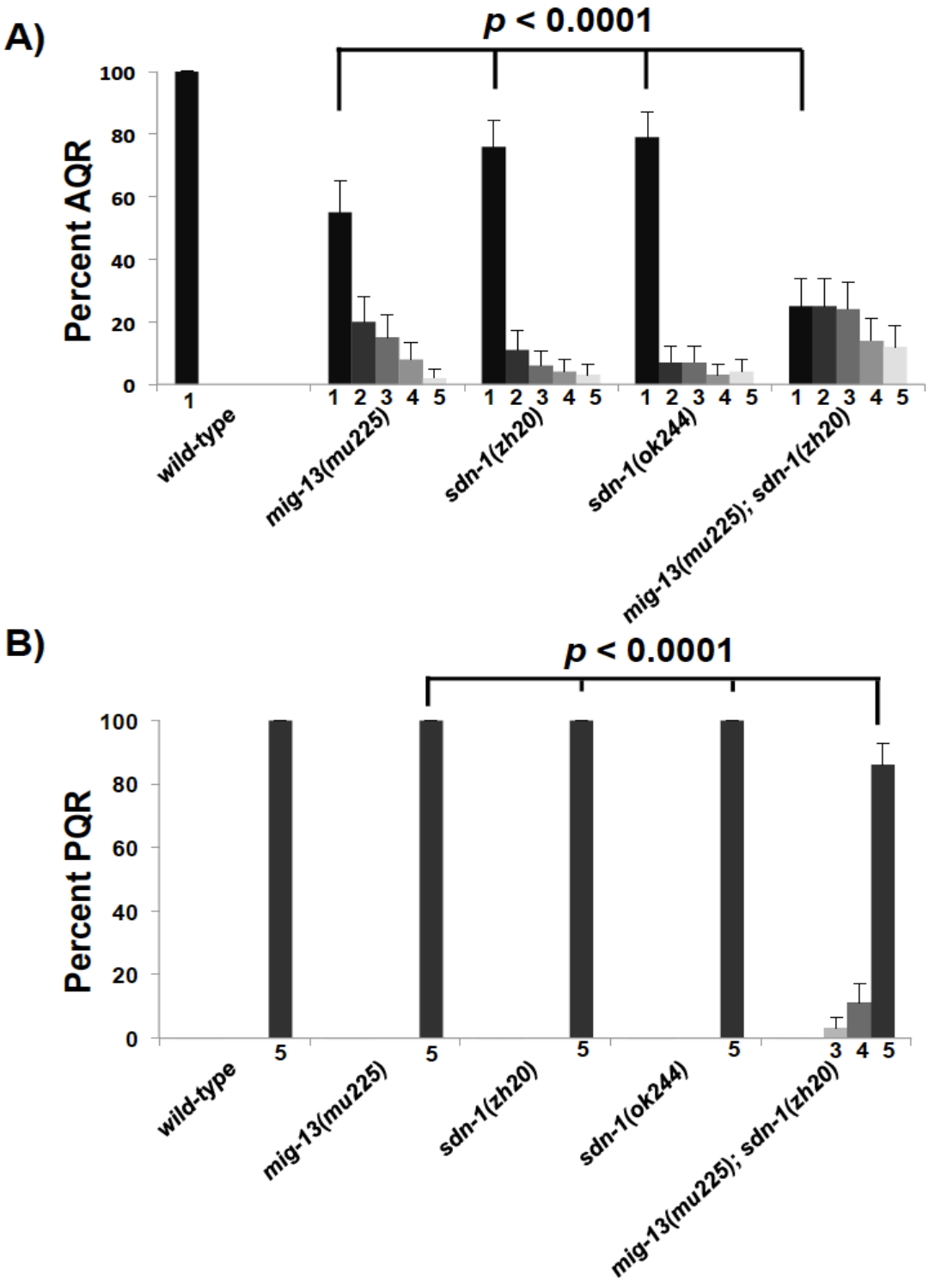
A)
p < 0.0001
Percent AQR
100
80
60
40
20
0
1
1 2 3 4 5
1 2 3 4 5
1 2 3 4 5
1 2 3 4 5
wild-type
mig-13(mu225)
sdn-1(zh20)
sdn-1(ok244)
mig-13(mu225); sdn-1(zh20)
B)
p < 0.0001
Percent PQR
100
80
60
40
20
0
5
5
5
5
3 4 5
wild-type
mig-13(mu225)
sdn-1(zh20)
sdn-1(ok244)
mig-13(mu225); sdn-1(zh20)

Figure 4.2. AQR and PQR migration defects in *sdn-1* and *mig-13* single and double mutants: These graphs represent the final positions of AQR and PQR neurons along the regions 1,2,3,4 and 5 as mentioned in figure 4.1A. The X-axis and Y-axis represent the same as Figure 4.1B. The statistical difference between the single and double mutants were determined using the Fischer Exact test and indicated on top of lines connecting the compared genotypes. The scale bars represent two times the standard error of proportion. At least 100 animals of each genotype were scored.

Figure 4.3.

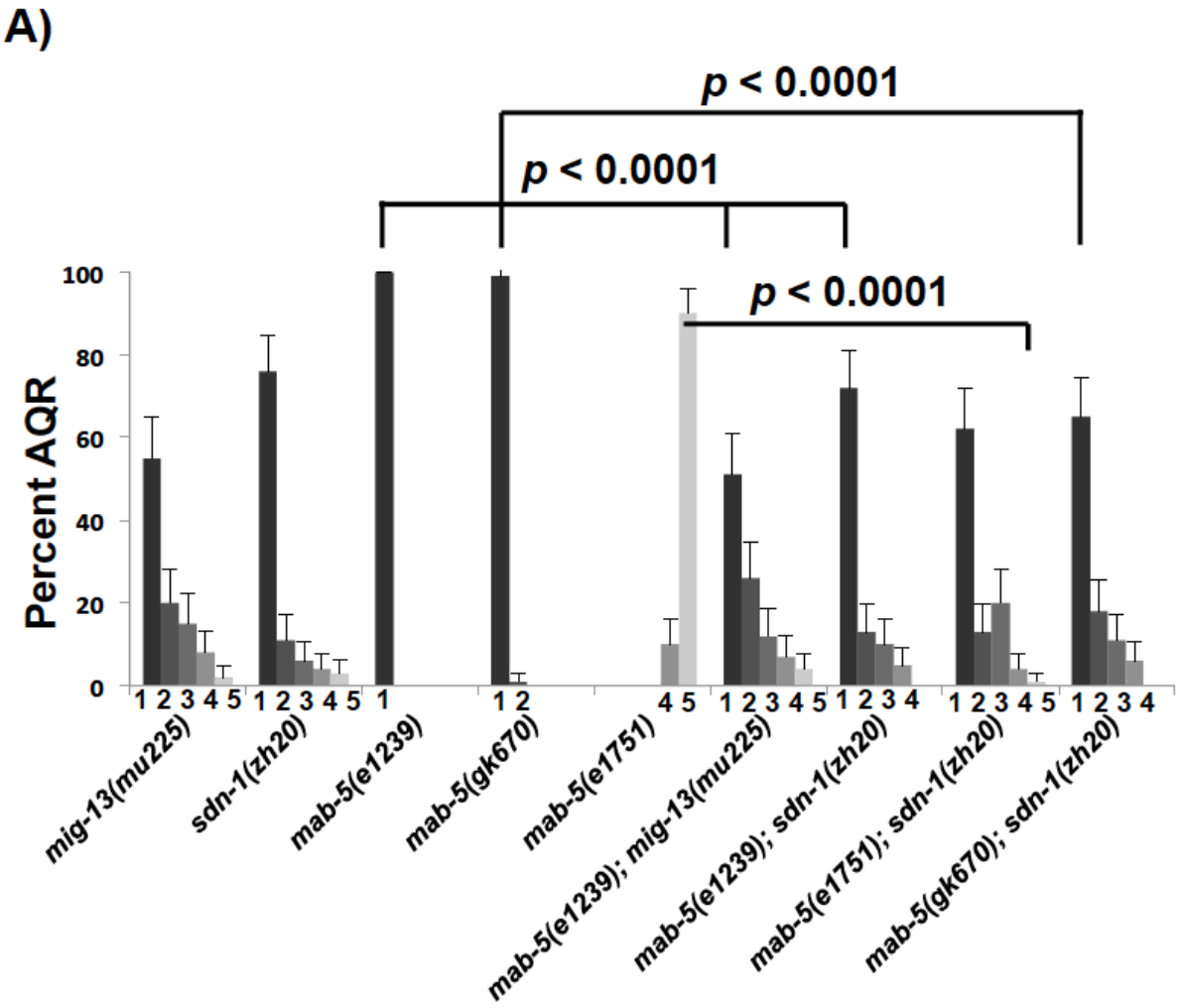
A)
p < 0.0001
p < 0.0001
p < 0.0001
Percent AQR
100
80
60
40
20
0
1 2 3 4 5
1 2 3 4 5
1
1 2
4 5
1 2 3 4 5
1 2 3 4
1 2 3 4 5
1 2 3 4
mig-13(mu225)
sdn-1(zh20)
mab-5(e1239)
mab-5(gk670)
mab-5(e1751)
mab-5(e1239); mig-13(mu225)
mab-5(e1239); sdn-1(zh20)
mab-5(e1751); sdn-1(zh20)
mab-5(gk670); sdn-1(zh20)

Figure 4.3.

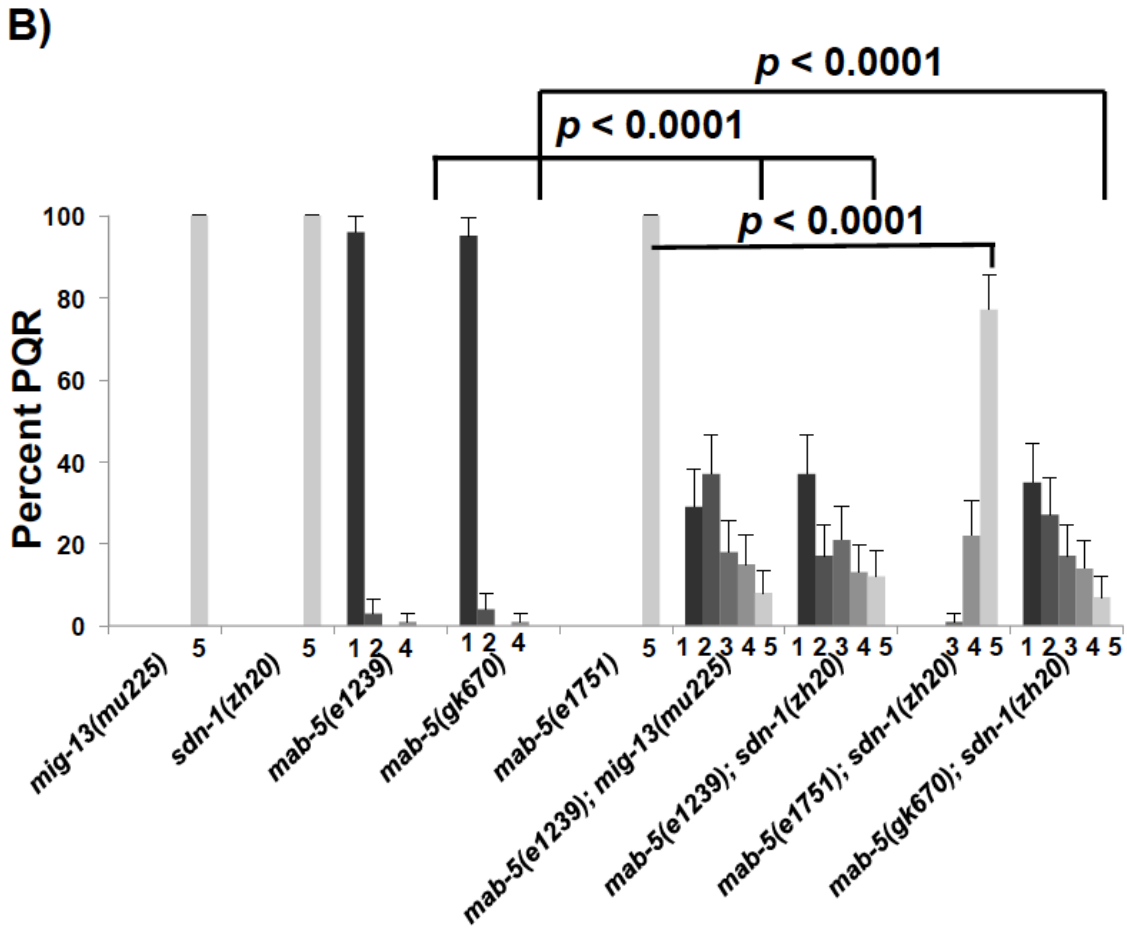
B)
p < 0.0001
p < 0.0001
p < 0.0001
Percent PQR
100
80
60
40
20
0
5
5
1 2 4
1 2 4
5
1 2 3 4 5
1 2 3 4 5
3 4 5
1 2 3 4 5
mig-13(mu225)
sdn-1(zh20)
mab-5(e1239)
mab-5(gk670)
mab-5(e1751)
mab-5(e1239); mig-13(mu225)
mab-5(e1239); sdn-1(zh20)
mab-5(e1751); sdn-1(zh20)
mab-5(gk670); sdn-1(zh20)

Figure 4.3. AQR and PQR migration defects in *sdn-1*, *mig-13* and *mab-5* single and double mutants: These graphs are structured similar to 4.1B and 4.2. A) Represents the percent AQR in their positions (1 2 3 4 5) B) Represents the percent PQR in their final positions (1 2 3 4 5). The statistical difference between the single and double mutants were determined using the Fischer Exact test and indicated on top of lines connecting the compared genotypes. The scale bars represent two times the standard error of proportion. At least 100 animals of each genotype were scored.

Figure 4.4.

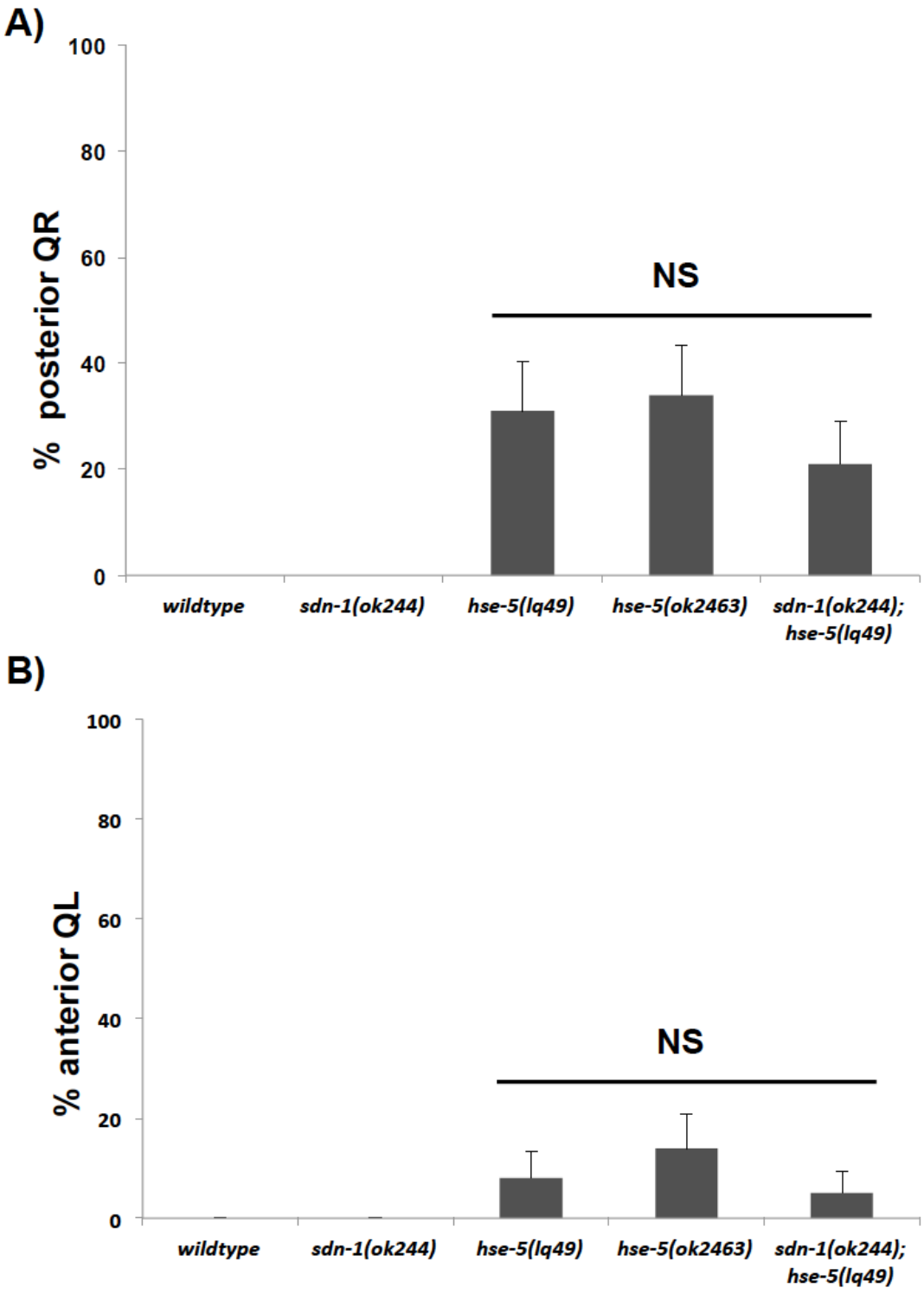
A)
100
80
60
40
20
0
% posterior QR
NS
wildtype
sdn-1(ok244)
hse-5(lq49)
hse-5(ok2463)
sdn-1(ok244); hse-5(lq49)
B)
100
80
60
40
20
0
% anterior QL
NS
wildtype
sdn-1(ok244)
hse-5(lq49)
hse-5(ok2463)
sdn-1(ok244); hse-5(lq49)

Figure 4.4. Quantification of early QR and QL defects in *sdn-1* and *hse-5* single and double mutants: Graphs represent the division stage of QR and QL at 4-4.5 hours post hatching. Genotype is on the X-axis and the percentage of defective posterior QR and anterior QL migration and division is the Y-axis. Migration was scored as defective when QR divided posterior on the seam cell V5 and when QL divided anterior on the seam cell V4. The error bars represent two times the standard error of proportion, and the statistical difference between the genotypes were determined by Fisher's Exact test. Twenty-five animals or more were scored for each genotype. A) QR defects in *sdn-1*, *hse-5* and the double mutants. B) QL defects in *sdn-1, hse-5* and the double mutants.

Figure 4.5.

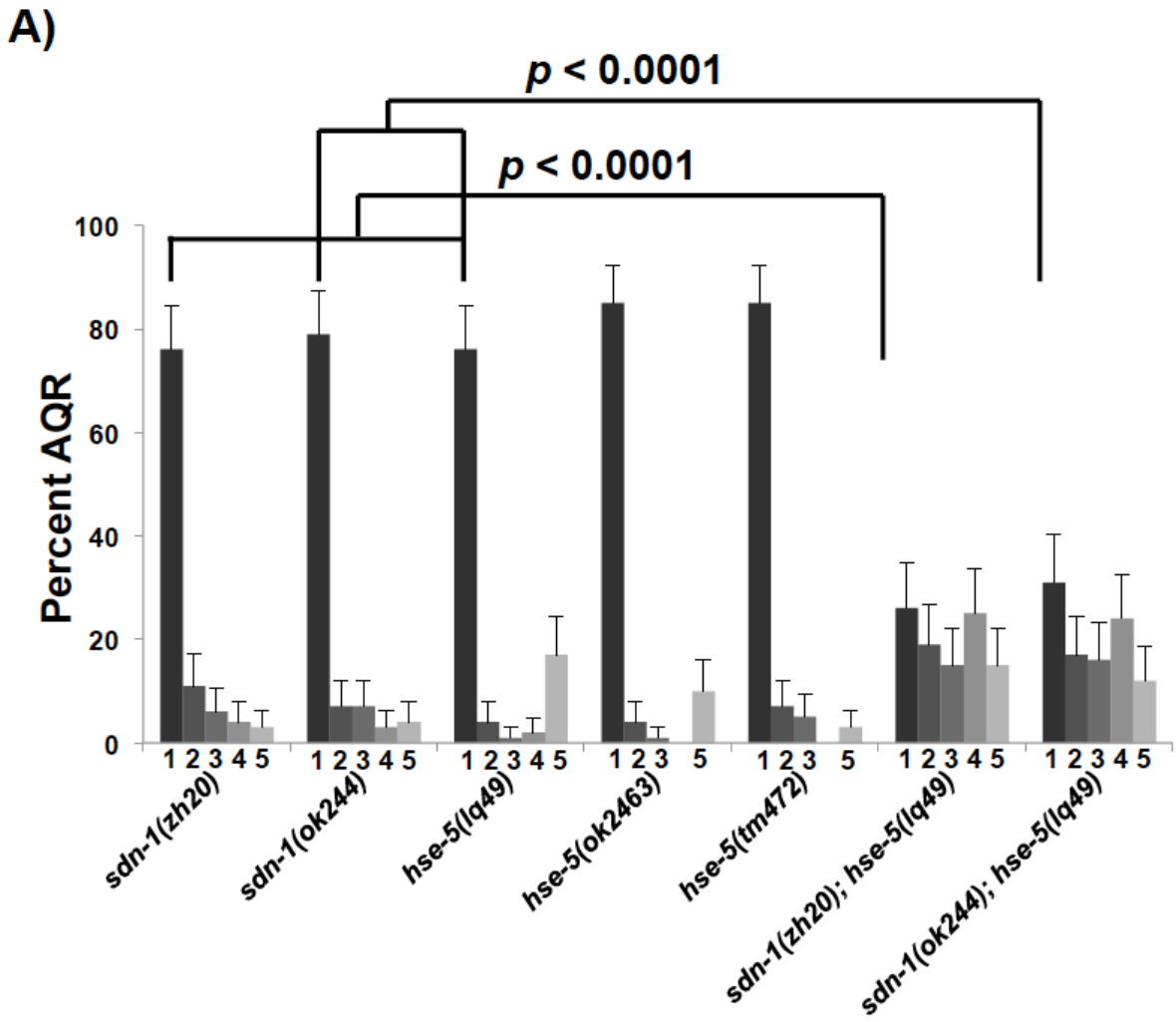
A)
p < 0.0001
p < 0.0001
Percent AQR
100
80
60
40
20
0
1 2 3 4 5
sdn-1(zh20)
sdn-1(ok244)
hse-5(lq49)
hse-5(ok2463)
hse-5(tm472)
sdn-1(zh20); hse-5(lq49)
sdn-1(ok244); hse-5(lq49)

Figure 4.5.

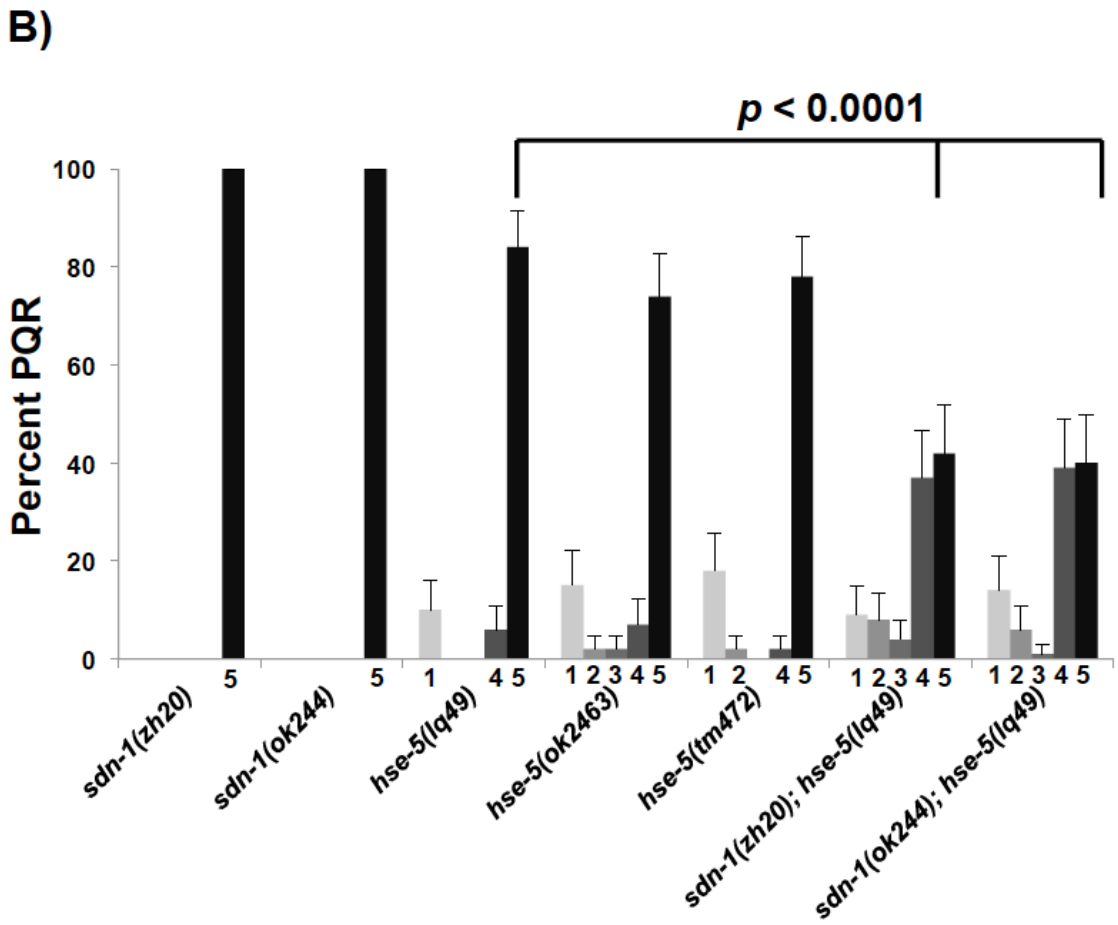
B)
p < 0.0001
Percent PQR
100
80
60
40
20
0
5
5
1
4 5
1 2 3 4 5
1 2
4 5
1 2 3 4 5
1 2 3 4 5
sdn-1(zh20)
sdn-1(ok244)
hse-5(lq49)
hse-5(ok2463)
hse-5(tm472)
sdn-1(zh20); hse-5(lq49)
sdn-1(ok244); hse-5(lq49)

Figure 4.5. Quantification of AQR and PQR defects in *sdn-1* and *hse-5* single and double mutants: Graph represents the percentage of defective AQR and PQR in *sdn-1* and *hse-5* single and double mutants. The genotypes are listed as X-axis and the percent of AQR in positions 1, 2, 3, 4 and 5 are represented in the Y-axis. The error bars represent two times the standard error of proportion, and the statistical difference between the genotypes were determined by Fisher's Exact test. At least a 100 animals were scored for each genotype.

Figure 4.6.

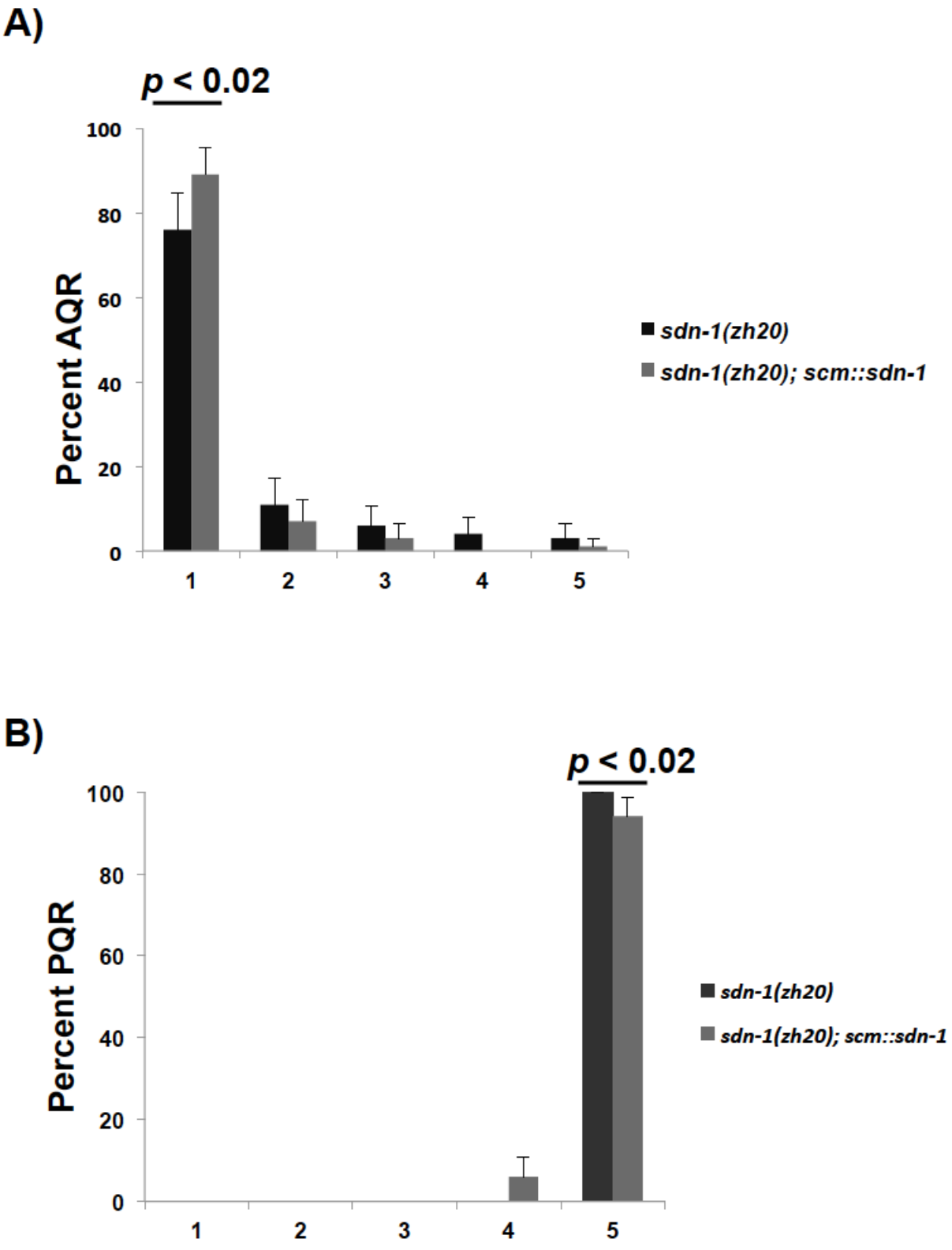
A)
p < 0.02
Percent AQR
100
80
60
40
20
0
1
2
3
4
5
sdn-1(zh20)
sdn-1(zh20); scm::sdn-1
B)
p < 0.02
Percent PQR
100
80
60
40
20
0
1
2
3
4
5
sdn-1(zh20)
sdn-1(zh20); scm::sdn-1

Figure 4.6. Cell specific rescue of a *sdn-1* mutant background using a *scm:: sdn-1* transgene: The X-axis shows the genotypes analyzed and the Y-axis represents the percent of AQR and PQR in positions 1, 2, 3, 4, and 5 as described in Figure 4.1A. *scm:: sdn-1* represents the transgene that consists of the *sdn-1* genomic region that is specifically expressed in the seam cells and the Q cell. Statistical significances of difference were determined by Fisher Exact analysis, and error bars represent 2x standard error of the proportion.

Chapter IV

Concluding remarks

4 Concluding remarks:

Chapter II revealed the role of transmembrane proteins UNC-40/DCC, PTP-3/LAR and MIG-21 in contributing to the inherent left right asymmetry existent in the Q neuroblasts (Sundararajan and Lundquist, 2012). The Q neuroblasts are daughters of the seam cell V5 and are born at the same time at about half hour post hatching (Chalfie and Sulston, 1981; Sulston and Horvitz, 1977). They undergo identical patterns of cell division and cell death to produce three neurons each. Despite their similarities, they posses some genetic asymmetries, that drives migration of these neuroblasts and their respective descendant neurons in opposite directions. Our work has established a genetic signaling system in QR Vs. QL with three transmembrane proteins UNC-40, PTP-3 and MIG-21. Our studies show that these transmembrane proteins interact differently in QR and in QL. In both QR and QL, our data is consistent with MIG-21 and PTP-3/LAR functioning in the same pathway. IN QL, MIG-21/PTP-3 and UNC-40 act in redundant pathways to direct posterior migration. In QR, MIG-21/PTP-3 and UNC-40 are required to direct posterior migration. However, these posterior pathways mutually inhibit each other's role to direct anterior QR migration.

Our work has helped us to start understanding the inherent differences in the genetic environment between QR and QL. Our observations have shown that despite directing identical functions in both QR and QL, UNC-40, PTP-3 and MIG-21 interact distinctly in both the cells. Hence, we wanted to identify genes in both QR and QL that might drive these distinct interactions in these cells or at least contribute to the asymmetries through interactions with our established genetic pathways. The unique nature of these genetic pathways is the mutual inhibition observed in QR but not in QL. We wanted to characterize genes that might be required to facilitate this mutual inhibition in QR.

In chapter III we identified and characterized the role of CDH-4/Fat in directing both QR and QL migrations. CDH-4 interacts distinctly with UNC-40/DCC, PTP-3/LAR and MIG-21 in QR and QL. In QL, CDH-4 function with

PTP-3 and possibly with MIG-21 in the same genetic pathway, redundantly with UNC-40 to direct posterior migrations. In QR, CDH-4 functions in both PTP-3 and UNC-40 pathways and possibly facilitates the mutual inhibition between the posterior directing pathways to direction anterior QR migrations. Here, we have identified an interaction that contributes to the asymmetries between QR and QL. CDH-4/Fat interacts with UNC-40/DCC in QR but not in QL suggesting that there is a difference in the genetic environments between QR and QL (Sundararajan et al., 2014).

Our work has also shown that UNC-40, PTP-3 and MIG-21 function cell autonomously i.e., they are required in the Q cells to direct their migrations (Sundararajan and Lundquist, 2012). However, our data is consistent with CDH-4/Fat functioning non-cell autonomously suggesting that CDH-4 was required outside the Q cells to direct their migrations (Sundararajan et al., 2014). In sum, we have characterized a novel-signaling pathway in QL Vs. QR with distinct genetic interactions between four transmembrane proteins. In QL, MIG-21, PTP-3/LAR and CDH-4/Fat possibly function in the same genetic pathway redundantly with UNC-40/DCC to direct posterior migrations. In QR, MIG-21/PTP-3 functions in parallel with UNC-40/DCC to direct posterior migrations. CDH-4/Fat functions with both MIG-21/PTP-3 and UNC-40 to direct mutual inhibition between the posterior directing pathways to direct anterior migration of QR. Hence, we have identified another player that is involved in directing the mutual inhibition in QR but not in QL thus contributing to the left-right asymmetries in the Q cells.

Our initial work has identified the role of transmembrane proteins in directing early Q neuroblast migrations and contributing to their inherent left-right asymmetries. The Q descendant neurons born from the Q neuroblasts also exhibit an anterior-posterior migratory trajectory similar to their parent cells. We were interested in characterizing the asymmetry in these descendant cells. Previous work characterized the role of MAB-5 in directing posterior QL descendant migrations (Chalfie et al., 1983; Eisenmann, 2005; Harris et al., 1996; Herman, 2001; Kenyon, 1986; Korswagen et al., 2002; Korswagen et al., 2000; Salser and Kenyon, 1992; Whangbo and Kenyon, 1999). We have

illustrated the role of SDN-1 in directing anterior QR descendant migrations. Our work also showed that SDN-1 functions in a redundant fashion with MIG-13, another previously characterized protein that has been shown to be require for QR descendant migrations (Sym et al., 1999; Wang et al., 2013). Furthermore, SDN-1 and MIG-13 function downstream of MAB-5 and are possibly regulated by MAB-5 in posterior migration. Our work also showed that SDN-1, MAB-5 and MIG-13 contribute to inherent asymmetry of the Q descendant neurons but did not function in early Q neuroblast migrations, suggesting that the early and subsequent descendant migrations may have some common players but definitely have some distinct genetic pathways directing their migrations.

Together, we have identified and characterized genetic pathways required to direct early Q neuroblast migrations and subsequent descendant migrations. Despite possessing identical times of birth and patterns of division, QR and QL undergo migrations in opposite directions. Our work has characterized distinct genetic pathways in QR and QL that contribute to their inherent asymmetry, which is causative to drive migrations in anterior-posterior directions. We have also identified a novel interaction of CDH-4/Fat with UNC-40 in QR but not in QL. This result strongly suggests that there might be an asymmetric genetic environment between QR and QL. Localization of proteins in QR but not in QL could facilitate this specific interaction between CDH-4 and UNC-40 in just QR. Identifying some asymmetrically expressed proteins in the Q cells would be a step towards understanding the distinct genetic interactions in QR Vs. QL. We propose performing a cell sorting experiment by sorting specifically for the Q cells using a cell specific *Pegl-17::RFP* marker. We then intend to perform a RNA sequencing on the Q cells and specifically screen for asymmetrical RNA levels of any gene from the sequencing data. Another experiment that could help us identify a QR specific CDH-4 interacting gene would be to perform a forward genetic screen in a *cdh-4* mutant background and isolate genes that suppress the posterior migration defects caused by *cdh-4* mutants in QR similar to that observed in *cdh-4; unc-40* mutant backgrounds. Through further genetic testing

we would able to positively identify the gene(s) required for the QR specific CDH-4 function.

References.

Abou Jamra, R., Becker, T., Georgi, A., Feulner, T., Schumacher, J., Stromaier, J., Schirmbeck, F., Schulze, T.G., Propping, P., Rietschel, M., Nothen, M.M., Cichon, S., 2008. Genetic variation of the FAT gene at 4q35 is associated with bipolar affective disorder. Mol Psychiatry 13, 277-284.

Ackley, B.D., 2013. Wnt-signaling and planar cell polarity genes regulate axon guidance along the anteroposterior axis in C. elegans. Dev Neurobiol.

Ackley, B.D., Harrington, R.J., Hudson, M.L., Williams, L., Kenyon, C.J., Chisholm, A.D., Jin, Y., 2005. The two isoforms of the Caenorhabditis elegans leukocyte-common antigen related receptor tyrosine phosphatase PTP-3 function independently in axon guidance and synapse formation. J Neurosci 25, 7517-7528.

Aicher, B., Lerch, M.M., Muller, T., Schilling, J., Ullrich, A., 1997. Cellular redistribution of protein tyrosine phosphatases LAR and PTPsigma by inducible proteolytic processing. J Cell Biol 138, 681-696.

Alexander, M., Chan, K.K., Byrne, A.B., Selman, G., Lee, T., Ono, J., Wong, E., Puckrin, R., Dixon, S.J., Roy, P.J., 2009. An UNC-40 pathway directs postsynaptic membrane extension in Caenorhabditis elegans. Development 136, 911-922.

Bernfield, M., Gotte, M., Park, P.W., Reizes, O., Fitzgerald, M.L., Lincecum, J., Zako, M., 1999. Functions of cell surface heparan sulfate proteoglycans. Annu Rev Biochem 68, 729-777.

Bigelow, H., Doitsidou, M., Sarin, S., Hobert, O., 2009. MAQGene: software to facilitate C. elegans mutant genome sequence analysis. Nat Methods 6, 549.

Branda, C.S., Stern, M.J., 2000. Mechanisms controlling sex myoblast migration in Caenorhabditis elegans hermaphrodites. Dev Biol 226, 137-151.

Buettner, F.F., Ashikov, A., Tiemann, B., Lehle, L., Bakker, H., 2013. C. elegans DPY-19 is a C-mannosyltransferase glycosylating thrombospondin repeats. Mol Cell 50, 295-302.

Bulow, H.E., Berry, K.L., Topper, L.H., Peles, E., Hobert, O., 2002. Heparan sulfate proteoglycan-dependent induction of axon branching and axon misrouting by the Kallmann syndrome gene kal-1. Proc Natl Acad Sci U S A 99, 6346-6351.

Calixto, A., Chelur, D., Topalidou, I., Chen, X., Chalfie, M., 2010. Enhanced neuronal RNAi in C. elegans using SID-1. Nat Methods 7, 554-559.

Ch'ng, Q., Williams, L., Lie, Y.S., Sym, M., Whangbo, J., Kenyon, C., 2003. Identification of genes that regulate a left-right asymmetric neuronal migration in Caenorhabditis elegans. Genetics 164, 1355-1367.

Chalfie, M., 1993. Homeobox genes in Caenorhabditis elegans. Curr Opin Genet Dev 3, 275-277.

Chalfie, M., Sulston, J., 1981. Developmental genetics of the mechanosensory neurons of Caenorhabditis elegans. Dev Biol 82, 358-370.

Chalfie, M., Thomson, J.N., Sulston, J.E., 1983. Induction of neuronal branching in Caenorhabditis elegans. Science 221, 61-63.

Chan, S.S., Zheng, H., Su, M.W., Wilk, R., Killeen, M.T., Hedgecock, E.M., Culotti, J.G., 1996. UNC-40, a C. elegans homolog of DCC (Deleted in Colorectal Cancer), is required in motile cells responding to UNC-6 netrin cues. Cell 87, 187-195.

Chapman, J.O., Li, H., Lundquist, E.A., 2008. The MIG-15 NIK kinase acts cell-autonomously in neuroblast polarization and migration in C. elegans. Dev Biol 324, 245-257.
Cho, E., Irvine, K.D., 2004. Action of fat, four-jointed, dachsous and dachs in distal-to-proximal wing signaling. Development 131, 4489-4500.
Cordes, S., Frank, C.A., Garriga, G., 2006. The C. elegans MELK ortholog PIG-1 regulates cell size asymmetry and daughter cell fate in asymmetric neuroblast divisions. Development 133, 2747-2756.
Davis, M.W., Hammarlund, M., Harrach, T., Hullett, P., Olsen, S., Jorgensen, E.M., 2005. Rapid single nucleotide polymorphism mapping in C. elegans. BMC Genomics 6, 118.
Du, H., Chalfie, M., 2001. Genes regulating touch cell development in Caenorhabditis elegans. Genetics 158, 197-207.
Dyer, J.O., Demarco, R.S., Lundquist, E.A., 2010. Distinct roles of Rac GTPases and the UNC-73/Trio and PIX-1 Rac GTP exchange factors in neuroblast protrusion and migration in C. elegans. Small GTPases 1, 44-61.
Eisenmann, D.M., 2005. Wnt signaling. WormBook, 1-17.
Esko, J.D., Selleck, S.B., 2002. Order out of chaos: assembly of ligand binding sites in heparan sulfate. Annu Rev Biochem 71, 435-471.
Esposito, G., Di Schiavi, E., Bergamasco, C., Bazzicalupo, P., 2007. Efficient and cell specific knock-down of gene function in targeted C. elegans neurons. Gene 395, 170-176.
Gilleard, J.S., Barry, J.D., Johnstone, I.L., 1997. cis regulatory requirements for hypodermal cell-specific expression of the Caenorhabditis elegans cuticle collagen gene dpy-7. Mol Cell Biol 17, 2301-2311.
Goodrich, L.V., Strutt, D., 2011. Principles of planar polarity in animal development. Development 138, 1877-1892.
Grimson, A., O'Connor, S., Newman, C.L., Anderson, P., 2004. SMG-1 is a phosphatidylinositol kinase-related protein kinase required for nonsense-mediated mRNA Decay in Caenorhabditis elegans. Mol Cell Biol 24, 7483-7490.
Haapasalo, A., Kim, D.Y., Carey, B.W., Turunen, M.K., Pettingell, W.H., Kovacs, D.M., 2007. Presenilin/gamma-secretase-mediated cleavage regulates association of leukocyte-common antigen-related (LAR) receptor tyrosine phosphatase with beta-catenin. J Biol Chem 282, 9063-9072.
Harrington, R.J., Gutch, M.J., Hengartner, M.O., Tonks, N.K., Chisholm, A.D., 2002. The C. elegans LAR-like receptor tyrosine phosphatase PTP-3 and the VAB-1 Eph receptor tyrosine kinase have partly redundant functions in morphogenesis. Development 129, 2141-2153.
Harris, J., Honigberg, L., Robinson, N., Kenyon, C., 1996. Neuronal cell migration in C. elegans: regulation of Hox gene expression and cell position. Development 122, 3117-3131.
Harterink, M., Kim, D.H., Middelkoop, T.C., Doan, T.D., van Oudenaarden, A., Korswagen, H.C., 2011. Neuroblast migration along the anteroposterior axis of C. elegans is controlled by opposing gradients of Wnts and a secreted Frizzled-related protein. Development 138, 2915-2924.

Hedgecock, E.M., Culotti, J.G., Hall, D.H., 1990. The unc-5, unc-6, and unc-40 genes guide circumferential migrations of pioneer axons and mesodermal cells on the epidermis in C. elegans. Neuron 4, 61-85.
Hedgecock, E.M., Culotti, J.G., Hall, D.H., Stern, B.D., 1987. Genetics of cell and axon migrations in Caenorhabditis elegans. Development 100, 365-382.
Herman, M., 2001. C. elegans POP-1/TCF functions in a canonical Wnt pathway that controls cell migration and in a noncanonical Wnt pathway that controls cell polarity. Development 128, 581-590.
Hofmeyer, K., Treisman, J.E., 2009. The receptor protein tyrosine phosphatase LAR promotes R7 photoreceptor axon targeting by a phosphatase-independent signaling mechanism. Proc Natl Acad Sci U S A 106, 19399-19404.
Honigberg, L., Kenyon, C., 2000. Establishment of left/right asymmetry in neuroblast migration by UNC-40/DCC, UNC-73/Trio and DPY-19 proteins in C. elegans. Development 127, 4655-4668.
Hudson, M.L., Kinnunen, T., Cinar, H.N., Chisholm, A.D., 2006. C. elegans Kallmann syndrome protein KAL-1 interacts with syndecan and glypican to regulate neuronal cell migrations. Dev Biol 294, 352-365.
Ishiuchi, T., Misaki, K., Yonemura, S., Takeichi, M., Tanoue, T., 2009. Mammalian Fat and Dachsous cadherins regulate apical membrane organization in the embryonic cerebral cortex. J Cell Biol 185, 959-967.
Johns, L., Grimson, A., Kuchma, S.L., Newman, C.L., Anderson, P., 2007. Caenorhabditis elegans SMG-2 selectively marks mRNAs containing premature translation termination codons. Mol Cell Biol 27, 5630-5638.
Johnson, K.G., Tenney, A.P., Ghose, A., Duckworth, A.M., Higashi, M.E., Parfitt, K., Marcu, O., Heslip, T.R., Marsh, J.L., Schwarz, T.L., Flanagan, J.G., Van Vactor, D., 2006. The HSPGs Syndecan and Dallylike bind the receptor phosphatase LAR and exert distinct effects on synaptic development. Neuron 49, 517-531.
Jung, Y.E., Jun, T.Y., 2013. Association between FAT Gene and Schizophrenia in the Korean Population. Clin Psychopharmacol Neurosci 11, 67-71.
Kamath, R.S., Ahringer, J., 2003. Genome-wide RNAi screening in Caenorhabditis elegans. Methods 30, 313-321.
Keino-Masu, K., Masu, M., Hinck, L., Leonardo, E.D., Chan, S.S., Culotti, J.G., Tessier-Lavigne, M., 1996. Deleted in Colorectal Cancer (DCC) encodes a netrin receptor. Cell 87, 175-185.
Kenyon, C., 1986. A gene involved in the development of the posterior body region of C. elegans. Cell 46, 477-487.
Korswagen, H.C., Coudreuse, D.Y., Betist, M.C., van de Water, S., Zivkovic, D., Clevers, H.C., 2002. The Axin-like protein PRY-1 is a negative regulator of a canonical Wnt pathway in C. elegans. Genes Dev 16, 1291-1302.
Korswagen, H.C., Herman, M.A., Clevers, H.C., 2000. Distinct beta-catenins mediate adhesion and signalling functions in C. elegans. Nature 406, 527-532.
Langmead, B., Trapnell, C., Pop, M., Salzberg, S.L., 2009. Ultrafast and memory-efficient alignment of short DNA sequences to the human genome. Genome Biol 10, R25.

Levy-Strumpf, N., Culotti, J.G., 2007. VAB-8, UNC-73 and MIG-2 regulate axon polarity and cell migration functions of UNC-40 in C. elegans. Nat Neurosci 10, 161-168.
Light, K.J., Miller, A.L., Doughty, C.J., Joyce, P.R., Olds, R.J., Kennedy, M.A., 2007. FAT and bipolar affective disorder. Mol Psychiatry 12, 899-900.
Lindahl, U., Kusche-Gullberg, M., Kjellen, L., 1998. Regulated diversity of heparan sulfate. J Biol Chem 273, 24979-24982.
Loveless, T., Hardin, J., 2012. Cadherin complexity: recent insights into cadherin superfamily function in C. elegans. Curr Opin Cell Biol 24, 695-701.
Maloof, J.N., Whangbo, J., Harris, J.M., Jongeward, G.D., Kenyon, C., 1999. A Wnt signaling pathway controls hox gene expression and neuroblast migration in C. elegans. Development 126, 37-49.
Matakatsu, H., Blair, S.S., 2004. Interactions between Fat and Dachsous and the regulation of planar cell polarity in the Drosophila wing. Development 131, 3785-3794.
Mello, C., Fire, A., 1995. DNA transformation. Methods Cell Biol 48, 451-482.
Merz, D.C., Alves, G., Kawano, T., Zheng, H., Culotti, J.G., 2003. UNC-52/perlecan affects gonadal leader cell migrations in C. elegans hermaphrodites through alterations in growth factor signaling. Dev Biol 256, 173-186.
Middelkoop, T.C., Williams, L., Yang, P.T., Luchtenberg, J., Betist, M.C., Ji, N., van Oudenaarden, A., Kenyon, C., Korswagen, H.C., 2012. The thrombospondin repeat containing protein MIG-21 controls a left-right asymmetric Wnt signaling response in migrating C. elegans neuroblasts. Dev Biol 361, 338-348.
Minevich, G., Park, D.S., Blankenberg, D., Poole, R.J., Hobert, O., 2012. CloudMap: a cloud-based pipeline for analysis of mutant genome sequences. Genetics 192, 1249-1269.
Minniti, A.N., Labarca, M., Hurtado, C., Brandan, E., 2004. Caenorhabditis elegans syndecan (SDN-1) is required for normal egg laying and associates with the nervous system and the vulva. J Cell Sci 117, 5179-5190.
Najarro, E.H., Wong, L., Zhen, M., Carpio, E.P., Goncharov, A., Garriga, G., Lundquist, E.A., Jin, Y., Ackley, B.D., 2012. Caenorhabditis elegans flamingo cadherin fmi-1 regulates GABAergic neuronal development. J Neurosci 32, 4196-4211.
Ou, G., Vale, R.D., 2009. Molecular signatures of cell migration in C. elegans Q neuroblasts. J Cell Biol 185, 77-85.
Pan, C.L., Howell, J.E., Clark, S.G., Hilliard, M., Cordes, S., Bargmann, C.I., Garriga, G., 2006. Multiple Wnts and frizzled receptors regulate anteriorly directed cell and growth cone migrations in Caenorhabditis elegans. Dev Cell 10, 367-377.
Pawson, C., Eaton, B.A., Davis, G.W., 2008. Formin-dependent synaptic growth: evidence that Dlar signals via Diaphanous to modulate synaptic actin and dynamic pioneer microtubules. J Neurosci 28, 11111-11123.
Popp, M.W., Maquat, L.E., 2013. Organizing principles of mammalian nonsense-mediated mRNA decay. Annu Rev Genet 47, 139-165.
Rawls, A.S., Guinto, J.B., Wolff, T., 2002. The cadherins fat and dachsous regulate dorsal/ventral signaling in the Drosophila eye. Curr Biol 12, 1021-1026.
Redies, C., Hertel, N., Hubner, C.A., 2012. Cadherins and neuropsychiatric disorders. Brain Res 1470, 130-144.

Rhiner, C., Gysi, S., Frohli, E., Hengartner, M.O., Hajnal, A., 2005. Syndecan regulates cell migration and axon guidance in C. elegans. Development 132, 4621-4633.
Robinson, J.T., Thorvaldsdottir, H., Winckler, W., Guttman, M., Lander, E.S., Getz, G., Mesirov, J.P., 2011. Integrative genomics viewer. Nat Biotechnol 29, 24-26.
Ruhe, J.E., Streit, S., Hart, S., Ullrich, A., 2006. EGFR signaling leads to downregulation of PTP-LAR via TACE-mediated proteolytic processing. Cell Signal 18, 1515-1527.
Saburi, S., Hester, I., Fischer, E., Pontoglio, M., Eremina, V., Gessler, M., Quaggin, S.E., Harrison, R., Mount, R., McNeill, H., 2008. Loss of Fat4 disrupts PCP signaling and oriented cell division and leads to cystic kidney disease. Nat Genet 40, 1010-1015.
Salser, S.J., Kenyon, C., 1992. Activation of a C. elegans Antennapedia homologue in migrating cells controls their direction of migration. Nature 355, 255-258.
Salser, S.J., Kenyon, C., 1996. A C. elegans Hox gene switches on, off, on and off again to regulate proliferation, differentiation and morphogenesis. Development 122, 1651-1661.
Sarov, M., Murray, J.I., Schanze, K., Pozniakovski, A., Niu, W., Angermann, K., Hasse, S., Rupprecht, M., Vinis, E., Tinney, M., Preston, E., Zinke, A., Enst, S., Teichgraber, T., Janette, J., Reis, K., Janosch, S., Schloissnig, S., Ejsmont, R.K., Slightam, C., Xu, X., Kim, S.K., Reinke, V., Stewart, A.F., Snyder, M., Waterston, R.H., Hyman, A.A., 2012. A genome-scale resource for in vivo tag-based protein function exploration in C. elegans. Cell 150, 855-866.
Schmitz, C., Wacker, I., Hutter, H., 2008. The Fat-like cadherin CDH-4 controls axon fasciculation, cell migration and hypodermis and pharynx development in Caenorhabditis elegans. Dev Biol 316, 249-259.
Schwabiuk, M., Coudiere, L., Merz, D.C., 2009. SDN-1/syndecan regulates growth factor signaling in distal tip cell migrations in C. elegans. Dev Biol 334, 235-242.
Solecki, D.J., Govek, E.E., Tomoda, T., Hatten, M.E., 2006. Neuronal polarity in CNS development. Genes Dev 20, 2639-2647.
Srinivasan, S., Mahowald, A.P., Fuller, M.T., 2012. The receptor tyrosine phosphatase Lar regulates adhesion between Drosophila male germline stem cells and the niche. Development 139, 1381-1390.
Strutt, H., Strutt, D., 2002. Nonautonomous planar polarity patterning in Drosophila: dishevelled-independent functions of frizzled. Dev Cell 3, 851-863.
Strutt, H., Strutt, D., 2005. Long-range coordination of planar polarity in Drosophila. Bioessays 27, 1218-1227.
Sulston, J., Hodgkin, J., 1988. Methods, in: Wood, W.B. (Ed.), The Nematode *Caenorhabditis elegans*. Cold Spring Harbor Laboratory Press, Cold Spring Harbor, New York, pp. 587-606.
Sulston, J.E., Horvitz, H.R., 1977. Post-embryonic cell lineages of the nematode, Caenorhabditis elegans. Dev Biol 56, 110-156.
Sundararajan, L., Lundquist, E.A., 2012. Transmembrane proteins UNC-40/DCC, PTP-3/LAR, and MIG-21 control anterior-posterior neuroblast migration with left-right functional asymmetry in Caenorhabditis elegans. Genetics 192, 1373-1388.
Sundararajan, L., Norris, M.L., Schoneich, S., Ackley, B.D., Lundquist, E.A., 2014. The fat-like cadherin CDH-4 acts cell-non-autonomously in anterior-posterior neuroblast migration. Dev Biol.

Sym, M., Robinson, N., Kenyon, C., 1999. MIG-13 positions migrating cells along the anteroposterior body axis of C. elegans. Cell 98, 25-36.
Tabara, H., Grishok, A., Mello, C.C., 1998. RNAi in C. elegans: soaking in the genome sequence. Science 282, 430-431.
Tanoue, T., Takeichi, M., 2004. Mammalian Fat1 cadherin regulates actin dynamics and cell-cell contact. J Cell Biol 165, 517-528.
Terns, R.M., Kroll-Conner, P., Zhu, J., Chung, S., Rothman, J.H., 1997. A deficiency screen for zygotic loci required for establishment and patterning of the epidermis in Caenorhabditis elegans. Genetics 146, 185-206.
Thomas, C., Strutt, D., 2012. The roles of the cadherins Fat and Dachsous in planar polarity specification in Drosophila. Dev Dyn 241, 27-39.
Thorvaldsdottir, H., Robinson, J.T., Mesirov, J.P., 2013. Integrative Genomics Viewer (IGV): high-performance genomics data visualization and exploration. Brief Bioinform 14, 178-192.
Wang, F., Wolfson, S.N., Gharib, A., Sagasti, A., 2012. LAR receptor tyrosine phosphatases and HSPGs guide peripheral sensory axons to the skin. Curr Biol 22, 373-382.
Wang, X., Zhou, F., Lv, S., Yi, P., Zhu, Z., Yang, Y., Feng, G., Li, W., Ou, G., 2013. Transmembrane protein MIG-13 links the Wnt signaling and Hox genes to the cell polarity in neuronal migration. Proc Natl Acad Sci U S A 110, 11175-11180.
Whangbo, J., Kenyon, C., 1999. A Wnt signaling system that specifies two patterns of cell migration in C. elegans. Mol Cell 4, 851-858.
White, J.G., Southgate, E., Thomson, J.N., Brenner, S., 1986. The structure of the nervous system of the nematode Caenorhabditis elegans. Philos Trans R Soc Lond B Biol Sci 314, 1-340.
Williams, L., 2003. Ph.D. thesis. A genetic analysis of the left-right asymmetric polarizations and migrations of the Q neuroblasts in C. elegans. University of California-San Francisco.
Winston, W.M., Molodowitch, C., Hunter, C.P., 2002. Systemic RNAi in C. elegans requires the putative transmembrane protein SID-1. Science 295, 2456-2459.
Wodarz, A., 2005. Molecular control of cell polarity and asymmetric cell division in Drosophila neuroblasts. Curr Opin Cell Biol 17, 475-481.
Yang, C.H., Axelrod, J.D., Simon, M.A., 2002. Regulation of Frizzled by fat-like cadherins during planar polarity signaling in the Drosophila compound eye. Cell 108, 675-688.
Zhao, X., Sawa, H., Herman, M.A., 2003. tcl-2 encodes a novel protein that acts synergistically with Wnt signaling pathways in C. elegans. Dev Biol 256, 276-289.
Zinovyeva, A.Y., Yamamoto, Y., Sawa, H., Forrester, W.C., 2008. Complex network of Wnt signaling regulates neuronal migrations during Caenorhabditis elegans development. Genetics 179, 1357-1371.